Geophysical Investigations on the Hydrogeological Situation in Nam Dinh Coastal area

Dissertation

zur Erlangung des Doktorgrades
der Naturwissenschaften

vorgelegt von
Nguyễn Trọng Vũ
aus Thai Binh, Vietnam

genehmigt von der Fakultät für
Energie- und Wirtschaftswissenschaften
der Technischen Universität Clausthal

Tag der mündlichen Prüfung
28. November 2012

Die Arbeit wurde am Institut für Geophysik der Technischen Univeristät Clausthal angefertigt.

Vorsitzender der Promotionskommission:	Prof. Dr. rer. nat. H. –J. Gursky
Hauptberichterstatter:	Prof. Dr. rer. nat. habil. A. Weller
Mitberichterstatter:	Prof. Dr. rer. nat. M. Sauter

Acknowlegments

I am grateful to Prof. Dr. Andreas Weller for supervising this work and for his keen assistance and intensive discussion that always lead to improve the results of this work. My grateful thanks are also to Prof. Dr. Martin Sauter for his valuable help and important suggestions that had brought this work in its present form.

I am grateful to Dr. Tang Dinh Nam from the Institute of Geosciences and Mineral Resources, Hanoi, for his support and discussions on resistivity imaging and data interpretation. I thank to Prof. Dr. Doan Van Canh from Universtity of Mining and Geology, Hanoi, for his suggestions and discussions on hydrogeological characteristics of Nam Dinh province. I am thankful to Dr. Wolfgang Debschütz from the Institute of Geophysics (TU Clausthal) for his support to perform the measurements of specific internal surface and his assistance in well logging data interpretation. Also my thanks go to Dr. Carl-Dietrich Sattler from the Institute of Geology and Paleontology (TU Clausthal) for performing the sieving process, the X-ray diffraction measurements, and his assistance in data interpretation. I thank also Marcus Möller for his assistance in resistivity data inversion.

From the Vietnamese side, first I am grateful to the Ministry of Education and Training that granted a 3 years scholarship for my study in Germany. I am thankful to the Head of the Institute of Geophysics at Vietnamese Academy of Science and Technology (VAST) for the support he has given to me to obtain this scholarship. I should not forget to thank Dr. Nguyen Nhu Trung from the Institute of Marine Geology and Geophysics, VAST, for his support.

I wish to express my gratitude to all my colleagues in the Institutes of Geophysics at VAST and TU Clausthal. Great thanks to all my colleagues for offering their assistance and help wherever needed. I wish also to thank Nguyen Tien Phong from the Institute of Geosciences and Mineral Resources for his helps in transient electromagnetic measurement and data interpretation.

I am grateful to Ass. Prof. Dr. Le Thi Lai from the Institute of Geology, VAST, and Ass. Prof. Dr. Jörn Kassbohm from Greifswald University, Germany, for their support and suggestions for this work. The funding for drilling of the three boreholes in the study area was supported by the project ‘Integrated Water Resource Management in Nam Dinh province’.

This dissertation would not have been finished without the endless love, encouragement and support from my parents, my wife and my son.

Geophysical investigations on the hydrogeological situation in Nam Dinh coastal area

Summary

Saltwater intrusion is a typical phenomenon that is observed in coastal aquifers. Geophysical methods are increasingly used to explore the hydrogeological situation in coastal areas. These investigations are usually focused on the differentiation in fresh and saline water bearing formations based on the electrical conductivity. A severe limitation of geoelectrical methods is the ambiguity of the resulting models caused by the principle of equivalence in inversion and interpretation. A combination of geophysical and hydrogeological investigations was carried out in Nam Dinh coastal area to improve the knowledge on the geological structures and the distribution of the aquifers. Additionally, the hydraulic properties of the aquifers were estimated from petrophysical data on the basis of empirical models. The study presents a methodological approach to identify the potential of different methods in the investigation of saltwater intrusion in coastal aquifers. The practical application of the tools, the achieved data quality, the reliability of the resulting models, and their relation to other results should indicate the advantages but also the limitations of the selected geophysical methods.

A total of 33 vertical electric soundings (VES), 26 transient electromagnetic soundings (TEM), and 8 km of resistivity imaging (RI) were carried out in the area of Giao Thuy and Xuan Truong districts (Nam Dinh province) to determine the geological structure based on the resulting electrical resistivity distribution. Three new boreholes were drilled to examine the exact stratification for the calibration of geoelectrical models. Soil samples were collected for laboratory investigation to determine the petrophysical properties. Natural gamma log and resistivity logs were performed in the three new boreholes to identify the geological structure and to verify the resistivity of different layers.

VES and TEM soundings were inverted by layered models. Thickness and resistivity of the layers were carefully adjusted on the basis of the principle of equivalence regarding the thickness and resistivity of the formations from neighboring boreholes. A combined inversion of VES and TEM at the position of the boreholes provides a suitable structural model, which considers the local stratification and the formation resistivity derived from well logging and laboratory measurements. The results indicated that the TEM method is restricted in the depth of investigation due to the screening effect of shallow conductive layers. The clay layer and the shallow saline water bearing formation absorbed the energy and prevented a deeper penetration of the

electromagnetic field. Based on the resistivity of the layered models from VES inversion, regional maps of resistivity distribution for the Holocene and the Pleistocene aquifers were constructed. A low resistivity value in almost all VES models indicated that the Holocene aquifer contains in wide area saline water. For the Pleistocene aquifer, the resistivity distribution map indicated fresh water only in the Southwestern part of the study area. Brackish and saline water was indentified in the remaining parts of the area. The large distance between VES stations caused a distortion of resistivity contour lines. The distance between stations should consider the depth of investigation. For the investigation of the Pleistocene aquifer at a depth of about 100 m, a distance between neighboring soundings of about 1000 m is recommended. RI presents the resistivity distribution in a 2D vertical cross section. The results are in good agreement with VES, TEM and resistivity logs. An obvious limitation is the principle of equivalence in data interpretation of the resulting images. Because clay layers and saline water bearing formations show a similar resistivity, a discrimination of these lithological units in the vertical sections is not possible. Two faults were identified in the study area by RI. The geological stratification in two boreholes confirmed the uplifted and depressed zone of a fault.

Soil samples collected from the boreholes were investigated in laboratory to determine the petrophysical parameters of samples such as grain density, water content, porosity, specific internal surface, electrical conductivity, and magnetic susceptibility. Additionally, grain size distribution and clay content were determined. A comparison between RI, well logging, and sample resistivity data at positions of the three boreholes demonstrated that different methods provide similar values of resistivity for a certain formation. The relationship between clay content of sample and the count rate of gamma ray activity was investigated. Additionally, the clay volume fraction was estimated from gamma log on the basis of count rate of gamma ray activity. An increasing clay fraction causes a decrease in resistivity of soil sample because the clay in wet samples acts as a conductor.

The electrical conductivity of groundwater from the Pleistocene aquifer was measured at the position of 80 domestic water wells. In the regional map of water conductivity, the distribution of water wells caused a distortion of the contour lines because the water wells are concentrated in the freshwater area. For an aquifer, the resistivity of the fully saturated formation is proportional to the resistivity of the water according to the first Archie’s equation. Based on this relationship, the resistivity formation factor of the Pleistocene aquifer was estimated. An average formation factor of 2 was determined. The electrical conductivity of ground water was inferred from the conductivity of the Pleistocene formations, which were derived from geophysical

investigations. A combination of water conductivity values, which were derived from geoelectrical methods and measured in the water wells, increases the number of data in both fresh and saline water area. The distortion of the contour lines is reduced and a reliable map of the distribution of water conductivity is provided that indicates clearly the boundary between fresh and saline water.

Based on the results of all geophysical investigations, the geological structure and the physical properties of the units have been determined. For sandy sediments, a resistivity of higher than 10 Ωm indicates a fresh water bearing formation while a resistivity of lower than 5 Ωm reflects the saline water in sandy sediment. Brackish water is presented by a formation resistivity in the range from 5 to 10 Ωm. The resistivity of the clay layer varies in the range from 0.7 to 10 Ωm. The Holocene aquifer, which extends from the surface down to a depth of 30 m, contains predominantly saline water. The Pleistocene aquifer, which is found at a depth of more than 56 m, contains both fresh and saline water. The aquiclude, which is formed by a clay layer with a thickness of about 40 m, separates the Holocene and the Pleistocene aquifers. It prevents a water movement in vertical direction between the Holocene and Pleistocene aquifers. A transition from fresh to saline water in the Pleistocene aquifer is observed in the study area. According to geophysical results the boundary between fresh and saline can be determined with an accuracy of around 100 m.

To evaluate the hydrogeological characteristics of the aquifers, the hydraulic conductivity of the Pleistocene samples were estimated from grain size distribution (sieving), specific internal surface (nitrogen adsorption), and interface conductivity (spectral induced polarization). The calculated results verified the validity of the different empirical equations. For a certain sample, the hydraulic conductivity, which is calculated from different equations regarding distinct values of the grain size distribution, exhibits only a low variation. For all Pleistocene samples, the hydraulic conductivity varies in the range of one order of magnitude. Two other values of hydraulic conductivity of the samples were calculated by the PaRiS equation using the specific internal surface and the complex interface conductivity. The results are comparable. The estimation of hydraulic conductivity based on different parameters including grain size distribution, specific internal surface, and complex interface resistivity varies in the range of one and half order of magnitude. This is a good result because the hydraulic conductivity values were determined by different empirical equations with different uncertainty of the methods. The hydraulic conductivity determined from pumping tests is higher than the hydraulic conductivity calculated from petrophysical parameters. The pumping tests more or less reflect the horizontal flow of groundwater at macroscopic scale while the laboratory investigations consider

the hydraulic properties of disturbed samples at microscopic scale. For the coarse grained samples, the hydraulic conductivity values determined by complex interface conductivity indicate a weaker deviation within one order of magnitude. An upscaling of the laboratory values to the field scale generally results in a higher hydraulic conductivity. A variation of one and a half order in hydraulic conductivity from different empirical equations and different scales can be regarded as a reasonable result.

All the information, which is gathered during geophysical and hydrogeological investigations, has been integrated in a cross section of a conceptual hydrogeological model. The hydrogeological situation along the coastline of the study area is clearly reflected by the model. The saline water may infiltrate into the Holocene aquifer via the local canals. For the Pleistocene aquifer, the saline water originates from the fault systems. The transition zone between fresh and saline water is about 1 km wide. A further extension of the transition zone in Southwestern direction will be expected when the ground water extraction increases in the freshwater area.

The methodological approach has shown that a combination of geophysical methods at field scale (VES, RI, TEM), in boreholes (resistivity, gamma log), and in laboratory (resistivity, specific internal surface, grain size distribution) provides sufficient data at different scales that can be integrated in a reliable hydrogeological model. Geoelectrical methods are generally recommended for hydrogeological investigations related to varying water salinity. The combination of sounding and mapping tools provides valuable structural information. The limitations caused by the principle of equivalence can be reduced if boreholes are available to calibrate the geoelectrical models with known depth data. Electrical investigations on samples provide insight into petrophysical relations that are helpful to estimate water conductivity or hydraulic conductivity of the investigated formations.

Contents

List of figures

List of Tables

Lists of Abbreviations and Symbols

Δs:	Drawdown difference of water table over one log cycle (m)
φ:	Phase angle (complex resistivity measurement – mrad)
σ:	Conductivity (mS/m)
σ_w:	Conductivity of water (mS/m)
σ_o:	Saturated conductivity of formation (mS/m)
σ'':	Complex interface conductivity (S/m)
ρ:	Resistivity (Ωm)
ρ_0:	Saturated resistivity of soil sample (Ωm)
ρ_{LAB}:	Resistivity of samples determined in laboratory (Ωm)
ρ_{Log}:	Resistivity of formation determined by resistivity well logging R32 (Ωm)
ρ_m:	Measured resistivity (including ρLAB and ρLog -Ωm)
ρ_{RI}:	Resistivity of formation determined by RI (Ωm)
ρ_w:	Resistivity of water (Ωm)
Θ:	Volumetric water content (%)
Φ:	Porosity (%)
κ:	Mass specific magnetic susceptibility (10^{-8} m^3/kg)
CC:	Clay content (%)
Chl:	Chloride (Clay mineral identification - %)
d_{10}:	Effective diameter of particles, which 10 % particle has a diameter smaller than grain size (mm)
d_k:	Grain density (kg/m^3)
d_n:	Draw density (kg/m^3)
EC:	Electrical conductivity of water (mS/m)
e_r:	Relative error (%)
F:	Formation factor (dimensionless)
G_R:	Count rate of gamma ray activity (cps)
K:	Kaolinite (Clay mineral identification- %)
K_P:	Hydraulic conductivity (pumping test - m/s)
K_A:	Hydraulic conductivity (following Alyamani equation - m/s)
K_B:	Hydraulic conductivity (following Beyer equation - m/s)
K_{Spor}:	Hydraulic conductivity regarding specific internal surface *Spor* (m/s)
$K_{\sigma''}$:	Hydraulic conductivity regarding interface conductivity σ'' (m/s)
M:	Muscovite or illite (Clay mineral identification- %)
Q:	Discharge of water in pumping test (m^3/s)
qh:	The Holocene aquifer
qp:	The Pleistocene aquifer
RI:	Resistivity imaging investigation
RMS:	Root Mean Square error (%)

S_m: Mass related specific internal surface (m^2/kg)
S_{por}: Specific internal surface ($1/\mu m$)
S_w: Saturation factor (dimensionless)
T_{KA}: Transmissivity factor (calculated from K_A - m^2/s)
T_{KB}: Transmissivity factor (calculated from K_B - m^2/s)
T_P: Transmissivity factor (pumping test - m^2/s)
TDS: Total Dissolved Solid (g/l)
TEM: Transient Electromagnetic Method
VES: Vertical Electric Sounding
V_{Shale}: Clay volume fraction regarding the gamma ray activity (%)
w: Gravimetric water content (%)

1. Introduction

1.1. Motivation

Water is an invaluable natural resource. It is a basic requirement for live and development of the communities. Considering increasing pollution of surface water, groundwater is the safest kind of water supply because the groundwater is normally protected by the covering layers which prevent the pollution from different surface sources. The supply of groundwater is the main source of freshwater for domestic, industrial and agricultural purposes in coastal regions. But saltwater intrusion in the aquifers is a large problem because it is directly linked to the lack of freshwater. Saltwater intrusion is a world-wide problem that occurs in the coastal zones of many countries. The increase of groundwater extraction causes saltwater intrusion in the coastal aquifers. The studies of saltwater intrusion phenomenon are useful for a sustainable exploitation of groundwater in the coastal zones. It is helpful to protect the freshwater resources for the development of the communities.

Saltwater intrusion is the movement of saline water into freshwater aquifers. The detection and quantification of this phenomenon is the target of geophysical methods in coastal environment. Geoelectrical methods have proven to be efficient tools for geoenvironmental investigations on saltwater intrusion in coastal areas because the salt content of water dominates the electrical conductivity of the sediments (Bear, 1999; Reynolds, 2005; Kirsch, 2006; Franco et al., 2009). Based on geophysical and hydrogeological investigations, the structure of aquifers and the transition zone between fresh/saline water can be delineated. Note that geophysical methods do not directly detect the saline water but they can measure the characteristic increase of formation conductivity, which is caused by the saltwater intrusion phenomenon. Geophysical methods are also indirect tools to estimate the hydraulic properties of the aquifers.

Vietnam has a long coastline of more than 3200 km. The salt water intrusion is one of the largest problems for coastal zones in Vietnam. The first trials of geophysical investigations to determine the saline water in aquifers were made using Vertical Electric Soundings (VES) about 30 years ago. Due to the limitations of instruments and method, the results of investigations were ambiguous. Recently, geophysical methods, such as VES, Resistivity Imaging and Transient electromagnetic method, were applied to investigate the saline water in the aquifers along the coastal zone (Nguyen Van Giang et al., 1998; Tang Dinh Nam et al., 2004; Nguyen Nhu Trung, 2005, Dang Thanh Hai et al., 2009). These investigations are carried out in field scale

to locate the boundary between fresh and saline water bearing aquifers. Saltwater intrusion is commonly indicated by a strong decrease in formation resistivity.

Nam Dinh province is located in Red River delta in the North of Vietnam with a coastline of 72 km. With deltaic characteristics, the geological structure is characterized by horizontally layered sediments. There are two main aquifers which are exploited: the Holocene aquifer and the Pleistocene aquifer. Almost all of the Holocene aquifer contains brackish (or saline) water. In the Pleistocene aquifer, freshwater exists in a part of Nam Dinh province and other parts of Pleistocene contain saline water (Doan Van Canh et al., 2005, Nguyen Trong Vu et al. 2007). Based on previous investigations (Nguyen Van Do et al., 1996; Doan Van Canh et al., 2004), the boundary between fresh and saline water runs parallel to the Red River and perpendicular to the coastline. The freshwater and saline water boundary was determined by the distribution of Total Dissolved Solids (TDS) content or chloride content which is measured in water samples. The boundary is not exactly defined because the water samples are non-uniformly scattered and almost all water samples are concentrated in freshwater areas. A movement of saline water into freshwater area (in the Pleistocene aquifer) is observed due to the increasing groundwater extraction. The previous geophysical and hydrogeological investigations were carried out over the whole areas of the province Nam Dinh. There has been no intensive use of geophysical tools to study saltwater intrusion in the coastal area.

Geophysical methods are not only used to determine the geological structure of the study area but also applied to predict the hydraulic properties of the aquifers. Böner et al. (1996) proposed a method to estimate the hydraulic conductivity of sediments from complex resistivity data. In previous studies in Vietnam, geophysical investigations are used to locate the geological structure and to identify the fresh or saline water bearing formation. A severe limitation of geophysical methods is the ambiguity in the results, which is related to the validity of the principle of equivalence in the inversion of geophysical data. Additionally, geoelectrical methods are limited to distinguish between clay sediment and saline water bearing formation because they present a similar resistivity. To study the extension of salt water intrusion in the coastal aquifers, a combination of geophysical and hydrogeological investigations should be used to get a better knowledge on the saltwater intrusion phenomenon in coastal aquifers.

1.2. International case studies

Saltwater intrusion occurs in virtually all coastal aquifers, which are in hydraulic connection with seawater. Stewart (1999) defined saltwater intrusion as the mass transport of saline water into a zone that has been previously occupied by

fresh water. Salt water intrusion leads to changing properties of water bearing formations which are subject of geophysical measurements. In the last few decades, many geophysical investigations have been carried out to study the process of salt water intrusion all over the world (Choudhury et al., 2001; Hodlur et al., 2006; Hamzah et al., 2007; Maurer et al., 2009; Falgas et al., 2009; Khalil et al., 2011). In this section, only a few typical examples of geophysical investigations are described.

A significant investigation of geophysical methods to delineate the fresh and saline water transition zone in Travis and Hays county (Texas, USA) has been performed by a group of American scientists (Payne et al., 2007). A combination of Time Domain Electromagnetic Method (TDEM) and resistivity log measurements has been applied to map the resistivity distribution of the aquifer. TDEM sounding results have shown a sharp change in resistivity along profiles. The effectiveness of TDEM soundings to delineate the transition zone was indicated by comparing the distribution of resistivity in the aquifer with the distribution of TDS concentrations in the aquifer along profiles. The higher resistivity regions correspond to lower TDS concentration (freshwater) and the lower resistivity regions correspond to higher TDS concentration (saline water). Payne et al. (2007) have shown the efficiency of TDEM and resistivity logs to delineate the transition zone in a deep aquifer.

The Leibniz Institute for Applied Geophysics (LIAG) has performed intensive studies on problem of the salt water intrusion in northern Germany using airborne electromagnetic measurements. The SkyTEM system was used with different frequencies to determine the potential saltwater intrusion zones (resistivity <10 Ωm) in the surroundings of the salt dome Segeberg. The boundary between fresh and saline water was detected down to about 60 m at the island Borkum (North Sea). In their investigations, Wiederhold et al. (2010) have shown that the SkyTEM is able to identify the freshwater lenses within the saline water area (Föhr Island).

In a case study of groundwater prospection in Zeeland, Netherlands, Geos et al. (2009) have applied geophysical and hydrological methods to estimate the depth of fresh and brackish groundwater in a predominantly saline region. The depth of fresh-brackish and brackish-saline groundwater interface has been detected by analyzing geophysical (1D, 2D geoelectrical measurements, electrical well logging, electromagnetic measurements) and hydrological (chloride content of groundwater samples) data. Geos et al. (2009) also indicated the regional map, which was formed by geophysical and hydrological results, maybe less reliable due to a low data density.

Another example of the application of geophysical methods to investigate the salt water intrusion in coastal aquifers was presented by Hwang et al. (2004). The authors used geophysical well logging and VES to assess seawater intrusion in a coastal

aquifer of Youngkwang, Korea. The layer boundaries of the aquifer were obtained from interpretation of 60 VES. Well logging (fluid conductivity, electromagnetic induction, caliper, natural gamma, gamma – gamma, and thermal neutron measurements) data were used to identify the aquifer (sand layer) and the resistivity of pore water in the aquifer. The estimated equivalent NaCl concentration in the aquifer was used to identify the boundary between fresh and saline water.

1.3. Case studies in Vietnam

Since 1990, geophysical methods have been applied to delineate the fresh and saline water in Vietnamese coastal zones. Nguyen Thi Kim Thoa et al. (1995) have applied the VES and Magnetotelluric methods to investigate the aquifers in Mekong delta (South of Vietnam). Based on the inversion technique, a layered model of geological structure has been constructed. Concerning the resistivity distribution of the layered model, the boundary between fresh and saline water has been identified.

The salt water intrusion was also investigated by geophysical methods in the centre of Vietnam. Tang Dinh Nam et al. (2004) used the induced polarization soundings and resistivity imaging to evaluate the salt water intrusion in the coastal aquifer of central provinces (from Quang Binh province to Quang Ngai provine). The authors obtained the relationship between the resistivity of the aquifers and the TDS contents of water. The boundary between fresh and saline water were determined based on the resistivity of the aquifer and the TDS content of water. The results were used to select the positions of boreholes. The extracted water from the boreholes has proven the efficiency of geophysical and hydrogeological methods in surveys of salt water intrusion.

Geophysical methods including electrical and electromagnetic methods have been used in the investigation of deep aquifers in Ninh Binh province (Nguyen Van Giang et al., 1998). Ninh Binh is an adjacent province of Nam Dinh (see Figure 2.1). The freshwater lens in Pleistocene extends from Ninh Binh to Nam Dinh province. The results of geophysical investigations were used to delineate the distribution of aquifers in Ninh Binh province. In the coastal area of Ninh Binh province, saline water exists in the Holocene aquifer which was indicated by geophysical results.

Thai Binh is a neighbouring province of Nam Dinh. Red River forms the natural boundary between the two provinces (see Figure 2.1). The hydrogeological situation is similar in both provinces. The salt water intrusion occurs in the western part of Thai Binh province which is connected with the eastern part of Nam Dinh province. After successful investigation of saltwater intrusion in Hai Phong province (Nguyen Nhu Trung, 2005), geophysical and hydrogeological investigations were applied to evaluate

the groundwater situation in Thai Binh province (Nguyen Nhu Trung et al., 2008). Geoelectrical methods were used to delineate the distribution of aquifers and aquitards. Hydrogeological measurements and the chemical analyses of groundwater samples were used to estimate the boundary between fresh and salt water in the study area. The results of geophysical (aquifer and aquitard structures, formation factor of aquifer) and hydrogeological measurements (TDS and chloride content) were used as input parameters for modelling and simulations. The modelling has predicted the movement of fresh and saline water boundary in the Pleistocene aquifer. Based on the number of wells, which are located in the freshwater area, the freshwater yields of the Pleistocene aquifer were estimated. The modelling has indicated that the saline water area in the western part of Thai Binh province is connected with the saline water area in the eastern part of Nam Dinh province.

The hydrogeological situation of Nam Dinh province has been investigated by several studies. The most important hydrogeological project resulted in the 'Hydrogeological map in Nam Dinh province and adjacent areas in scale 1:50.000' (Nguyen Van Do et al., 1996). In the frame of this project, Nguyen Van Do and his co-workers carried out many investigations in the fields of geology, hydrogeology, and geophysics to map the hydrogeological situation of Nam Dinh province. 35 boreholes were drilled to determine the geological structure, to analyze the rock constituents, and to perform hydrogeological experiments. 523 VES stations and 1515 m well logging measurements were carried out to determine the geological structure, thickness of aquifers, and boundaries between fresh and saline water. More than one hundred water samples were collected and analysed. During the project, 12 permanent groundwater monitoring wells were established. The project has provided an overview of the geological and hydrogeological situation of Nam Dinh province. Based on all geological, hydrogeological, and geophysical data, the authors have designed hydrogeological maps for the main aquifers in scale 1:50000 for Nam Dinh province. The hydrogeological maps indicate the potential, quality, and distribution of groundwater in the province. Following the hydrogeological maps, Nam Dinh province was divided in three zones corresponding to the quality of groundwater distribution. The TDS and chloride contents in groundwater were used to distinguish between fresh, brackish, and saline groundwater.

The boundary between fresh and saline water was only roughly estimated because of the limited number of data and water samples. To get more information on the hydrogeological situation of Nam Dinh province, Doan Van Canh et al. (2004) have carried out more hydrogeological measurements to improve the quality of hydrogeological map. Based on the hydrogeological measurements and chemical

analyses of groundwater samples, the boundary between fresh and saline water was estimated with more accuracy.

Based on all available information on the Pleistocene aquifer in Nam Dinh province, Dang Dinh Phuc (2000) constructed a model of the aquifer. He calculated several scenarios of the saltwater movement in the aquifer with varying groundwater extraction. Using the hydrogeological software ModFlow, he predicted a depressed water table for different periods. Following his modelling, the difference of water table between the saline and fresh groundwater area will reach 11 m after 27 years and 18 m after 50 years later due to groundwater extraction from domestic wells. The increased potential difference will cause a further salt water intrusion into the Pleistocene aquifer.

According to the yearly report of Hydrogeological Federation of North Vietnam (2006) on the statistical data set from the national monitoring wells located in Hai Hau district, the groundwater table of Pleistocene aquifer in Nam Dinh province is decreased approximately 8 m in the period from 1996 to 2005. The depression seems to be much faster than the predicted levels from previous studies. More extraction of groundwater leads to an increased salt water intrusion.

The water supply for the communities is very important, especially in the area of saline groundwater. To solve this problem, Dang Thanh Hai et al. (2009) have tried to estimate the depth of freshwater aquifers in the predominantly saline groundwater area of Nam Dinh province (especially for Giao An commune, Giao Thuy district) by geophysical methods. Resistivity imaging and TDEM measurements have been applied to find a deep aquifer in the study area. The geophysical results have confirmed that the Holocene and Pleistocene aquifers contain saline water in the study area. Fortunately, the TDEM results have shown a potential freshwater bearing aquifer (resistivity of formation in the range 23.8 Ωm to 80.0 Ωm) at a depth of more than 300 m. Further investigations and drilling became necessary to confirm the freshwater containing aquifer.

All geophysical investigations, which were mentioned above, just concentrated to identify the fresh or saline aquifer and to locate the boundary between fresh and saline water in the aquifer. There is no intensive geophysical investigation which is focused on saltwater intrusion problem in a small area. Hydraulic characteristics of the aquifer, which related to geophysical parameters, are not investigated. The spatial density of data set was not discussed in detail to prove the advantages and disadvantages for each geophysical method. Because the hydraulic properties the aquifer were not fulfilled, the prediction of saline water movement from modelling and simulation is ambiguous.

Following the results of geophysical and hydrogeological investigation in the whole province, salt water intrusion occurs not only in the coastal area but also in the central part of province. The main aquifer (the Pleistocene aquifer) is a high potential groundwater aquifer but the North and the Northeastern parts of the Pleistocene aquifer contain saline groundwater. The boundary between fresh and saline groundwater runs in parallel to the Red river and perpendicular to the coastline. The transition zone from freshwater to saline water is not exactly determined. The previous investigations were sparse over whole area of province. There is no detailed investigation with geophysical and hydrogeological methods in the coastal area of Nam Dinh province, so far. Therefore, a combination of geophysical and hydrogeological investigations in the area of saltwater intrusion should be carried out to determine the quality of groundwater, to locate the boundary between fresh and saline water and to characterize the hydraulic properties of the aquifers.

1.4. Objectives of my study

In the frame work of my study, geophysical and hydrogeological investigations were performed which focused on saltwater intrusion problems in the coastal aquifers. The area of investigation was chosen in the Eastern part of Nam Dinh province. It includes the districts Xuan Truong, Giao Thuy and a part of Hai Hau district. The study area contains three zones of groundwater: fresh water, brackish water and saline water.

In the study area, geophysical investigations were carried out to explore the geological structures of the water bearing formations. Vertical Electric Soundings were carried out to delineate the aquifers and aquitards. Resistivity and thickness of geological structure were determined by inversion technique. Resistivity Imaging (RI) investigations were performed to evaluate the distribution of resistivity of geological structures along RI profiles. Transient Electromagnetics method (TEM) was investigated parallel to the RI profiles to delineate the geological structures and compare with the results of geoelectrical investigations. Three new boreholes were drilled to determine geological structures and to confirm the results of VES, RI and TEM measurements. Soil samples were taken from the boreholes to be analysed in the laboratory for determining the petrophysical parameters such as grain density, water content, grain size distribution, specific internal surface, electrical and magnetic properties. Well logging, including natural gamma log and resistivity logs, was performed after drilling to confirm the geological structure and properties of the aquifers and aquicludes. The resulting logs are used to verify the other geophysical investigations. The electrical conductivity of water samples was measured at domestic water wells, which extract groundwater from the Pleistocene aquifer.

The thesis presents a recent study on saltwater intrusion in coastal zone of Nam Dinh province based on the new investigations of geophysical, hydrogeological and petrophysical methods. The aims of geophysical investigations are to determine the geological structure of aquifers and aquicludes, to identify the fresh and saltwater bearing formations, to locate the extension of saltwater intrusion in both vertical and horizontal directions. The hydraulic conductivity of the aquifer was calculated by petrophysical parameters such as grain size distribution, specific internal surface and interface conductivity. The results demonstrate a new approach to evaluate the hydraulic properties of the aquifer. Finally, a conceptual model of the hydrogeological situation along coastline of the study area was constructed on the basis of all collected data. The study presents a methodological approach to identify the potential of different methods in the investigation of saltwater intrusion in coastal aquifer. The practical application of the tools, the achieved data quality, the reliability of the resulting models, and their relation to other results should indicate the advantages but also the limitations of the selected geophysical methods. The ambiguity of geophysical models, which is related to the principle of equivalence, is discussed. Recommendation should be given to design a cost-effective program for further investigation of saltwater intrusion in the Red River delta in Vietnam.

My thesis includes six sections. The section 1 provides an introduction in the topic of saltwater intrusion. The geological and hydrogelogical situation in Nam Dinh province is presented in the section 2. In the section 3, the theoretical fundamentals methods which are used in the study are described. The results of the geophysical investigations are presented in section 4. The data interpretations and discussions are presented in section 5. Section 6 presents a conclusion and recommendation of the study.

2. Natural conditions and geological situations

2.1. Natural conditions

Nam Dinh province is located in Red river delta, about 100 km to the south of Hanoi capital. Nam Dinh province has a total area of 1638 km^2 including 10 administrative divisions with approximately two million inhabitants (Nam Dinh statistical yearbook, 2009). The neighbour provinces of Nam Dinh are Ha Nam province at the Northwest, Thai Binh province at the Northeast and Ninh Binh province at the Southwest. The Southeastern boundary of Nam Dinh province is the Eastern Sea (international name is so-called South China Sea), which has a 72 km long coastline with three large estuaries: Ba Lat, Lach Giang and Day (Figure 2.1).

Nam Dinh province has a plain terrain with almost all areas at the altitudes up to 3 m with a gradual slope trend to the Eastern Sea. A small part belonging to Y Yen and Vu Ban districts is a hilly region with altitudes up to 100 m (Nguyen Van Do et al., 1996).

Nam Dinh province has a monsoon tropical climate which can be divided into two main seasons, dry and rainy seasons, according to the precipitation distribution. The rainy season extends from May to September with hot weather and heavy rain. The heavy shower and Southeastern wind, tropical hurricanes and storms are happening in the rainy season with precipitation reaching from 400 mm to more than 1000 mm and average daily temperature from 27 to 29 degree Celsius. The dry season lasts from October to April with cold weather and high humidity. In the dry season, the Northeastern monsoon and drizzling rain are occurring. The precipitation is less than 100 mm, average daily temperature is from 17 to 25 degree Celsius.

In Nam Dinh province, the river system is dense with three large rivers: Red river, Ninh Co river and Day river. The river system is connected by small rivers and canals. The Red river is the largest river in Nam Dinh province. It forms the natural boundary between Nam Dinh and Thai Binh provinces and joins to Eastern Sea at Ba Lach estuary. The width of Red river is about 500 m and the depth is about 15 m. The water level on Red river is clearly changing with the seasons. The highest water level at Phu Hao (Nam Dinh) hydraulic station is 13.2 m (dated 18.08.1969) above sea level and lowest water level is 1.8 m (dated 26.04.1999). Since Nam Dinh province has a plain terrain, the velocity of water flow is low. The saltwater intrusion at the estuary changes with the tides. Saline water intrusion along the river affects about 4.5 km from the estuary inland in flood-tide time and it is around estuary in low tide.

The Ninh Co river is a tributary of Red river. It starts from Xuan Truong district and runs over Hai Hau dictrict. It forms also the natural boundary between Xuan Truong,

Hai Hau and Truc Ninh districts. Ninh Co river has a total length of about 40 km and it joins to the Eastern Sea at Lach Giang estuary. The average statistical water level at Truc Phuong hydraulic station shows that the highest altitude of water level is 2.26 m above sea level and the lowest is -0.41 m below sea level. The boundary between fresh water and saline water is about 5 km from the estuary in flood-tide time and about 2.5 km in low tide (Nguyen Van Do et al., 1996). The Day river is a tributary of Red river. It starts from Hanoi and runs over Ninh Binh and Nam Dinh province. It marks the natural boundary between Nam Dinh and Ninh Binh province. The Dao river is an interior river of Nam Dinh province. It connects the Red and Day rivers.

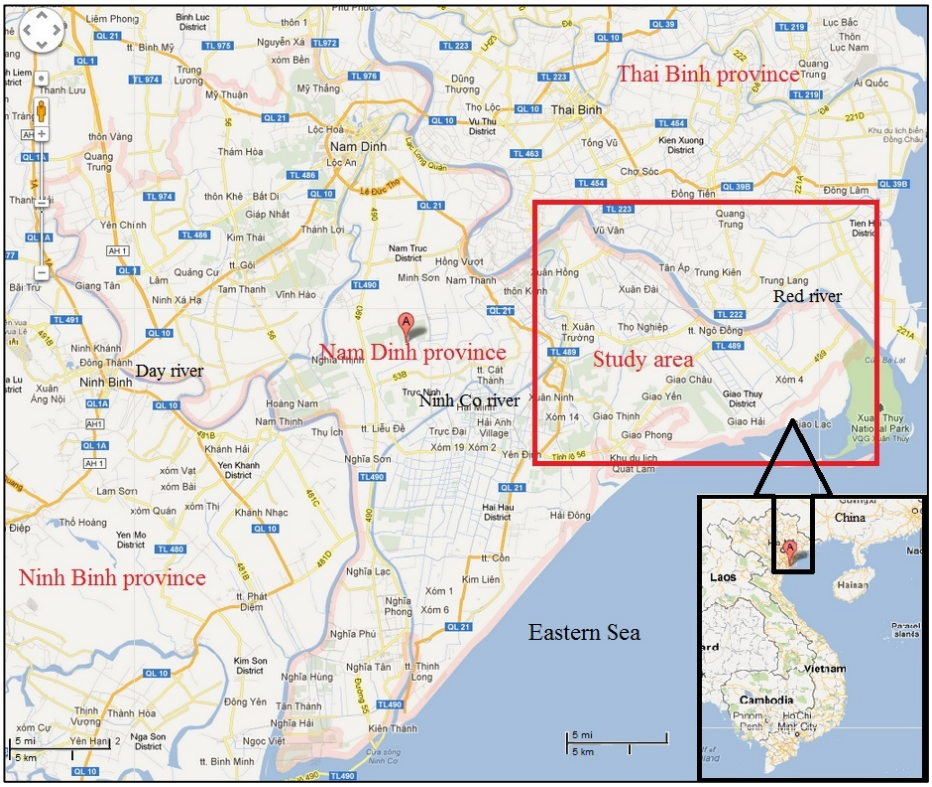

Figure 2.1. Map of Nam Dinh provice (www.maps.google.com).

2.2. Geological characteristics in Nam Dinh province

In the last few decades, there have been many investigations on the geological and hydrogeological situation in Nam Dinh province and adjacent areas. There are two main investigations which are related to the hydrogeological situation in Nam Dinh province. The first research is the project 'Hydrogeological map in Nam Dinh province and adjacent areas in scale 1:50.000' (Nguyen Van Do et al., 1996). In this project, a huge amount of geophysical, geological and hydrogeological measurements

were carried out to form a hydrogeological map of Nam Dinh province and adjacent areas. The second research is 'Estimating the groundwater potentials and proposal the safe exploitation methods for Nam Dinh province' (Doan Van Canh et al., 2004). This project focuses on hydrogeological measurements to improve the hydrogelogical map of Nam Dinh province. A modeling of groundwater movement was performed. Several scenarios of hydrogeological situations were forecasted for different periods.

The available geological and hydrogeological information is very important for my study. In this section of the thesis, I describe the available geological and hydrogeological information which summarizes the two above projects.

Nam Dinh province has geological characteristics of a plain area. Geological sediments are deposited in many geological periods. They have different sources such as marine origin, alluvial marine origin, and marshy marine origin. Stratification of geological structure is described by the sedimentary process and its sources. The description of the stratification follows the geological time scale. To classify lithological components according to grain size of particles, the classifications given in Table 2.1 is used.

Table 2.1. Grain size classification of sediment according to Vietnamese standard, a simplified from Tiab and Donaldson (2004).

Grain size classification	From	To
Clay		< 0.002 mm
Silt	0.002 mm	0.063 mm
Fine Sand	0.063 mm	0.2 mm
Middle Sand	0.2 mm	0.63 mm
Coarse Sand	0.63m	2 mm
Gravel	>2 mm	

Figure 2.2 presents a typical stratification of geological structure in the study area. The interface between two sedimentary layers is not fixed. It is adjustable according to the position of the borehole. Following the classification of sediments, the aquifers are separated. There are four aquifers including the Upper Holocene, Lower Holocene, Pleistocene and Pliocene aquifers (Figure 2.2). In Nam Dinh province, the Upper Holocene and the Pleistocene aquifers are two main aquifers where the groundwater is extracted. Following is the detailed description for each formation corresponding to the aquifers and aquicludes.

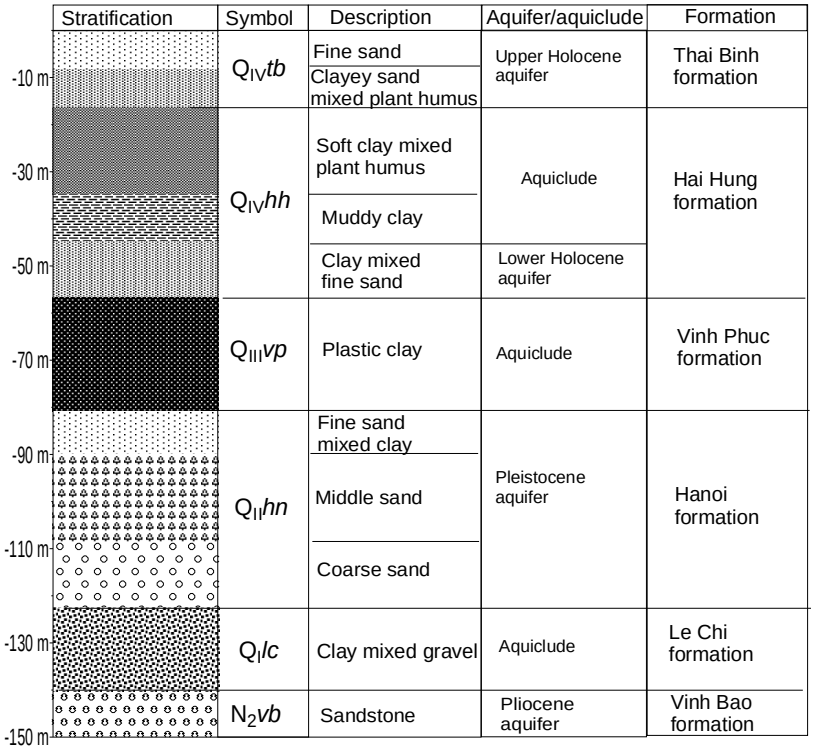

Figure 2.2. A geological profile integrated from stratification of boreholes in Nam Dinh area.

2.2.1. Neocene period - Pliocence epoch – Vinh Bao formation (N_2vb)

The Vinh Bao formation is found in deep boreholes. Vinh Bao formation is distributed widely except the North Western part of Nam Dinh province. The depth and thickness of Vinh Bao formation increases from the interior to the seaside. The lithological components of Vinh Bao formation mainly include sandstone with fine to middle grain size. The Vinh Bao formation is buried at the depth of 149 m (at Hai Son commune Hai Hau district) with 85 m of thickness in the coastal area. The Vinh Bao formation covers directly older rock formations such as Dong Giao formation (Triasic period) and Red river complex.

2.2.2. Quaternary period – Lower Pleistocene epoch – Le Chi formation (Q_Ilc)

The Le Chi formation belongs to Lower Pleistocene epoch, Quaternary period. It is not exposed to the surface. The Le Chi formation sediment distributes in the tectonic-depressed zone. The depth and thickness increase from North-West to South-East. The Le Chi formation's lithologies are mainly including fine sand to coarse sand and pebbles mixed with clay. Le Chi formation found in borehole 30 (at Nam Hong

commune Nam Truc district) at a depth from 136 to 146 m. The Le Chi formation covers the denuded surface of Vinh Bao formation.

2.2.3. Quaternary period – Middle-Upper Pleistocene epoch – Hanoi formation (a, am, $Q_{II-III}^{1}hn$)

The Hanoi formation is not exposed to the surface. It is found in the boreholes except for the central part of lifted block in the North-West of province. Hanoi formation has alluvial origin ($aQ_{II-III}^{1}hn$) and alluvial marine origin ($amQ_{II-III}^{1}hn$).

Hanoi formation, which has alluvial origin, is distributed at the depth from 92 m to 157 m in depressed zone and at the depth from 46 m to 61.5 m in up lift zone. The maximum thickness in coastal area (Hai Hau district) is 55 m. The stratification of borehole 110a at Hai Cuong commune, Hai Hau district shown that Hanoi formation sediments are presented at depth from 62.8 m to 100 m with grain size sorted from fine sand to pebbles. The coarse grained sediments have alluvial origin and belong to Hanoi formation ($aQ_{II-II}^{1}hn$). It is a thick layer and covers directly on Le Chi formation. Hanoi formation is the main water bearing formation of Pleistocene aquifer.

Hanoi formation, which has alluvial marine origin, was found in 20 boreholes in the whole areas of province. It extends from 41 m to 105.7 m with the maximum thickness reaches 42.5 m at Hai Son commune, Hai Hau district (borehole 54). The alluvial marine sediments belonging to Hanoi formation have lithological components including mainly silt and clayey silt.

2.2.4. Quaternary period – Upper Pleistocene epoch – Vinh Phuc formations (a, am, $Q_{III}^{2}vp$)

Vinh Phuc sedimentary formations are found in the boreholes from a depth of 15 m to the depth of 87 m. It is not exposed to the surface. The Vinh Phuc formation can be divided into three types of origins:

- Alluvial origin: $aQ_{III}^{2}vp$
- Alluvial marine origin: $amQ_{III}^{2}vp$
- Marine origin: $mQ_{III}^{2}vp$

The alluvial sediments ($aQ_{III}^{2}vp$) are usually distributed at the bottom of Vinh Phuc formation's cross section. The buried depth ranges from 27 m to 87 m with a thickness from 8 to 30 m. This type of sediment is deposited in alluvial environment with fluvial facies in coastal plains.

The alluvial marine sediments ($amQ_{III}^{2}vp$) are found in almost all boreholes in the area of province. The buried depth depends on the position of borehole. The average thickness is 20 m. The lithological component of this layer includes clay, silty clay, and clayey silt bearing pebbles with diameter up to 3 cm.

The marine sediment ($mQ_{III}^{2}vp$) of Vinh Phuc formation found at a depth from 15 m to 60 m with a thickness ranging from 6.5 to 30 m. The lithological components are clay, silty clay interbeded by grey plant humus. The marine sediment has a weathered surface with motley colour and laterite grit, and iron-oxide clots. The Vinh Phuc formation is an aquitard, which plays an important role for freshwater bearing in Red River Delta.

2.2.5. Quaternary period –Middle Lower Holocene epoch – Hai Hung formation ($Q_{IV}^{1-2}hh$)

The Hai Hung formation is exposed to the surface only in the North-Western part of Nam Dinh province. In other parts of the province, it is found in boreholes at a buried depth from 2 to 57 m. The Hai Hung formation can be divided into two formations, Lower Hai Hung formation and Upper Hai Hung formation, following the palaeo-biological, sedimentary, palaeo-environmental, palaeo-geographical characteristics:

The Lower Hai Hung formation ($Q_{IV}^{1-2}hh_1$) includes sediments which have origin from alluvial marine, marshy marine and marine sediments. The alluvial marine sediment is buried at the depth from 11 to 54 m with a thickness from 4 to 20 m. The lithologic component is silty clay, sometimes interbeded by fine sand lenses. The marshy marine sediment is not exposed to the surface. It is found in the boreholes at a depth from 9 to 49 m with a thickness from 11 to 27.5 m. The lithologic component includes silty clay, silty sand, and clayey silt bearing fine sand. The marine sediment is usually buried at the bottom of Lower Hai Hung formation and it is not exposed to the surface. It is found in borehole from 8.5 to 57 m of depth. Lower Hai Hung formation covers directly the surface of Vinh Phuc formation and it is gradually changing to sediments belonging to Upper Hai Hung formation.

The Upper Hai Hung formation ($mQ_{IV}^{1-2}hh_2$) is distributed in North-Western part of the province. This sediment is found in almost all boreholes from 2 to 44 m depth. The lithologic components are mainly silty clay or silt bearing fine grained sand. The thickness of Upper Hai Hung formation ranges from 3.5 to 25 m.

2.2.6. Quaternary period – Upper Holocene epoch – Thai Binh formation ($Q_{IV}^{3}tb$)

Thai Binh formation is divided into three sub-formations:

- Lower Thai Binh formation (am, mb, $mQ_{IV}^3 tb_1$) is the sediment which was deposited in the period before marine transgression process in Middle Holocene. It includes alluvial marine sediments and marshy marine sediments. The lithological components consist of clayey silt bearing fine grain sand or plant humus. The Lower Thai Binh sediments are not exposed to the surface. It is found in borehole from 5.6 to 8.5 m (alluvial marine sediment) or 5 to 15 m (marshy marine sediment).
- Middle Thai Binh formation (am, $mQ_{IV}^3 tb_2$) is the sediment which was deposited during the marine transgression process. It includes alluvial marine sediments and marine sediments. It is distributed at a depth from 0.0 to 10 m. The lithological component is mainly clayey silt interbeded by plant humus. The Middle Thai Binh formation, which is marine origin, is exposed in the interior parts of the province and it is found at the depth from 2 to 12 m in the coastal areas. The lithological components include fine grained sand, clay, and silty clay bearing shell, shellfish and micaceous operculums.
- Upper Thai Binh formation (m, amb, mv, am, ab, $aQ_{IV}^3 tb_3$) is the recent sediment which was formed following marine transgression process. The youngest sediment is the marine sediment belonging to Upper Thai Binh formation which has been deposited from 1500 years ago to present. It includes the sediments which have marine, eolian marine, alluvial marshy marine, alluvial marine, alluvial marshy and alluvial origins. The lithological component of Upper Thai Binh formation is fine sand bearing silt, which forms sand dunes along coastal zone.

2.3. Tectonic characteristics

Tectonic activity plays an important role to subdivide the geological structures. Fracture zones, which are formed by fault systems, may cause a connection between different aquifers and act as a hydrogeological window. In Nam Dinh province, the saline water in the Pleistocene aquifer originates from fault systems. The knowledge of tectonic characteristics in the study area is useful to understand the saltwater intrusion process.

2.3.1 Fault systems

As shown in Figure 2.3, there are two main fault systems in the area which run in the North Western – South Eastern direction and the South Western – North Eastern direction. The North Western – South Eastern fault system is dominant. It includes Song Chay fault, Red River fault, and Nam Dinh fault. The fault systems play an important role to subdivide the geological structures.

Song Chay fault is the first level Neotectonic fault. It is the boundary between uplifted

zone and depressed zone. The fault is the left transform normal fault in period from Middle Paleogene to Lower Neogene (P_2 - N_1) and the right transform normal fault in Middle Neogene to Quatenary (N_2 – Q). It is an active fault. The depth of fault may reach down to Mohorovicic surface.

Red River fault is the second level Neotectonic fault. It is the boundary between two uplifted zones with different rates. The slope surface of the fault is 72°. The depth of fault reaches from 0.5 km down to 30 km. It is an active fault.

Ninh Binh and Nam Dinh faults are the secondary faults. They are affected by the above faults. They play a role in geotectonic subdivision.

The South Western – North Eastern faults include Xuan Truong fault and Van Ly fault. They are second level faults. They play an important role in subdivision of geotectonic zones. Xuan Truong fault is the boundary between the strongly uplifted zone in Neotectonics on Paleoproterozoic bed rocks and the weakly uplifted zone in Neotectonics on Paleoproterozoic bed rocks. Van Ly fault is running along the coastline of Ninh Binh, Nam Dinh, Thai Binh, and Hai Phong provinces.

2.3.2 Tectonic structures

There are two types of tectonic zones in Nam Dinh province, the uplifted zone and depressed zone. They are divided by the fault system.

A strongly uplifted zone on Palaoproterozoic bed-rocks is located in the area between the Red River fault in the South West, Nam Dinh fault in the North East and Xuan Truong fault in South East. The bed rocks are paleo-metamorphic formations which belong to Song Hong complex (PR_1sh). The paleo-metamorphic rocks are exposed in Vu Ban district and found in Nghia Thai commune, Nghia Hung district (borehole 35 – close to Xuan Truong fault) at a depth of 121 m. This zone is uplifted in Paleogene, Neogene period and weakly depressed in Quaternary period. This uplifted zone can be seen on Figure 2.3.

The uplifted zone in period from Upper Paleogene to Lower Neogene (P_3 – N_1) and depressed in period from Middle Neogene to Quatenary (N_2 – Q) on Paleoproterozoic (PR_1) bed rocks has a width of 60 to 70 km. The uplifted zone is bounded by Nam Dinh fault (South West), Song Chay fault (North East) and Xuan Truong fault (South East).

The weakly uplifted zone in Quaternary period on Proterozoic bed rocks is limited by Red River fault, Song Chay fault, Xuan Truong fault and Van Ly fault including Xuan Truong, Hai Hau, and Truc Ninh districts. The bed rocks are paleometamorphic rocks

of Paleoproterozoic age at a depth of 234 m in Hai Son commune, Hai Hau district (borehole 54).

The depressed zone in Neotectonics is a subsidence zone which covers a small area of Giao Thuy district. The subsidence zone extends to Lo River fault (Thai Binh province). The Vinh Ninh fault divides the depressed zone into the South Western and the North Easten areas with different subsiding rates. The depressed zone belonging to Giao Thuy district is strongly subsiding in period from Upper Paleogene to Neogene (P_3 – N) and weakly uplifting in period from Neogene to Quaternary (N – Q).

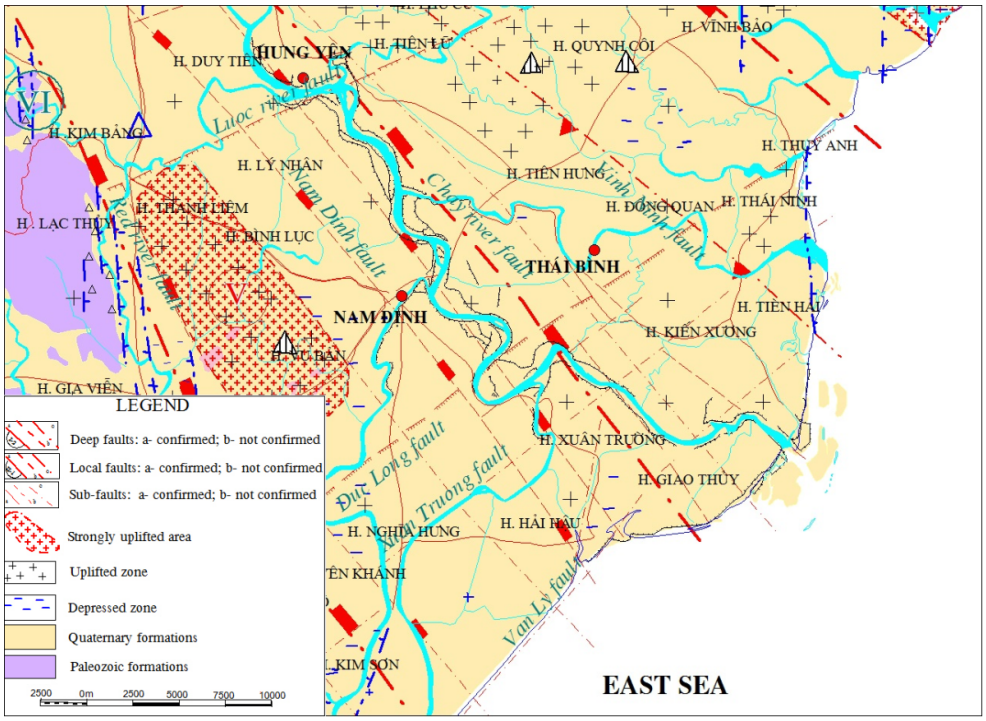

Figure 2.3. The fault system of Red River delta simplified from Tran Van Thang (2009).

2.4. Hydrogeological situation in Nam Dinh province

To estimate the quality of groundwater in Nam Dinh province, Doan Van Canh et al. (2004) divided the groundwater bearing formation into three zones with different Total Dissolved Solids (TDS) content, Iron content (Fe^{++}) and Ammoniac content (NH_4^+) following Vietnamese Standard TCVN 5944 – 1995.

The parameters in Table 2.2 can be used to estimate the type of pollution in groundwater aquifers (both Holocene and Pleistocene aquifers). The hydrogeological situation of an aquifer can be presented in separated parameters such as TDS, Iron

content, ammoniac content. These contaminations come from natural origin. The boundary between fresh and saline groundwater is determined by results of water sample measurements on the wells and water sample analyses. Doan Van Canh et al. (2004) used the TDS values of groundwater samples to map the groundwater situation of the aquifers in three zones of salt contamination.

Table 2.2. Quality of groundwater (Doan Van Canh et al., 2004).

Groundwater quality	TDS	Iron content (Fe^{+2})	Ammoniac content (NH_4^+)
Fresh water	< 1 g/l	< 1 mg/l	< 1 mg/l
Lightly contaminated	1 – 3 g/l	1 – 5 mg/l	1 – 3 mg/l
Strongly polluted	> 3 g/l	> 5 mg/l	> 3 mg/l

In Nam Dinh province, groundwater exists in the water bearing formations including porous groundwater and fractured groundwater aquifers. Following the previous study on geology and hydrogeology, groundwater bearing formations can be divided into four aquifers including Holocene aquifer (qh), Pleistocence aquifer (qp), Pliocene formation aquifer (m_4) and Middle Triassic formation aquifer (t_2) (Nguyen Van Do et al., 1996). Among those aquifers, only two aquifers, the Holocene and the Pleistocene aquifers were explored because they are shallow aquifers. Almost all of the exploiting wells are extracting groundwater from Pleistocene aquifer (Doan Van Canh et al., 2004).

The Pliocene aquifer is located above the Triassic aquifer. It is a fractured groundwater bearing formation. Pliocene aquifer is widely distributed in the whole area of Nam Dinh province. It is not exposed to the surface and it is covered by younger sediments. The groundwater bearing formations are the sediments belonging to Vinh Bao formation (N_2vb). The lithological components are sandstone from fine to middle grain size. The thickness of Pliocene aquifer depends on geological structure and terrain. The thickness of the aquifer is thin in the North and thick in the South Eastern part of the province. The thickness varies in a range from 35 to 85 m. In the coastal area, Pliocene aquifer is layered from 125 to 189 m depth (borehole 54 at Hai Son commune, Hai Hau district). The water table is in the range from 0.6 m to 1.2 m below the ground surface. The boundary between fresh and saline groundwater is not determined exactly. However, the TDS value is 0.58 g/l at the well 54 (Hai Son commune, Hai Hau district) indicating that this area is fresh groundwater area. At the borehole 56 (Giao Thuy district), the TDS value is 16 g/l. It indicates a saline groundwater. The water table of the Pliocene aquifer shows little seasonal variation. This aquifer is not used for water supply, so far.

In the frame of my study, I focus on porous groundwater aquifers including the Holocene and the Pleistocene aquifers. It follows a presentation of the Holocene and the Pleistocene aquifers which based on the results of Nguyen Van Do et al. (1996) and Doan Van Canh et al. (2004).

2.4.1. Holocene aquifer

The Holocene aquifer (qh) is the shallowest aquifer. The Holocene aquifer can be divided into Upper Holocene and Lower Holocene aquifers following lithological components of groundwater bearing formation.

The Upper Holocene aquifer (qh_2) is widely distributed in the province except a small area in the North Western part of the province. The Upper Holocene aquifer is formed by loose sediments including fine sand, silt bearing plant humus which belongs to Thai Binh formation. Groundwater exists and moves in the porous sediments. The thickness of aquifer ranges from 2 m to 28 m. The average thickness is 13 m. The Upper Holocene aquifer is a poor water bearing formation. The results of Total Dissolved Solids (TDS) analyses show that the aquifer contains both fresh and saline groundwater. The TDS value is larger than 1 g/l which indicates groundwater in the Upper Holocene aquifer is brackish or saline groundwater. The water table of groundwater in the Upper Holocene aquifer varies with the seasons between 0.7 m in the rainy season and 1.4 m in the dry season. Based on the results of water sample analyses, Doan Van Canh et al. (2004) constructed a hydrogeological map of the Upper Holocene aquifer according to TDS and Iron content (Figure 2.4). Although the aquifer contains freshwater the water quality is poor.

The Lower Holocene aquifer (qh_1) is covered by the aquifuge of Upper Hai Hung formation ($mQ_{IV}^{1-2}hh_2$). It is not exposed to the surface. This is a confined groundwater aquifer. The components of the aquifer are fine sand and silty sand which have the origin from alluvial marine, marshy marine and marine origin. It belongs to Lower Hai Hung formation ($Q_{IV}^{1-2}hh_1$). The thickness of this aquifer varies from 1.3 to 27.5 m. The water table varies between 0.5 to 3.4 m. The discharge changes from 0.5 l/s to 5 l/s in the water wells. This is a potential groundwater bearing formation. However, the results of water quality analyses from ground water samples have shown that almost all water wells provide brackish water in the area. The TDS value ranges from 1.1 g/l to 30.23 g/l. Almost all groundwater in the Lower Holocene aquifer is saline water. The Lower Holocene aquifer can be divided into two areas following the chemical analyses of groundwater samples:

An area of brackish groundwater is located in the North and the North-Western parts of province. An area of saline groundwater is located in the South East, along coastal

zones of province with the TDS value ranging from 16 g/l to 30 g/l. The Lower Holocene groundwater bearing formation is a potential aquifer but almost all groundwater is brackish or saline water. It cannot be use for water supply and agriculture. This aquifer covers directly the aquifuge of Vinh Phuc formations *(*a, am, Q_{III}^{2}*vp)*.

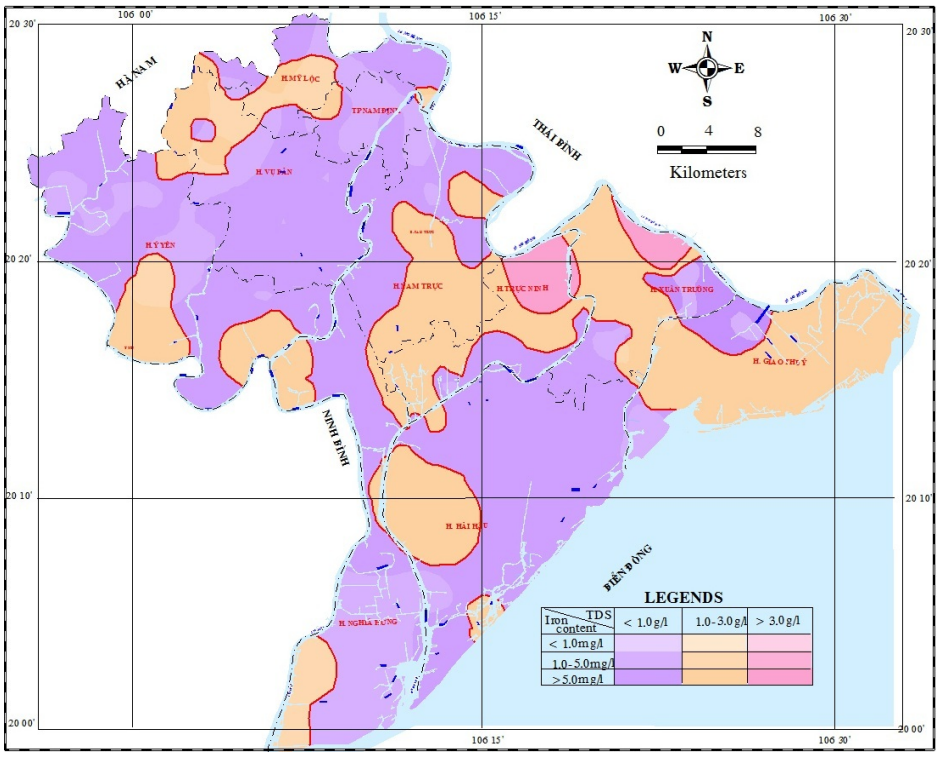

Figure 2.4. Total dissolved solids and iron content distributions of the Upper Holocene aquifer in Nam Dinh province after Doan Van Canh et al. (2004).

2.4.2. Pleistocene aquifer

The Pleistocene aquifer (qp) is widely distributed in the whole province. It is not exposed to the surface. It is covered by Vinh Phuc-formation sediments which are an aquitard. The sediments of the Pleistocene aquifer include the sediments belonging Hanoi formation (Q_{II-III}*hn*). The lithologic components are mainly sand and gravel. The thickness of Pleistocene aquifer ranges from 10 to 78 m. The average thickness is 45 m. The Le Chi formation separates Pleistocene aquifer and Pliocene aquifer as an aquifuge.

The Pleistocene aquifer is a confined aquifer. The water table is located above the top of aquifer from 40 to 60m. There are many water wells in the area which are exploiting groundwater from Pleistocene aquifer. The results of pumping experiments

in the water wells have shown a high potential for groundwater exploitation. Almost all the pumping experiments show a discharge higher than 5 l/s.

The Pleistocene aquifer shows a boundary between fresh and saline groundwater. The Northern part of province provides saline groundwater in the Pleistocene aquifer. It can be recognized that the saline groundwater bearing formation extends to the Eastern part of Nam Dinh province. It extends over the Red River about 5 km. The boundary between fresh and saline groundwater runs parallel to the Red River.

The observation of pumping in a bunch of water wells did not reveal any relationship between hydraulic pressure of Pleistocene aquifer and Holocene aquifers (including qh_1 and qh_2). The tide shows no effect on the groundwater in the Pleistocene aquifer following the monitoring results in groundwater wells. The groundwater table in the Pleistocene aquifer shows only little changes. The differential water table between dry and rainy seasons is about 0.2 - 0.5 m. The chemical composition of groundwater does not show any seasonal variation.

The Holocene aquifer and Pleistocene aquifer are separated by an aquifuge which belongs to Vinh Phuc formation. The aquifuge prevents saline water intrusion from the Holocene aquifer to the Pleistocene aquifer. The water table of Pliocene aquifer is higher than water table of Pleistocene aquifer therefore the water from the Pliocene aquifer (m_4) can be supplied for the Pleistocene aquifer through fractures. At the centre of fresh water area, the Pleistocene aquifer is located in the strongly uplifted zone which is formed by the tectonic fault systems. The fresh water of the Pleistocene aquifer originates from Pliocene aquifer in vertical direction through the fault systems.

The Pleistocene aquifer shows high potential of groundwater. It is widely distributed and of sufficient thickness. The quality of groundwater is good water which can be used for water supply. This is the main aquifer in Nam Dinh province. Almost all exploiting wells extract water from Pleistocene aquifer. The quality of the groundwater mainly depends on the TDS and Iron content, especially for groundwater in coastal areas. Following Vietnamese standards of water supply, the fresh water supply must have TDS value less than 1 g/l and the Iron content less than 1 mg/l (see Table 2.2). Figure 2.5 shows the distribution of TDS content and iron content for the Pleistocene aquifer after Doan Van Canh et al., (2004). It indicates that the South West part of province is containing fresh water with the TDS less than 1 g/l and iron content less than 1 mg/l , the North part of province is containing brackish water with the TDS in range 1-3 g/l and the iron content in range 1-5 mg/l (the yellow colour area), the North East part of province is containing saline water with TSD value above 3 g/l and the iron content value above 5 mg/l.

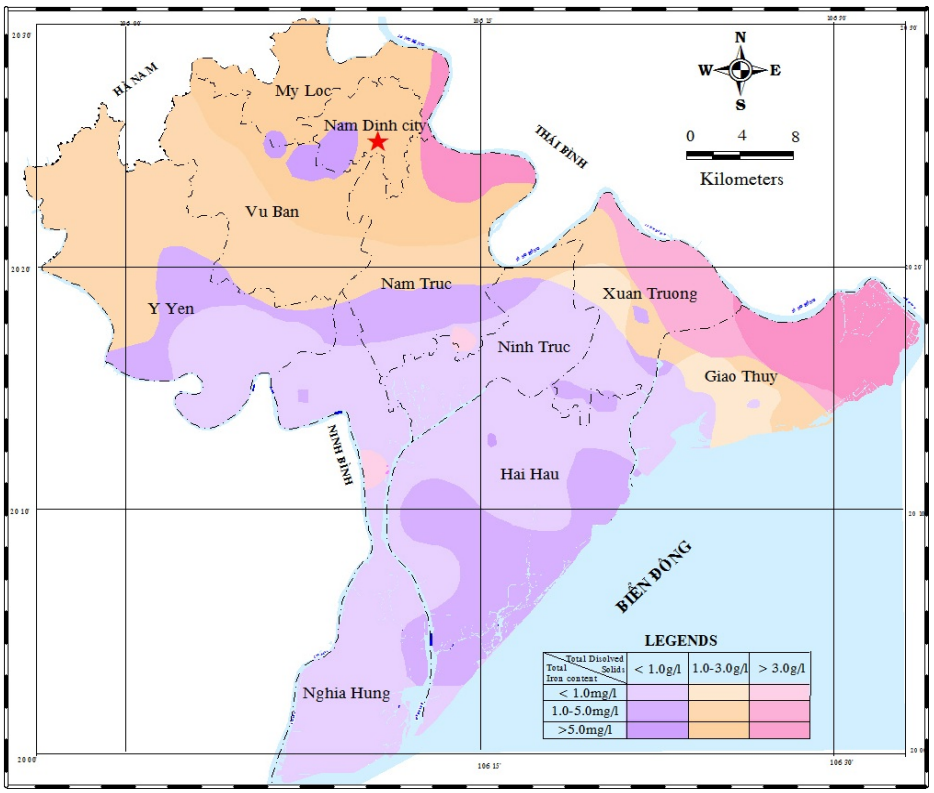

Figure 2.5. Total dissolved solids and iron content distributions of the Pleistocene aquifer in Nam Dinh province after Doan Van Canh et al. (2004).

2.5. Hydrogeological situation in the study area

The study area is located in the Eastern part of Nam Dinh province. It inludes whole areas of Xuan Truong and Giao Thuy districts. In the area, almost all the Holocene aquifer contains saline groundwater. Additionally, the Holocene aquifers represent poor aquifers. The Pleistocene aquifer is the main aquifer in Xuan Truong and Giao Thuy districts. The Pleistocene aquifer includes three zones of ground water: fresh water, brackish water and saline water. This section focuses on the description of the geological and hydrogeological situations of the Pleistocene water bearing formation.

The study area has a flat terrain with an altitude up to 3 m above the sea level. The terrain of area slopes to the sea. The whole area is covered by Thai Binh formation sediments ($Q_{IV}^{3}tb$) which belongs to Upper Holocene aquifer (qh_2). Almost all of aquifer contains saline water. Below Thai Binh formation sediments are Hai Hung formation sediments including alluvial, marine and marshy sediments. The lithological components of Hai Hung formations contain mainly fine sand interbeded clayey lenses. This is the Lower Holocene aquifer (qh_1). It is a confined aquifer. The Lower

Holocene aquifer has a high potential of water and close to the surface. Unfortunately, almost all of aquifer contains brackish water. The TDS value from boreholes show a range from 1.1 g/l to 30 g/l. The Vinh Phuc formation sediments are an aquiclude which separates Lower Holocene and Pleistocene aquifers.

The Pleistocene aquifer is present in the whole area. It is not exposed to the surface. The lithological components of water bearing formation include sand and gravel which belong to Hanoi formation sediments. The Pleistocene is a confined aquifer. The water table is higher than the top of aquifer from 40 to 60 m. It is about 2.5 m below ground surface. Following the boreholes, the depth distribution of Pleistocene aquifer is stable in the whole area. The thickness of aquifer increases from inland to the sea. There are 20 boreholes in the study area including 17 old boreholes and 3 new boreholes. The thicknesses of Pleistocene aquifer are compiled in Table 2.3. Following boreholes, Pleistocene aquifer extends from 54 m of depth (LK1 – Xuan Hong commune, Xuan Truong district) to 140 m (LK7 – Bach Long commune, Giao Thuy district). The average thickness of Pleistocene is about 45 m.

Figure 2.6 shows the TDS distribution of the Pleistocene aquifer in the study area. The contour lines are interpolated from TDS dataset. Following the TDS distribution, the study area can be divided into three zones with different TDS value which corresponding with fresh, brackish and saline water zones:

- Blue area: TDS value lower than 1 g/l – fresh water area
- Green area: TDS value in range 1 – 3 g/l: brackish water area
- Yellow area: TDS value higher than 3 g/l: saline water area

The Pleistocene aquifer is not influenced by the tidal. The water table is 3.4 m below the ground at the well GT-1 (freshwater area) and 2.3 m at the well GT-3 (saline water area). The difference of water table indicates that the saline water intrudes in to fresh water zone of the Pleistocene aquifer.

To determine the geological structure of area, a cross section profile was sketched from the Northwest to the Southeast direction. The stratifications of geological structures are presented in Figure 2.7. The sediments found in the boreholes can be divided in to three layers from surface down to 120 m of depth. The first layer is fine sand which belongs to the Upper Holocene aquifer. The second layer consists of clays which belong to Vinh Phuc formation. It is an aquifuge. The third layer with mainly sand and gravel belongs to Hanoi formation sediments. It is the Pleistocene aquifer. Clay lenses are identified in the LK XV and GT-2 boreholes.

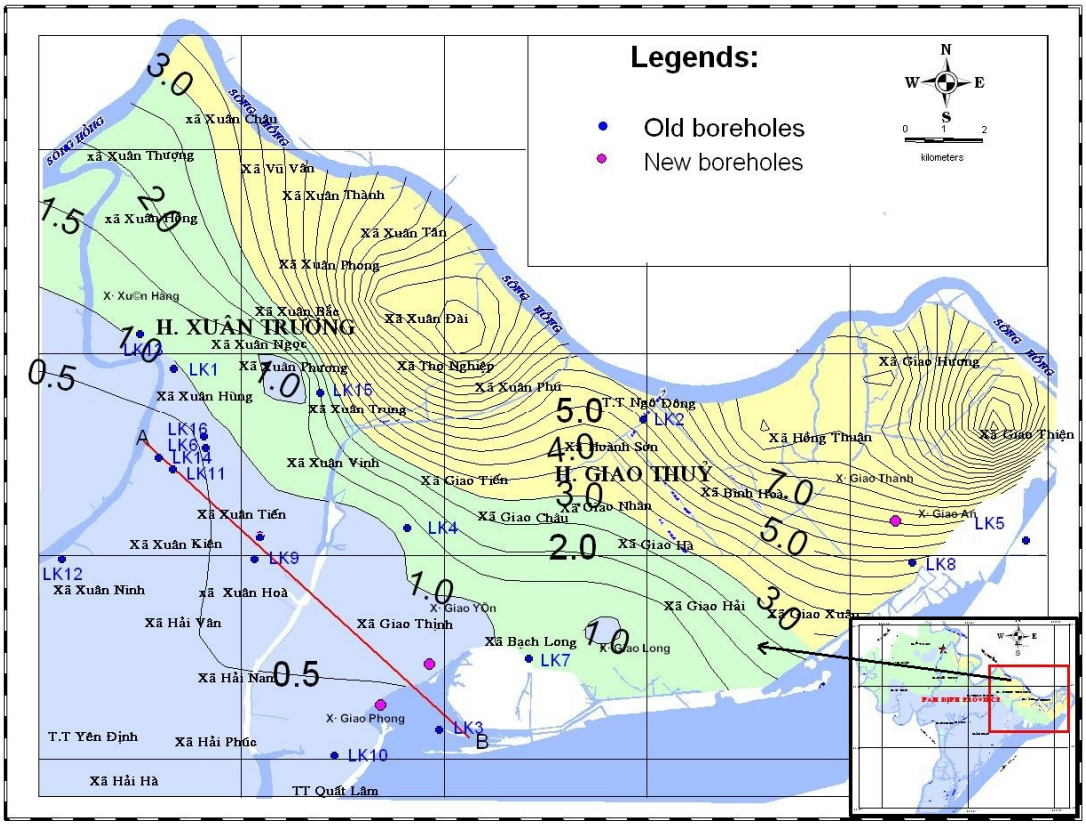

Figure 2.6. Distribution of total dissolved solids the study area after Doan Van Canh et al. (2004).

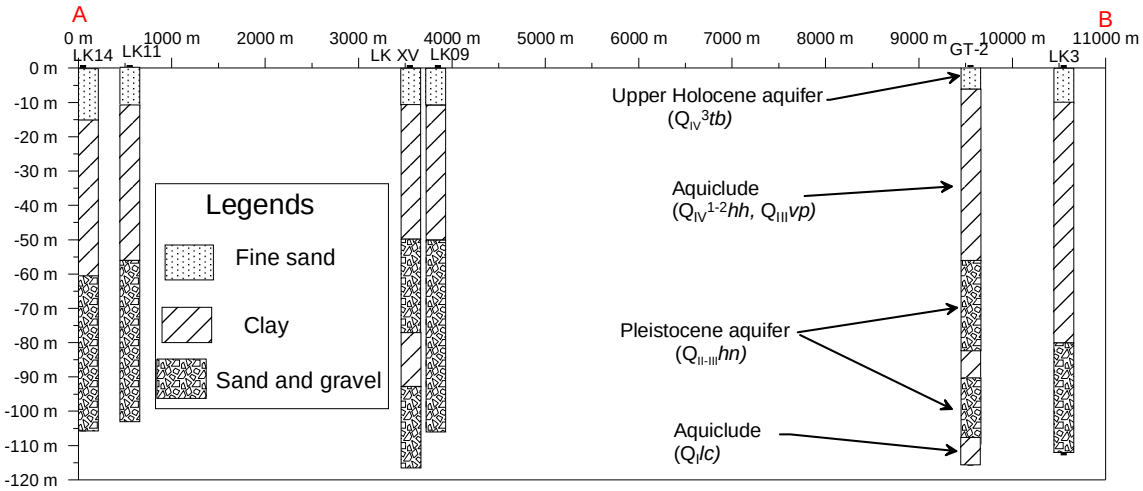

Figure 2.7. The geologic stratification of boreholes along profile AB (see Figure 2.6).

Table 2.3. Thickness statistics for Pleistocene aquifer following boreholes.

Number	Name of borehole	Depth distribution		Thickness
		From (m)	To (m)	
1	LK1	54	105	>51
2	LK2	45	120	>75
3	LK3	80	112	>32
4	LK4	55	130	>75
5	LK5	60	120	>60
6	LK6	50	100	>50
7	LK7	90	140	>50
8	LK8	84	110	>26
9	LK9	50	105	>55
10	LK10	86	114	>28
11	LK11	50	100	>50
12	LK12	84	100	>16
13	LK13	66	80	>14
14	LK14	60	105	>45
15	LK15	65	95	>30
16	LK16	60	100	>40
17	GT-1	81	115	>34
18	GT-2	65	113	48
19	GT-3	56	90	34
20	LK XV	56	110	54

3. Methodology in hydrogeophysical studies

3.1. Geoelectrical methods

Geoelectrical methods are widely used in groundwater explorations and environmental studies, especially for coastal aquifers. The objective of geoelectrical methods is to determine the variation of resistivity in the subsurface. Geoelectrical methods can be used to sketch the geological structure of the underground and to discriminate between freshwater and saltwater.

The geoelectrical methods were described in details in many textbooks (e.g. Keller and Frischknecht, 1970; Kearey and Brooks, 1984; Sheriff, 1989; Sharma, 1997). To estimate the resistivity of ground, an electric current is injected into ground while the resulting potential difference between potential electrodes is measured. Geoelectrical methods require two pairs of electrodes to determine the apparent resistivity of geological structures. A pair of current electrodes (*A* and *B*) is used for current injection into the ground, while another pair of potential electrodes (*M* and *N*) is used for measurements of potential difference. For a homogeneous ground with an arbitrary arrangement of electrodes, resistivity of the ground (ρ_a) can be calculated from the current *I* and the potential difference *U* by

$$\rho_a = K\frac{U}{I}. \tag{3.1}$$

K is called geometric factor (unit: meter) and is calculated from the electrode spacings:

$$K = 2\pi\left[\left(\frac{1}{AM}-\frac{1}{BM}\right)-\left(\frac{1}{AN}-\frac{1}{BN}\right)\right]^{-1}. \tag{3.2}$$

Practically, there is no homogeneous ground media under real geological conditions. The resistivity which is calculated from equations 3.1 and 3.2 is not the true resistivity. It is called apparent resistivity of the ground because the resulting resistivity corresponds to a weighted average integrating over the resistivity distribution in the whole subsurface media. Resistivity surveys can be performed as sounding and mapping.

3.1.1. Vertical electric sounding

Vertical Electric Soundings (VES) are intensively used by geophysicists for evaluation of subsurface to explore groundwater in coastal areas (Nguyen et al., 2009; Nguyen Nhu Trung et al., 2008; Hwang et al., 2003). Geological targets of VES are sediments of different lithologies or layered structures of different properties. The interpretation of VES results in the number of layers, their thickness and resistivity. The depth of penetration of a VES is proportional to the electrode spacing. Varying electrode

separation provides information about the successively deeper stratification of the ground. The VES is based on measuring the potential between one pair of electrodes while transmitting a direct current between another pair of electrodes. From that data the electrical properties of the geologic units can be derived and thereby the geologic properties inferred. The most common VES are using four electrodes in Wenner or Schlumberger configurations. VES soundings are usually applied at approximately horizontally layered earth.

In the case study in Nam Dinh (Vietnam) coastal area, VES measurements are performed to determine the geological structure of aquifers. A Schlumberger configuration is chosen because of practical and methodical advantages. The Schlumberger configuration uses the potential electrodes *M* and *N* closely spaced and fixed to the center of the array and the current electrodes *A* and *B* move outwards. The geometric factor K for a Schlumberger configuration (*AM* = *BN* and *AN* = *BM*) can be inferred from equation 3.2:

$$K_{Schlumberger} = \frac{\pi}{4}\frac{AB^2 - MN^2}{MN}. \qquad (3.3)$$

In my study, the spacing between current electrodes *A* and *B* increases from 4 to 800 m while the spacing between potential electrodes changes from 0.5 to 60 m (Table 3.1).

Table 3.1. Electrode spacings and geometrical factors used for VES.

AB (m)	MN (m)	K factor (m)
4	0.5	24.74
8	0.5	100.14
10	1.0	77.75
14	1.0	153.15
20	2.0	155.51
30	2.0	351.86
40	5.0	247.40
60	5.0	561.56
80	10.0	494.80
100	10.0	777.54
140	10.0	1531.52
200	20.0	1555.09
300	20.0	3518.58
400	40.0	3110.18
600	60.0	4665.27
800	60.0	8330.46

For Schlumberger array, the potential electrode spacing should be much less than the current-electrode spacing (*MN*<<*AB*). The depth of investigation is approximately equal to one-eighth of the current electrode spacing (Beck, 1981; Reynolds, 2005). A problem of VES measurements in coastal areas is the low resistivity of sub-surface. This is a disadvantage because higher currents are needed to generate a measureable voltage signal. To get a reliable data, a high power transmitter was used to inject the DC current into the ground. The transmitter is supplied by an electric generator. The strength of injected currents increases up to 2 A. The ABEM SAS 300C equipment is used to measure the potential between two electrodes M and N. Stainless steel rods are used for current and potential electrodes. The isolated cables connect the current and potential electrodes with the field equipment.

The measurement starts with the smallest potential electrode spacing. Then the spacing of current electrodes increases while the potential electrode spacing remains fixed at the center of array for several readings. The measured voltage between potential electrodes decreases with increasing distance between the current electrodes. Thus, the spacing of potential electrodes must be increased as well in order to guarantee a reliable signal to noise ratio. The measurements are continued and the potential electrode spacing increases again if necessary until the VES is completed. For each arrangement of electrodes, a number of stacking measurements are performed to get a reliable value of resistivity. Almost all VES soundings were measured under good conditions during the field work. It was sunny weather. The electrodes were arranged in a straight line. Some electrodes had to be watered at arid ground positions to improve the contact.

Resistivity sounding provides the apparent resistivity as a function of spacing between the electrodes. Assuming a layered earth, the true resistivity and the thickness of all layers are determined by curve fitting techniques. An inversion algorithm determines a layered model which enables a sufficient fitting between theoretical and measured curves. In the actual application of VES inversion, the result exhibits considerable ambiguity, because the resistivity and layer thicknesses are related to each other (Parasnis, 1986). This phenomenon is called principle of equivalence. It results in different layer models which all fit the sounding curves within a selected fitting error range.

There are two main types of equivalence in VES inversion. If a resistive layer is embedded by two adjacent conductive layers, only the product of layer thickness and layer resistivity, which is called transversal resistance of the embedded layer ($T=h*\rho$), can be properly determined. This case corresponds to so-called T-equivalence. In the other case, here called S-equivalence, a conductive layer is embedded by adjacent resistive layers. The product between conductivity and layer thickness, which is called

longitudinal conductance ($S=h*\sigma$), is properly determined (Seidel and Lange, 2007). A reliable interpretation requires the knowledge on either layer thickness or resistivity. The layer thickness can be adopted from neighboring boreholes. In other case, a reliable estimation on the resistivity of the layer can be derived from logging or samples.

3.1.2. Resistivity imaging

The greatest limitation of one dimensional (1D) sounding is that the assumption of horizontal layering is not fulfilled. VES are restricted to approximately horizontally layered strata. Resistivity profiling measurements are usually applied to map the near surface resistivity distribution. Two dimensional (2D) resistivity imaging is a combination of sounding and profiling in a single process to investigate complicated geological structures with lateral resistivity changes. This combination provides detailed information in both lateral and vertical direction along profile (Ernstson and Kirsch, 2006).

Resistivity Imaging (RI) is also known as Continued Vertical Electrode Sounding (CVES) or Electrical Resistivity Tomography (ERT). RI is particularly useful to determine geological structures of layered aquifers. The method helps to define transitional boundaries which are not easily detectable by other geophysical methods.
Practically, 2D RI investigates the resistivity of geological units with the assumption that the resistivity of the ground varies only in the vertical and the horizontal direction along the profile (Loke, 1999). 2D RI provides a high vertical and lateral resolution along the profile. The data acquisition can be done automatically using computer-driven switching boxes connected with multi-core cables and a large number of electrodes.

Based on the geological structure and their electrical properties, a suitable electrode configuration should be chosen for the 2D RI. The Wenner – Schlumberger array is a common array for resistivity imaging surveys that provides several advantages. Wenner – Schlumberger configuration is actually a combination of the Wenner and Schlumberger arrays adapted for the use of a line of electrodes with a constant spacing. In this array, the spacing between potential electrodes is '*a*'. The distance between current and potential electrodes is '*n*a*'. A Wenner – Schlumberger array becomes a Schlumberger array when the *n* factor is greater than two and becomes the normal Wenner array when the *n* factor is equals to one. The Wenner – Schlumberger configuration has a better horizontal coverage and the maximum depth of penetration of this array is about 15% larger than the Wenner array (Manual of software RES2DINV, 2004). The application of Wenner-Schlumberger array is limited by the

large separation of current electrodes that becomes necessary if a greater depth of penetration is required. The long current cables cause electromagnetic coupling effects and may be considered as a potential problem for the safe operation in the field. Therefore, the inverse Wenner – Schlumberger configuration is a more suitable proposal for 2D RI. In the inverse Wenner – Schlumberger array, the current electrodes are placed close to the center of configuration and the potential electrodes are located symmetrically at a larger distance to the center of configuration. The inverse Wenner – Schlumberger configuration enables the simultaneous measurement the several pairs of potential electrodes. Since the cables to the current electrodes are shorter the operation in the field becomes safer.

In my case study in Nam Dinh province, the inverse Wenner – Schlumberger configuration with three pairs of potential electrodes was used (Figure 3.1). The current electrodes are located in the middle of an array while three pairs of potential electrodes are located outside. The spacing between two current electrodes is '*a*' while the distances between potential electrode and current electrode are *1a, 2a,* and *3a,* respectively.

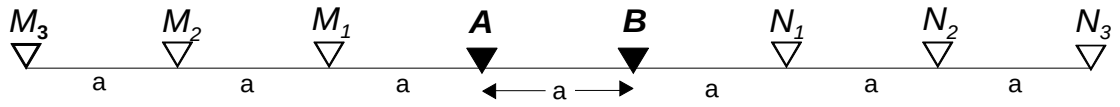

Figure 3.1. The inverse Wenner – Schlumberger configuration with three pairs of potential electrodes M_1 N_1, M_2 N_2, M_3 N_3.

Using the inverse Wenner – Schlumberger configuration with three pairs of potential electrodes, three values of apparent resistivity with different depth of penetration are measured simultaneously. For each current injection, three values of voltages between three pairs of potential electrodes are measured. Three apparent resistivity values are determined by

$$\rho_{a_n} = K_n \frac{U_n}{I} \tag{3.4}$$

with n=1, 2, 3 being the number of the pair of potential electrodes. The geometric factor *K* of inverse Wenner – Schlumberger configuration is determined by equation:

$$K = n\pi(n+1)a. \tag{3.5}$$

The depth of investigation depends on the electrode spacing. Loke (2001) defined a ratio between the median depth 'z_e' of investigation and electrode spacing '*a*'. For Wenner – Schlumberger configuration with *n* = 1, 2 and 3, the ratio between the median depth of investigation and electrode spacing is equal to 0.519, 0.925, and

1.318, respectively. In my case study in Nam Dinh province, 2D RI is carried out with four levels of electrode spacing a = 20, 40, 80 and 160 m. The total length (*L*) of electrode spacing reaches up to 1120 m and the median depth of investigation reaches down to 211 m of depth (see Table 3.2).

Following the geological condition of study area, the objects of studies are the aquifers which are distributed from the surface down to more than two hundred meters. The Scintrex equipment, which was made in Canada, was used to measure the current and voltages between electrodes. The Scintrex system includes two separated units: the transmitter TSQ-3 unit and the receiver IPR-12 unit. The power for TSQ-3 transmitter unit is supplied by a generator that has a power of 3000 W. The IPR-12 receiver unit allows to measure up to eight channels simultaneously. Since the potential signal becomes low, only three channels were measured using the inverse Schlumberger-Wenner configuration. The current intensity increases up to 3 A. Telford (1976) recommended using stainless steel for current electrodes and non-polarizable electrodes for the potential electrodes. In my case study in Nam Dinh province, the current electrode is a bunch of four stainless steel electrodes which are connected together in parallel to reduce the transfer resistance and to improve the contact to the ground. Non-polarizable electrodes, which are porous pots with a copper rod immersed in copper-sulfate solution, are used for the potential electrodes to reduce noise. In the dry ground position, the contact between electrodes and the ground may be improved by watering the electrodes. Isolated cables are used for both current and potential cables. The current cable and the potential cable are separated to each other and the transmitter and receiver instruments are placed at two different sides of profile to reduce the electromagnetic coupling effects. The field measurements starts with the electrodes arranged in inverse Wenner – Schlumberger configuration with an electrode spacing of a=20 m. Three values of resistivity are recorded at each location and the whole array is moved to the next position where the next measurement is carried out. The measurements are continued to the end of profile. The electrode spacing increases to 40 m and the measurement is continued in the back way to other end of profile. Finally, the electrode spacing is increased to 80 m and 160 m. The measured data file is complied as shown in Figure 3.2.

The true resistivity distribution in a 2D vertical section can be obtained by inversion processes. All data set, including twelve data levels, were used for data inversion. Some bad data points were eliminated before the inversion process. In 2D inversion, ambiguity is influenced by several factors such as structure of the grid used to approximate the geological structure, limited data density, errors in the data and sensitivity distribution of the electrode configuration. Generally, the inversion of geoelectrical data represents an ill posed problem, which has not a unique solution.

The principle of equivalence becomes relevant. Additional constraints are necessary to get a solution of the mathematical problem. Considering the selected constraints, the resulting model may be characterized by a smooth model or by models with a high resistivity contrast. The 2D inversion results are evaluated on the basics of Roots Mean Square (RMS) error. Different model (2D resistivity distribution sections) can be obtained if the RMS errors vary within the range of data errors.
Beside the ambiguity of resistivity determination in 2D model, which is related to the uncertainty of the 2D inversion (principle of equivalence of the geoelectrical survey), we encounter another difficulty that is related to the interpretation of the resulting resistivity model. A clay layer may be reflected by the same resistivity like a saltwater bearing sandy layer. This effect results in a principle of equivalence in interpretation of geoelectrical data. The determination of a layer boundary between clay and a saltwater bearing aquifer is impossible. In this case, the interface can be determined by natural gamma log or stratification of borehole.

Table 3.2. Electrode spacing, geometric factor and median depth of investigation (Loke, 2001) for inverse Wenner – Schlumberger array.

a (m)	n	L (m)	K (m)	z_e (m)
20	1	60	125.7	10.4
20	2	100	377.0	18.5
20	3	140	754.0	26.4
40	1	120	251.3	20.8
40	2	200	754.0	37.0
40	3	280	1508.0	52.7
80	1	240	502.7	41.5
80	2	400	1508.0	74.0
80	3	560	3016.0	105.4
160	1	480	1005.3	83.0
160	2	800	3016.0	148.0
160	3	1120	6032.0	210.9

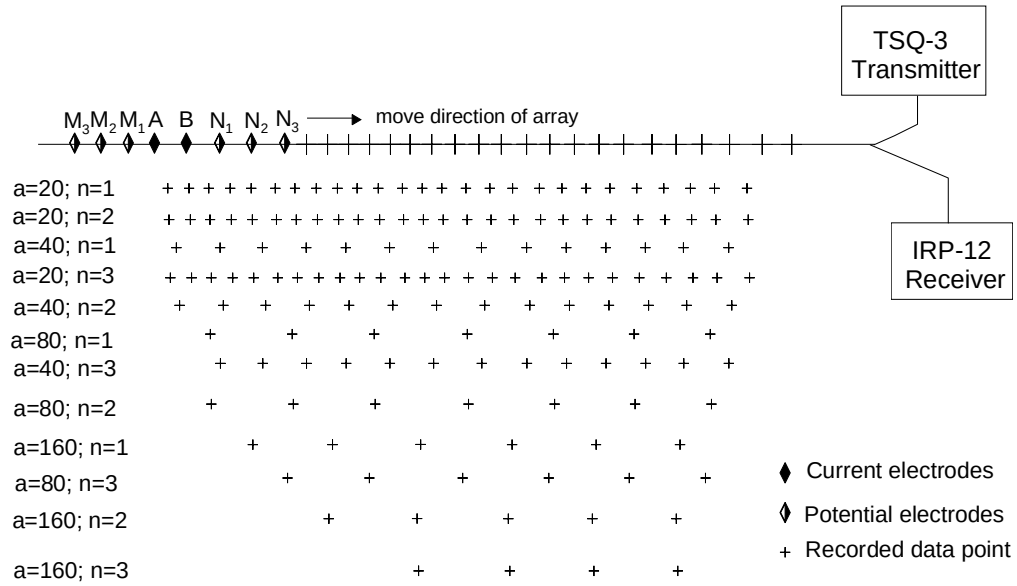

Figure 3.2. Setup for 2D resistivity imaging with inverse Wenner – Schlumberger electrode array.

3.2. Transient electromagnetic method

Conventional geoelectrical techniques have been applied for many years to determine the resistivity distribution of hydrogeological structures. Recently, electromagnetic techniques have been used to investigate the resistivity distribution of geological structures. Time-domain Electromagnetic methods (TDEM) or Transient Electromagnetic methods (TEM) are used to measure the resistivity of subsurface layers. The TEM method has been used in hydrogeological investigations as well as in geological mapping (Rabinovich, 1995; Meju et al., 2000; Land et al., 2004; Spichak, 2007). It was applied for delineating of saline groundwater in the aquifers (Yang, 1999; Kafri, 2005). The TEM method provides more advantages compared with Frequency Electromagnetic method (FEM) or geoelectrical resistivity methods such as deeper investigations, shorter time of measurements, and smaller spacings.

The TEM is based on the induction phenomenon of electromagnetic fields. A varying magnetic field results in a varying electric field which in turn causes another magnetic field. The TEM instrument transmits a direct current though a transmitter loop which is normally located on the ground. The current is abruptly interrupted and the rate of change of the secondary field due to the induced eddy currents in the conductive ground is measured using an induction coil. The primary field is absent while the measurements are carried out. The TEM measures the varying secondary electromagnetic field in time-domain after the transmitter current is shutoff in time

windows which often called gates. The gates are arranged with a logarithmically increasing length in time to improve the signal to noise ratio at late times.

In my case study in Nam Dinh coastal area, the TEM measurements are carried out using TEM-FAST 48 equipment which was developed by AEMR Ltd. company (Netherland). The TEM-FAST 48 instrument generates rectangular pulses of a current which pass though the transmitter loop. Figure 3.3 shows the form of the pulses. The real pulses can be presented as an inertial electrical system with distributed inductance, capacity and resistance. At the moments of switching on and off, the current in the transmitter loop differs from the ideal rectangular sharp (Manual of TEM-FAST 48, 2006). The secondary electromagnetic field decays with time. The TEM FAST 48 measures the secondary field in periods of decay process following the channels or time gates (Figure 3.4).

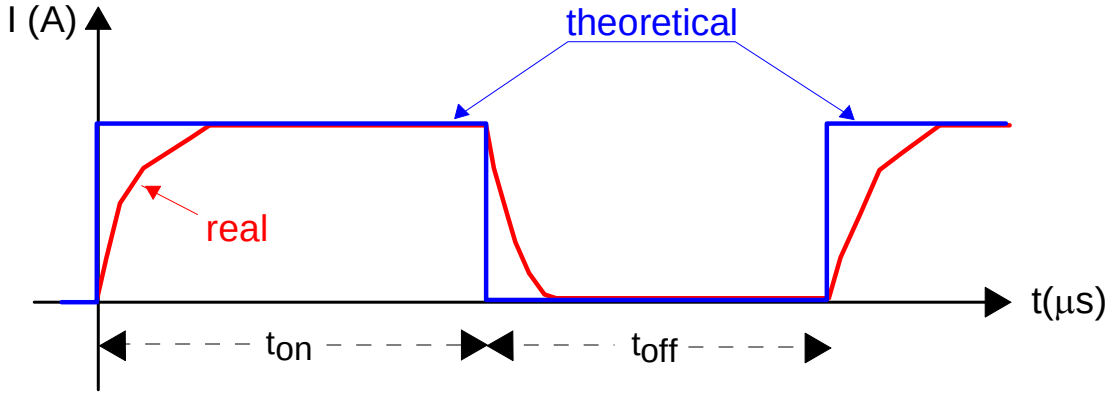

Figure 3.3. The current pulses in TEM-FAST 48 transmitter loop.

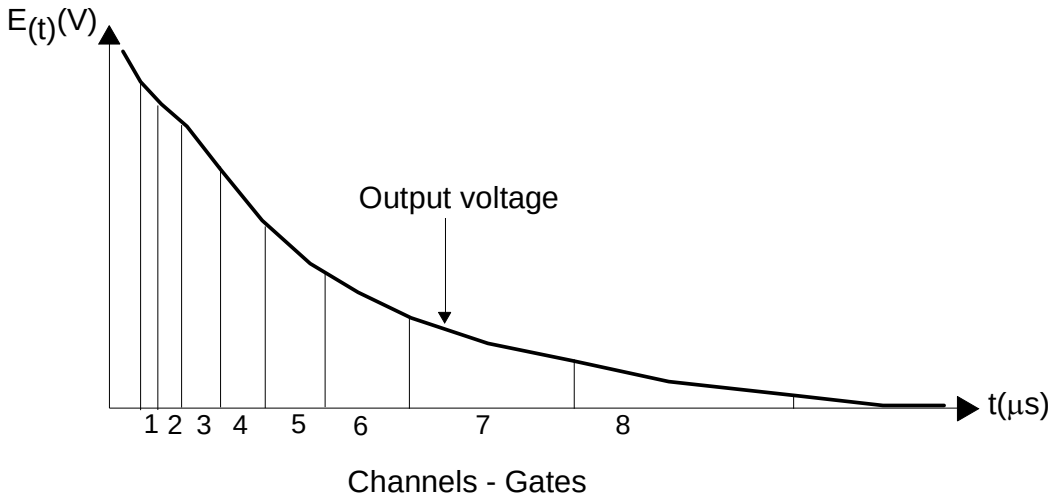

Figure 3.4. The location of channels – gates.

The depth of TEM investigation depends on a lot of parameters such as measured moment after switching off, electrical conductivity and magnetic permeability of the ground. In TEM technique, the term 'diffusion depth' (z) defines the maximum depth which a transient electromagnetic field can reach. This depth can be estimated by

$$z = \sqrt{\frac{2\rho t}{\mu}} \tag{3.6}$$

(Reynolds, 2005).

In the equation (3.6), t is time after switching off in μs, ρ is resistivity Ωm and μ is magnetic permeability of the ground.

In the time domain, the diffusion depth is directly proportional to the square root of time t. The local maximum of the electromagnetic propagates downward with a finite velocity (v). In a conducting half-surface, the downward velocity of the electromagnetic field is given by:

$$v = 2\left(\frac{\pi\mu t}{\rho}\right)^{-1/2}. \tag{3.7}$$

The measurement of a TEM sounding is reliable when the signal to noise ratio is high. When the signal during the decay process reaches the noise level the measurement should be stopped. At the late time, the signal decay is proportional to $t^{-5/2}$ which means that the transition from a good to a very poor measureable signal happens quite suddenly. To get the data at the later stages, Christiansen et al. (2006) suggested two ways: reduce the noise by stacking or increase the moment of transmitter. The maximum depth of investigation can be determined by the time at which the measurements are still reliable.

TEM-FAST 48 provides the possibility to start the process of measurements of decay of the voltage signal beginning from 4 μs (TEM FAST 48 manual, 2006). This parameter determines the minimal time of registration of a signal and minimal depth of investigation in TEM-FAST measurements. TEM FAST 48 includes 48 channels (the time gates) to measure the induced field at 48 intervals of time. Table 3.3 compiles the number of time gates and their intervals of measurements. The parameter t_{center} indicates the center of the time gate. Δt is the length of time window.

In the field, TEM soundings with TEM FAST 48 device use one loop configuration with transmitter and receiver loop coinciding. The transmitter (and receiver) is a square loop with the size 100 x 100 m. An external battery is a requirement for a long working day. A current of 4 A is injected into the transmitter loop. A filter of 50 Hz is applied to reduce the influence of nearby electrical power lines.

Table 3.3. The time gates and the intervals of time for registration input voltage in TEM FAST 48 device.

# time gates	t_{center} (μs)	Δt (μs)	# time gates	t_{center} (μs)	Δt (μs)
1	4.06	1	25	285	64
2	5.07	1	26	350	64
3	6.07	1	27	414	64
4	7.08	1	28	478	64
5	8.52	2	29	570	128
6	10.53	2	30	699	128
7	12.55	2	31	828	128
8	14.56	2	32	956	128
9	17.44	4	33	1152	256
10	21.46	4	34	1408	256
11	25.49	4	35	1664	256
12	29.50	4	36	1920	256
13	35.28	8	37	2304	512
14	43.30	8	38	2816	512
15	51.40	8	39	3328	512
16	59.41	8	40	3840	512
17	71.60	16	41	4608	1024
18	87.60	16	42	5632	1024
19	103.60	16	43	6656	1024
20	119.60	16	44	7680	1024
21	143.60	32	45	9216	2048
22	175.60	32	46	11264	2048
23	207.60	32	47	13312	2048
24	239.60	32	48	15360	2048

TEM results in a resistivity sounding curve *ρ(t)*. The transformation from *E(t)* to *ρ(t)* is made according to asymptotic estimations of signals for late and early stages (TEM FAST 48 manual, 2006). At the late stages of transient ($\frac{t\rho}{\mu_0 R^2} \gg 1$) for a one turn transmitter loop, the transformations are described by the equation:

$$\frac{E(t)}{I} = \frac{1}{20}\frac{\pi^{1/2}\mu_0^{5/2}r^2R^2}{\rho^{3/2}t^{5/2}} \qquad (3.8)$$

where $E(t)$ is the output voltage (in Volt) from the secondary electromagnetic field, I is the current strength (in Ampere) passed thought the transmitter loop, μ_0 is the magnetic permeability in a vacuum, R and r are the equivalent radii of transmitter and receiver antennas ($\pi R^2=L^2$; $\pi r^2=l^2$) and ρ is the resistivity of the ground.

The registered signal is proportional to conductivity $\sigma^{3/2} = 1/\rho^{2/3}$ and to product R^2r^2. Thus, in TEM the amplitude of signals at late stages is rather sensitive to changes in the conductivity of the subsurface. At the early stages of transient for the coincident antennas $R=r$, the transformation does not depend on the resistivity of the ground:

$$\frac{E(t)}{I} = \frac{\mu_0 R}{2t}. \quad (3.9).$$

TEM measurement is very fast using TEM FAST 48 device. It takes only several minutes for one sounding. In the study area, a profile including 20 TEM soundings was carried out along the profile of resistivity imaging. The TEM soundings are located in the rice field in a flat terrain. The location of TEM profile is far away from electrical power lines and radio transmitter stations. TEM measurements were carried out in good condition for field work, i. e. it was sunny weather.

3.3 Electrical conductivity of groundwater

Electrical conductivity (σ) is the ability of a medium to transfer an electric current. The electrical conductivity of water is strongly related to the concentration of ions which are inorganic dissolved solids. The SI unit of conductivity is Siemens per meter (S/m). In practice, the unit milli Siemens per meter (mS/m) is usually used.

The electrical conductivity is measured by determining the conducting of the water between two flat or cylindrical electrodes. A current is passed though two electrodes. The electrical conductivity changes with storage time and temperature. Therefore, the electrical conductivity measurement should be made in the field directly after sampling. Nowadays, almost all electrical conductivity devices automatically compensate the readings at a temperature of 25^0 C.

Because the electrical conductivity is a measure of the ability of water to conduct electrical current, it is directly related to the concentration of salts dissolved in water, and therefore to the TDS. TDS and electrical conductivity are comparable. It is difficult to measure TDS in the field but the electrical conductivity of the water is used as a measure. Electrical conductivity values can be converted to TDS using the following equation:

$$\text{TDS (g/l)} = 0.0067 * \text{EC (mS/m)}. \quad (3.10)$$

Equation (3.10) provides only an estimate. When the salt concentration reaches a certain level, electrical conductivity is no longer directly linearly related to salt concentration. The factor of conversion between TDS and electrical conductivity is normally in the range from 0.005 to 0.009. It depends on the chemical components in the water.

The electrical conductivity is strongly related to the concentration of chloride ions in the water which are dissolved from salts such as sodium chloride (NaCl), potassium chloride (KCl), calcium chloride ($CaCl_2$). Depending on the content of chloride ions, Nguyen Van Do et al., (1996) classified the groundwater as freshwater (<380 mg/l), brackish water (380 – 1420 mg/l) and saline water (>1420 mg/l). The electrical conductivity also depends on the temperature of water samples because the mobility of ions increases with rising temperature. A chloride concentration of 200 mg/l at 18^0 C results in an electrical conductivity of 60 mS/m or a resistivity of 16.6 Ωm (Kirsh, 2006). This is only an estimation of the transformation between concentration of chloride ions and electrical conductivity of the water.

In the field, electrical conductivity of groundwater was measured using the MultiLine P4 device, which was made in Germany. MultiLine P4 records the electrical conductivity with an accuracy of 1% in the temperature range 15^0 C to 35^0 C. Besides the measurement of electrical conductivity, the temperature of ground water samples is measured. The measurements are directly performed in the groundwater wells. The water in the well was pumped out before water sampling to be sure that the static water column in the well is removed and the groundwater sample originates directly from the aquifer. The measurement of water conductivity is directly performed after water sampling. The depth of investigated groundwater samples is also determined to be sure that the groundwater is taken from the relevant aquifer.

3.4. Geophysical well logging

Well logging, also known as borehole logging, performs geophysical measurements in the borehole. The borehole measurements are combined with surface measurements to acquire detailed information on the characteristics of the subsurface geological layers. Well logging can be classified into several kinds of measurements according to the parameters of measurements (Ellis and Singer, 2007). In my case study in Nam Dinh province, well logging is performed in three open boreholes using the Mount Sopris MGX II system. The Mount Sopris MGX II logger provides measurements of natural gamma, electrical resistivity, self potential, and temperature. Parasnis (1986) suggested a speed of the downward (or upward) movement of the tool of 330 m/hour for natural gamma ray survey. In the case of Nam Dinh coastal investigation, the

Mount Sopris MGX II sensor was moved both downward and upward direction with an approximate speed of 300 m/hour. The measurement was carried out every 0.05 m.

3.4.1. Natural gamma ray log

Gamma ray logging records the naturally occurring gamma radiation to characterize the sediments around the borehole. It is usually used in mineral exploration and investigation of water-wells. Different types of rock emit different amounts and different spectra of gamma radiation. In particular, clay shows a very high radioactivity while sand is weakly radioactive. Gamma ray radiation of clay is higher because it commonly contains the potassium isotope ^{40}K. The high cation exchange capacity of clay causes them to adsorb uranium and thorium. The gamma ray tool consists of a gamma ray detector and a preamplifier that is lowered in a borehole by means of a waterproof electrical cable. The number of gamma ray counts per second (cps) is the unit of a gamma ray measurement. A high value of count rates from gamma ray detector indicates a high content of clay fraction in the sediments.

3.4.2. Resistivity log

A resistivity log measures the resistivity of the formation around the borehole. The resistivity of sediments is a fundamental formation property. Resistivity logging can be used to determine porosity and fluid saturation if the formation is fully saturated (Sherriff, 1989).

The conventional resistivity measurement in geophysics can be adapted to borehole logging. The Mount Sopris MGX II system provides the resistivity tools as normal devices which consist of two electrodes *A* and *M*. Similar to conventional resistivity measurement, a DC current is injected into the formation sediment through electrode *A* (electrode *B* placed at a large distance). The potential at electrode *M* is measured (electrode *N* the reference is placed at a large distance then U_N =0). The apparent resistivity can be calculated by equation (3.1) with the geometric factor $K=4\pi\ AM$ for a pole-pole configuration (Daknov and Keller, 1962). The distance between electrode *A* and *M* is called the spacing of the tool. The electrode spacing is direct proportional to the depth of investigation. When the electrode spacing is much larger than the radius of borehole, the measured resistivity becomes asymptotic to the true resistivity of the formation. Otherwise, when electrode spacing is much less than the radius of the borehole, the measured resistivity reflects the resistivity of mud.

The Mount Sopris MGX II system provides normal resistivity tools with electrode spacings equal to 8, 16, 32 and 64 inches. The resistivity of fluid is also measured.

Besides the normal resistivity logs, a self potential log and single point resistance log are also supported by the Mount Sopris MGX II system. The self potential measures the natural voltage between an electrode in the borehole and one at the surface. Due to the bentonite solution is used to stabilize the wall of borehole, the single point resistance log and self potential log are not useful for further interpretation.

3.5. Laboratory investigations.

3.5.1. Sample collection

Besides surface geophysical and well logging measurements, the petrophysical investigation of soil samples, which are collected from the subsurface layers, is carried out to gather detailed information on the aquifers and aquitards. In the study area, three boreholes are drilled to take soil samples and to perform well logging measurements. The depth of boreholes is 115 m. The bottom of the borehole is located in the main Pleistocene aquifer. The drilling work was performed by a drilling rig. The drilling process is controlled by observation of drilling mud and the water supply for drilling process. The depth of soil samples is estimated by the number of drilling rods. To take a sample, the drilling rod is stopped and the water supply for drilling process is closed while the drill probe is pressed by the drill machine to keep the cores in original state. The soil sample, which is cut out from the drilling core, is protected in an enclosed nylon bag. Forty samples are collected from three boreholes in the study area. The petrophysical investigation of soil samples are performed in laboratory at the Institute of Geophysics of Clausthal Universitiy of Technology.
The well logging is performed immediately after the drilling and sampling collection. The borehole is completed as groundwater well after well logging. Finally, a pumping test of the groundwater well is carried out.

3.5.2. Electrical resistivity

Electrical properties of soil samples are investigated by Spectral Induced Polarization (SIP) method. The method of SIP investigates the dispersion of complex electrical conductivity. The electrical conductivity of porous material can be written as a complex number $\sigma^*(\omega)$, given by

$$\sigma^*(\omega)=\sigma'(\omega) + i\omega\sigma''(\omega), \qquad (3.11)$$

where ω is the frequency of the excitation current, $i^2 = -1$, and σ' and σ'' are the measured real and imaginary components of the conductivity, respectively.

The real part of conductivity is related to the electrolytic conductivity in the pore space. The imaginary part originates from polarization phenomena. The conductivity

of sediments can be described by a real electrolytic volume conductivity and a complex interface conductivity. It was shown that the complex interface conductivity is related to specific internal surface S_{por} (Börner et al., 1996; Weller et al., 2010b). The specific internal surface and the formation factor are used in a Kozeny – Carman type equation to estimate the hydraulic conductivity. Weller and Börner (1996) proposed a procedure to use SIP data for a prediction of hydraulic conductivity of fully water saturated sediments.

Measurements of complex conductivity (resistivity) can be performed under field, borehole, and laboratory condition with different resolution scales. In the case study in Nam Dinh province, soil samples, which were taken from boreholes, were investigated in laboratory using a SIP FUCHS system. The SIP FUCHS system records complex conductivity spectra in the frequency range from 3 mHz to 750 Hz. The soil sample is packed in a cylindrical sample holder with a diameter of 40 mm and a length of 75 mm. Two circular electrodes with a distance of 55 mm at the inner surface of the sample holder monitor the potential difference while a sinusoidal current signal of a fixed frequency is passing through the sample (Nguyen Trong Vu et al., 2005). The current electrode is a net-plate of platinum wires. The current electrodes are placed in the tanks filled with water of the similar salinity as the natural groundwater of soil samples. In order to reduce the influence of electromagnetic noise and temperature fluctuations, the sample holders were kept in an incubator at a constant temperature of 20° C. The SIP investigations provide a measurement of resistivity amplitude and phase shift of soil samples at different frequencies.

3.5.3. Water content, porosity and saturation

The water content is the quantity of water contained in the soil sample. There are two types of water content: volumetric water content Θ and gravimetric water content *w*. The volumetric water content is defined by ratio between volume of water and volume of total sample:

$$\theta = \frac{V_w}{V_T}. \tag{3.12}$$

The gravimetric water content is expressed by ratio between mass of water and the dry mass of sample:

$$w = \frac{m_w}{m_{dry}} \tag{3.13}$$

The water content of the soil samples were determined by observing the weight loss during the drying process. Firstly, the samples were dried at room temperature at atmospheric conditions. Later, the drying process was continued in a vacuum oven at a temperature of 35° C.

Because the volume of sample can be determined, the volumetric water content can be determined by equation:

$$\theta = \frac{m_w}{d_w}\frac{1}{V_T}, \quad (3.14)$$

where d_w=1000 kg/m^3 is density of the water, m_w is mass of water and V_T is total volume of sample.

The porosity and the saturation of soil samples can be determined when the volume of water and total volume of soil sample are known. The volume of the air can be derived from the volume of water and total volume of sample. The porosity is calculated by equation

$$\emptyset = \frac{V_w + V_a}{V_T}. \quad (3.15)$$

The saturation factor is determined by

$$S_w = \frac{V_w}{V_w + V_a}. \quad (3.16)$$

where S_w is water saturation of sample, V_a is air volume containing in the sample.

3.5.4. Density

The density of soil sample is defined as its mass per unit volume. The density is the basic parameter of petrophysical properties. The density of soil sediments depends on the mineral content, porosity, pore-filing fluid and the saturation. The soil samples which were collected from the boreholes in the study area were determined in two types of density: raw density d_n and grain density d_k. The raw density is directly determined when the volume and mass of natural sample are known.

The grain density measurements regard only the volume of the solid constituents. The grain density was measured using the ULTRAPYCNOMETER-1000 system (Quantachrome corporation), which is designed to measure the volume of solid objects. The ULTRAPYCNOMETER-1000 is used Helium gas to displace the pore space to determine the volume of dry sample. The Helium has a small atomic dimension that makes it possible to penetrate into pores approaching one Ångstrom (10^{-10} m) in dimension. The Helium has a behavior as ideal gas. In the process of petrophysical investigation, the samples were dried at room temperature then continued at 35^0 C in vacuum oven for several days. The instrument is calibrated before the measurements. The calibration is performed using steel spheres with known volume. The mass of sample was determined because the equipment requires the input mass of sample. The sample is placed in the sample holder and the measurement could

be performed. The output sheet of the instrument includes the total volume of the grains, mass of dry sample and the grain density is printed out.

3.5.5. Specific internal surface

The internal surface may be useful to estimate the permeability or complex interface conductivity of loose sediments. It is an important structural parameter that is strongly related to fluid transport in porous media (Weller and Börner, 1996). The specific internal surface S_m is defined by ratio between the total surface area of porous space and the unit mass of dry sample. The specific internal surface is usually expressed in square meters per gram (m^2/g).

The specific internal surface is determined by the nitrogen adsorption method which applied the BET (Brunauer, Emmett, and Teller) theory. The adsorption isotherm of nitrogen is generally used for surface area measurements of samples. The volume of gas physically adsorbed as a uni-molecular layer is determined by arranging the adsorption parameters in the form of a straight line (Tiab and Donaldson, 2004):

$$\frac{P}{V(P_{N2}-P)} = \frac{1}{V_m C} + \frac{(C-1)P}{V_m C P_{N2}}, \qquad (3.17)$$

where: P is equilibrium vapor pressure

P_{N2} is pressure of saturated nitrogen vapor at the measurement temperature,

V is volume of nitrogen adsorbed at pressure P and the measurement temperature,

V_m is volume of gas required to form a monolayer,

C is dimensionless constant related to the heat of adsorption.

To measure the internal surface with the nitrogen adsorption system, the sample preparation is required. Soil sample is grinded to powder and dried at 35^0C in vacuum oven. The dried sample was determined the mass and placed into the sample cell. The sample cell is evacuated at temperature about 50^0C to degas the air in the pore space of sample. Then the sample cell cools to ambient temperature and connects to the system. The system could be performed the measurements. It may take a long time if the sample has a large internal surface.

3.5.6 Magnetic susceptibility

The magnetic susceptibility is a dimensionless proportionality factor between the magnetization M induced in a sample and the external magnetic field H

$$\kappa = M/H. \qquad (3.18)$$

The mass related susceptibility of soil samples was determined using a Kappabridge KLY-2 (Geofyzika Brno - Agico Inc., 1994). The Kappabridge KLY-2 operates based on measurements of inductivity changes in a coil due to the soil specimen. The soil sample is dried and is determined the mass. A high value of magnetic susceptibility measurement may indicate that the soil sample contains ferromagnetic minerals (Nguyen Trong Vu et al., 2005). This relation indicates an increased iron content in the aquifers.

3.5.7. Grain size classification

Sieve analysis is a simple method of separating particles of soil sample into size fraction. To classify the grain size of soil samples, the sieve analysis is performed using wet sieving method. Only the samples which were taken from the aquifers are chosen to sieve. Before the sieving process, the sample is dissolved in hydrogen peroxide (H_2O_2) to eliminate the organic materials. The clay faction (particles less than 2 μm) was separated from the sample using the Centrifuge machine with a rotation of 1037 circles/minute. The remaining sample was sieved using the mechanical shaker which involves a nested column of sieves with wire mesh screen. The wire mesh screens include different sizes of mesh. During the shaker sieving process, Ammonia (NH_3) solution was sprayed on the sample. The sample was separated according to grain size classification (Tucker, 1988) with diameter of particles up to 63, 125, 200, and 400 μm. After sieving, the sample was dried in the oven at temperature of 50^0 C.

To find the percentage of aggregates passing through each sieve, the mass of sample in each sieve is determined. The percent passing is calculated by:

$$\%\text{passing} = \frac{m_{below}}{m_{total}} \times 100\%, \tag{3.19}$$

where m_{below} is the mass of the aggregates within the sieves below the current sieve,
m_{total} is the total mass of all of the aggregates in the sample.

Grain size distribution curve is constructed from percentage of grain size factions. The curve is used to determine the diameters of particle size which are used to predict the hydraulic conductivity of soil sample. The grain size distribution is related to the hydraulic conductivity of sample, and therefore the aquifer.

3.5.8. Clay mineral identification

The clay fraction which was separated from sieving process was used to determine the types of clay minerals. X-ray diffraction (XRD) was used to identify clay minerals of

heterogeneous samples. X-ray diffraction is an analytical technique which reveals information about the crystallographic structure and chemical composition.

The X-ray diffraction method is based on Bragg' law (Tucker, 1988):

$$n\lambda = 2d\sin\Theta, \tag{3.20}$$

where n is an integer number, λ is the wavelength of the X-rays, d is the lattice spacing in Ångstroms and Θ is the angle of diffraction of the X-ray beam.

By observing the scattered intensity of an X-ray beam striking a sample as a function of incident and scattered angle, polarization, and wavelength (or energy), the *d*-spacing could be calculated. The mineral can be identified.

The clay fraction sample is smeared on a glass pad and dried at room temperature. The samples were measured by X-ray powder diffractometer. The main aim of the XRD measurements was to classify the clay minerals in the samples.

4. Measurements

4.1. Study area and geophysical investigations

In my study, the coastal area is investigated by geophysical and hydrogeological methods focused on salt water intrusion in the coastal aquifers. The area of investigation, which is shown in Figure 4.1, was chosen in the Eastern part of Nam Dinh province. It includes the districts Xuan Truong, Giao Thuy and a part of Hai Hau district. The study area has a length of 25 km and a width of 20 km. Red River, Ninh Co River and Eastern Sea form the natural boundaries of the area of investigation. The study area is confined by coordinates of 106.300^0 to 106.555^0 longitudes and 20.180^0 to 20.377^0 latitudes. The study area contains the transition zone of groundwater in the Pleistocene aquifer. Groundwater of the Pleistocene aquifer changes from freshwater in the South West to saline water in the North East of the study area. The boundary between freshwater and saline water runs parallel to the Red River and perpendicular to the coastline.

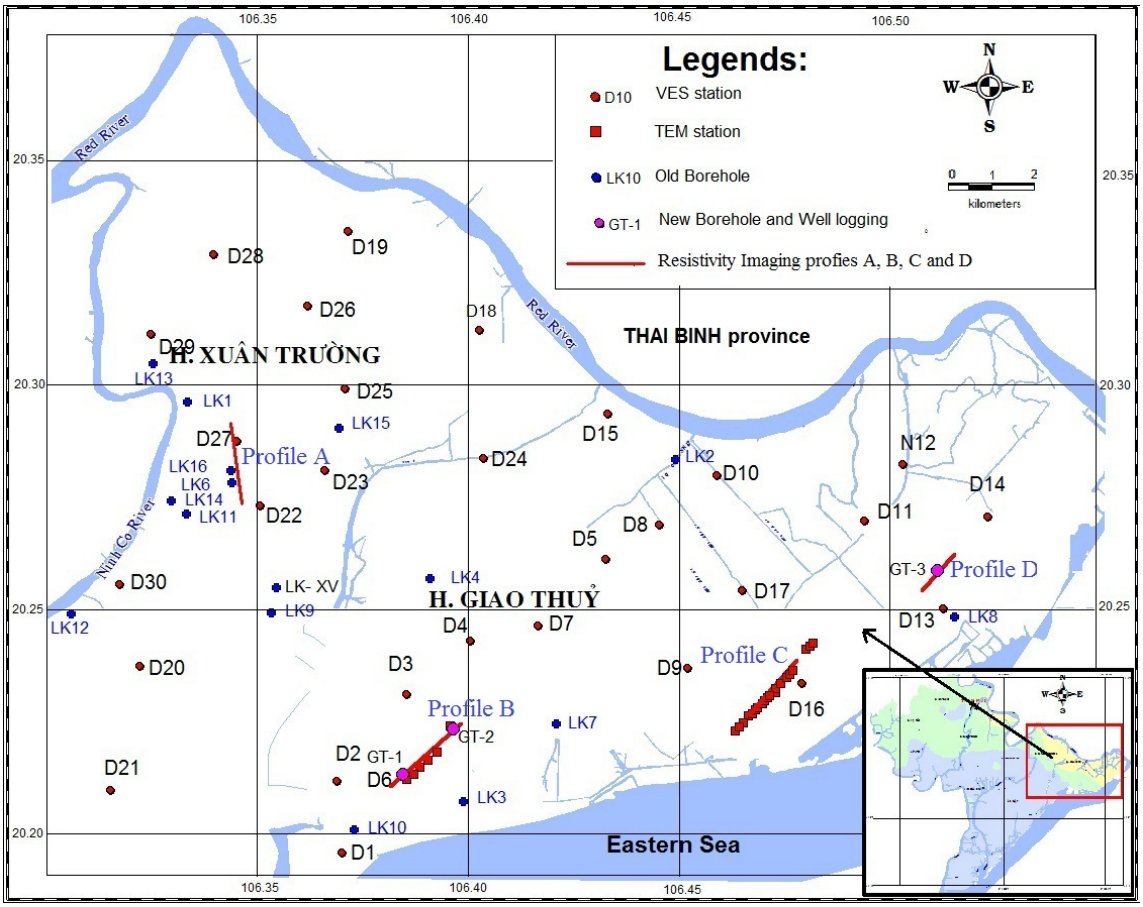

Figure 4.1. Study area and locations of geophysical investigations.

Figure 4.1 shows the area of investigation and the locations of the geophysical surveys. In the study area, geophysical investigation includes 33 VES stations, four profiles of resistivity imaging which are called Profile A, B, C, and D (see Figure 4.1) and 26 TEM stations. Three new boreholes were drilled that reach down to a depth of 115 m. Forty soil samples were taken from the boreholes to be analysed in the laboratory. Approximately 300 m of well logging was carried out after drilling. The boreholes are used as water wells after borehole geophysical measurements. Pumping tests have been performed in three water wells to determine the hydraulic conductivity of the Pleistocene aquifer. The electrical conductivity of water samples was measured at 80 wells which extract groundwater from the Pleistocene aquifer.

4.2. Geophysical investigations

4.2.1. Geoelectrical measurements

Geoelectrical methods, including Vertical Electric Sounding and Resistivity Imaging were used to determine the structure of geological formations in the study area and to delineate the boundary between fresh and saline groundwater in the aquifers. 30 VES have been carried out using Schlumberger configuration with electrodes spacings AB reaching up to 800 m. Generally, the VES are interpreted individually using the free software IPI2Win from Moscow State University. The depth of investigation of VES is estimated to be approximately one eighth of the maximum electrode spacing AB (Roy and Apparao, 1971). The resistivity sounding curves can be grouped into two types: sounding in fresh and saline groundwater area. The stratification of boreholes was used as information on geological structures. VES curves are interpreted using four to six layer models providing resistivity and thickness of each layer. Figure 4.2a shows the VES curve and interpreted result of VES station D6, which is located close to borehole GT-1 (see Figure 4.1). The VES curve D6 was fitted by a four layer model that is compared with the stratification of borehole GT-1. The average difference between the measured and modelled apparent resistivity is 6.5 %. This value is referred to as root mean square (RMS) fitting error of the inversion. The first layer from the surface with 5 Ωm resistivity and 1 m thickness corresponds to the overburden layer. The second layer has a resistivity of 13.5 Ωm and a thickness of 28 m. This layer corresponds to the Holocene aquifer consisting of fine sand and silt. The third layer with 1.8 Ωm resistivity is related to the soft clay layer with a thickness of 52 m. The fourth layer shows a resistivity of 15 Ωm and an infinite thickness. It is related to the Pleistocene aquifer with sand formation bearing fresh groundwater. The resistivity of groundwater sample from water well GT-1 is 8.2 Ωm. This is fresh groundwater.

A typical resistivity sounding curve, which is located in the saline groundwater area, is depicted in Figure 4.2b. The VES D13 is divided into five layers and considers the stratification of borehole GT-3. The first layer is related to the top soil with a resistivity of 2.2 Ωm and a thickness of 1.7 m. The second layer has a very low resistivity, which is related to the saline groundwater of the Holocene aquifer. The third layer is a clay layer. The fourth layer with low resistivity (1.5 Ωm) and a thickness of 42 m corresponds to the sand and gravel layer in boreholes LK8 and GT-3 (the Pleistocene aquifer). The resistivity of groundwater sample from the well GT-3 is 0.68 Ωm indicating that the Pleistocene aquifer contains saline water. This explains why the groundwater bearing sandy layer is characterized by very low resistivity. The deepest layer with a resistivity of 5.2 Ωm belongs to the clay layer mixed with gravels, which is found in the borehole GT-3 at a depth of more than 90 m. The model of VES D13 results in a fitting error of 3.9 %.

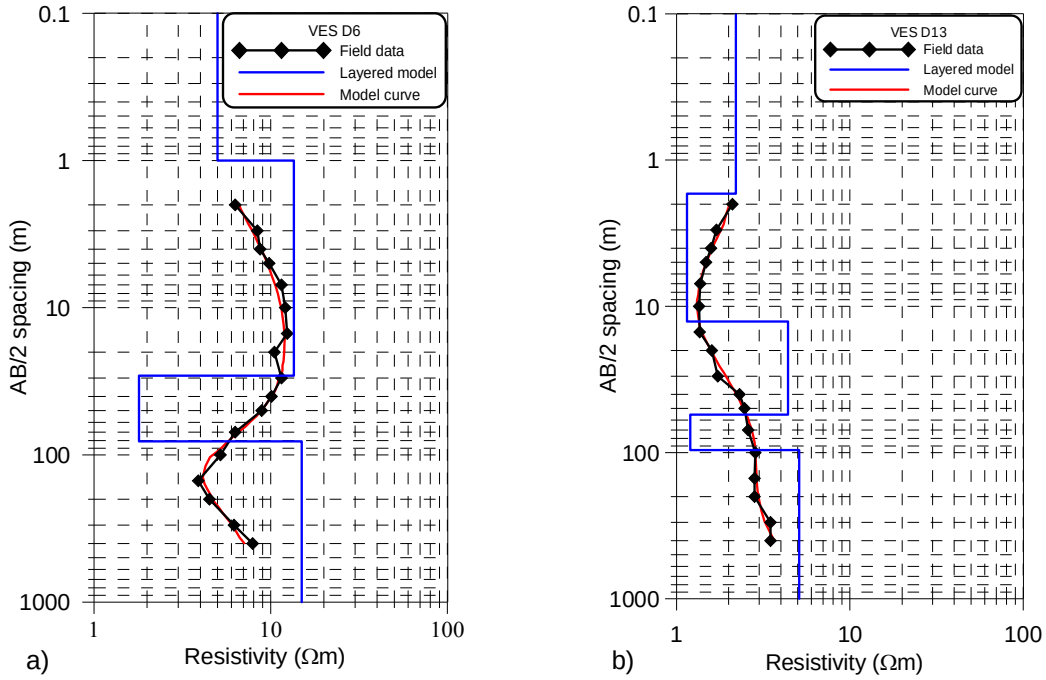

Figure 4.2. Data interpretation of VES: a) VES D6, b) VES D13.

The principle of equivalence in inversion technique is applied to get the best model which reflects the local structure and formation resistivity. Resistivity and thickness of the layered model vary in a certain range for which the RMS error of VES inversion yields a value of less than 10 %. The resulting models are compared with the stratification of boreholes, which are located close to the VES stations. Resistivity of layered models is considered the resistivities of formations which derived from well

logging and laboratory investigation. The best model shows a similar structure of the borehole and the resistivity of layers presents the formation resistivities.
Based on VES results, the geological situation of the study area can be divided into three main layers. The first layer from the surface down to an approximate depth of 30 m is the Holocene formation. The lithologies of the Holocene formations include fine sand or clayey sand. The second layer located below the Holocene formation with an average thickness of about 40 m is characterized by low resistivity. It corresponds to the clay of the Vinh Phuc formation, which is confirmed in the boreholes. The clay layer is identified in the whole area. The third layer corresponds to Hanoi formation belonging to Pleistocene epoch. This layer is covered by Vinh Phuc formation. The lithologies of Pleistocene formation consist of coarse sand and gravel. The resistivity of this layer varies from 1.5 Ωm to 45 Ωm.

At the position of the three new boreholes, three VES are carried out by IPR-12 system using an inverse Schlumberger Wenner configuration. The IPR-12 system provides a higher power and accuracy than SAS 300C equipment, which is used to measure voltage between potential electrodes in the VES investigations. The electrode spacing reaches 1120 m to increase the depth of penetration. Data interpretation is performed regarding the geological structure of the borehole. The inverted results of these VES are in agreement with the local geological structures and hydrogeological situation. At the boreholes GT-1 and GT-2, VES inversion results in a resistivity of 15 and 25 Ωm for the Pleistocene formations, corresponding to a fresh groundwater bearing formation. At the borehole GT-3, the resistivity of the Pleistocene formation is only 1.5 Ωm. This value implies that the Pleistocene aquifer contains saline water.

The results of VES analyses were used to map the distribution of resistivity of the Holocene and the Pleistocene aquifers in the study area. Figure 4.3 shows the distribution of resistivity of the Holocene formation resulting from VES models at a depth of 12 m (AB/2=50 m). In the whole area, almost all resistivity values of the Holocene formation are very low. There is only a small area in which the Holocene formation indicates a resistivity higher than 10 Ωm. Figure 4.3 presents an image of resistivity distribution for the Holocene aquifer. For this regional map, the low density of data affects the interpolated image. In my investigation, the distance between two VES stations is in the range from 1 to 5 kilometres. A large distance between VES stations may cause a distortion of resistivity contours. To get a higher resolution, an increase of data density is required. In VES surveys, the depth of investigation is proportional to the electrode spacing. For the Holocene aquifer, the depth of investigation is 12 m corresponding to an electrode spacing of 100 m. Therefore, the distance between VES stations should be in the range of 200 m.

Figure 4.4 presents the resistivity distribution of the Pleistocene formation at a depth of 90 m corresponding to AB/2= 400 m. In general, the resistivity decreases from the Southwestern part to the Northeastern part. High resistivity is identified in the Southwest of the study area at locations of VES stations D1, D2, D20, D21 and D30. This area corresponds to the fresh water area of the Pleistocene aquifer. The Northern and the Eastern areas show lower resistivity which indicates the brackish and saline water area of the Pleistocene aquifer. The map of resistivity distribution represents the hydrogeological situation of the Pleistocene aquifer. It reflects the subdivision of the Pleistocene in fresh and saline bearing areas. The fresh water area is presented a resistivity of more than 10 Ωm. A resistivity of less than 10 Ωm reflects the brackish and saline water area. The resulting map presents a smooth resistivity distribution for the Pleistocene aquifer. The resistivity contours are less affected by the density of VES station using for interpolation. For the Pleistocene aquifer, the depth of investigation is approximate 100 m corresponding to the spacing AB/2=500 m. That means that the best distance between VES station is less than 1000 m.

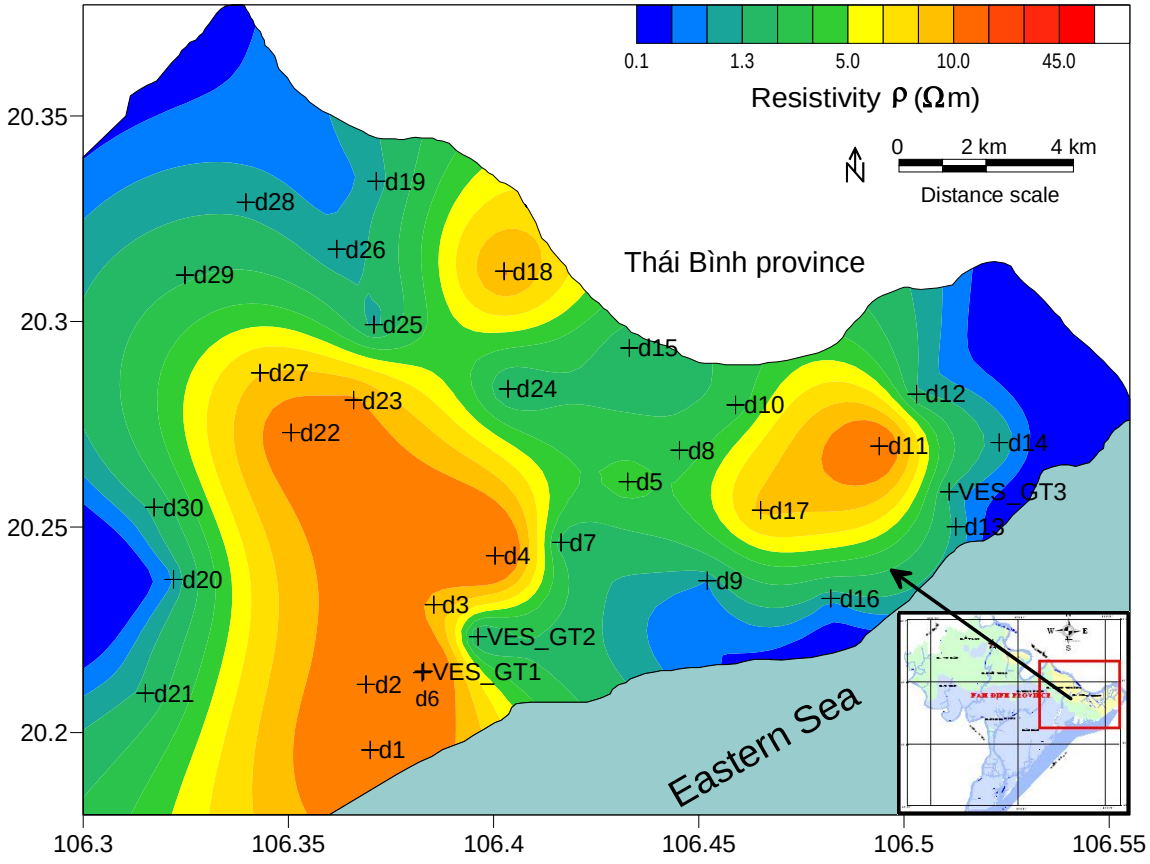

Figure 4.3. Resistivity distribution of Holocene formation at a depth of 12 m derived from VES models.

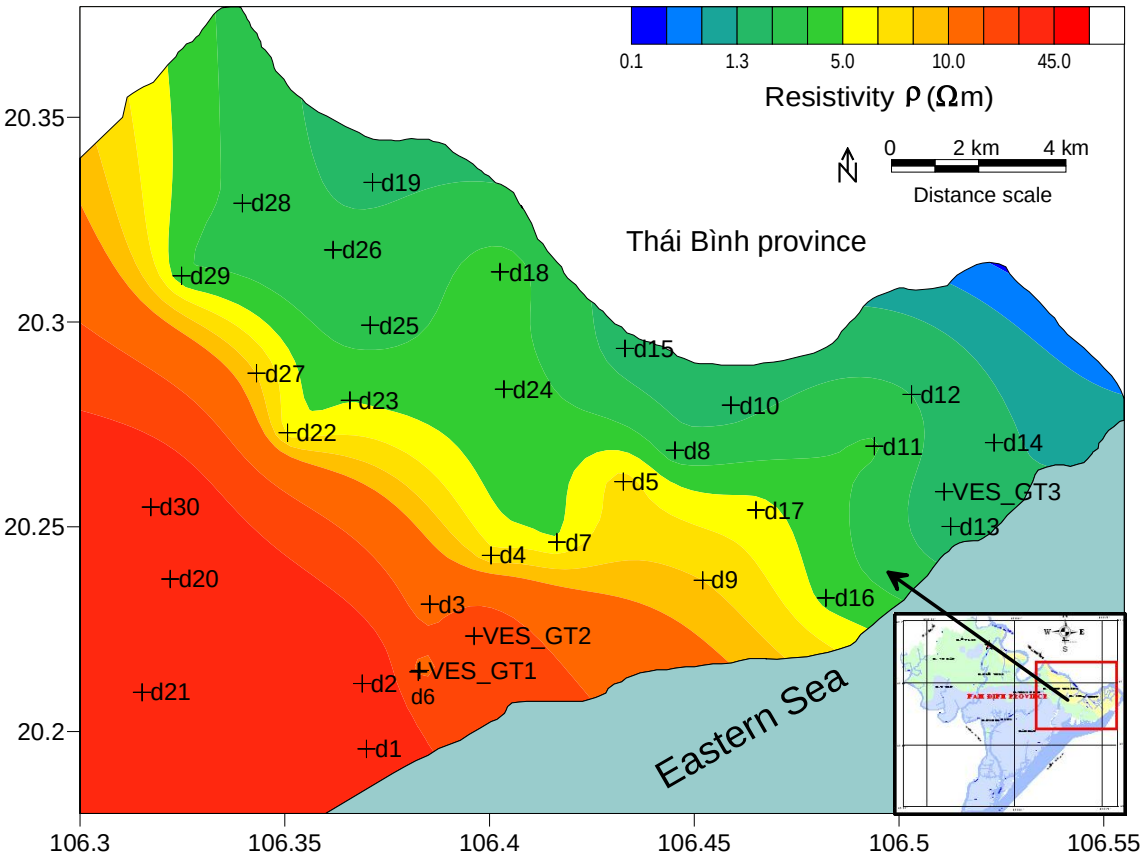

Figure 4.4. Resistivity distribution of Pleistocene formation at a depth of 90 m derived from VES models.

The results of 33 VES stations are compiled in Table 4.1 indicating the depth, thickness and resistivity of Holocene and Pleistocene aquifers. The thickness of the Holocene aquifer varies from 8.5 m to 31.5 m with the resistivity in the range from 0.7 Ωm to 14 Ωm. Almost all VES stations indicate a resistivity of the Holocene formation of less than 5 Ωm. The depth to the top of Pleistocene aquifer varies in the range from 45 m to 82 m. The depth to the bottom of the Pleistocene aquifer is not determined at some VES stations. The resistivity of Pleistocene formation varies from 1.5 Ωm to 45 Ωm. High resistivity of Pleistocene formation implies that the Pleistocene aquifer contains fresh water. Otherwise, low resistivity is related to a saline water bearing formation. The fitting error of the VES models is also compiled in the Table 4.1. It varies in the range from 3 to 11%. A fitting error of less than 5% indicates a reliable fitting quality. High error may be caused by noisy data or in area where the condition of horizontal stratification is violated.

Table 4.1. Resistivity, depth and thickness of Holocene and Pleistocene aquifers derived by VES.

VES ID	Holocene aquifer			Pleistocene aquifer			Fitting error (%)
	Resistivity (Ωm)	Depth to top (m)	Thickness (m)	Resistivity (Ωm)	Depth to top (m)	Thickness (m)	
D1	14	9	22	35	81.5	-	6.7
D2	12	10	20	45	80	-	4.1
D3	9.2	3	20	14	83	-	8.1
D4	16	4.2	11	6.7	68.2	-	8.8
D5	4.5	1.5	14	7	65.5	-	5.8
D6	13.5	1	28	15	81	-	6.5
D7	1.7	1	11.5	5	55	40	7.4
D8	3	3	15	3	51	40	6.1
D9	0.7	2.2	23.3	8	65.5	-	3.9
D10	3	7	7	2	45	48	7.1
D11	14	2	10.5	4	57.5	40	6.3
D12	1.2	2,5	10	2.5	58	39	5.3
D13	1.1	2	12	1.5	54.7	42	3.9
D14	1.1	7.5	9	1.5	51.5	44	5.7
D15	1.6	2	12	1.9	54	40	7.3
D16	0.7	1.6	12	4.6	77	-	10.6
D17	8.5	2.2	11.8	5.5	80.8	-	7.6
D18	10.5	2.2	11	4.5	73.2	-	11.2
D19	0.9	2.5	25.5	2.3	80	-	7.2
D20	0.6	3.5	15	41	78.5	-	6.1
D21	1.5	3	22	40	78	-	5.3
D22	12	3	14	5.5	72.5	-	7.3
D23	10.5	6	25	5	77	-	7.4
D24	1.2	1.6	15	4.5	54.6	41	5.9
D25	0.9	4	8.5	3.5	71.5	-	6.3
D26	0.8	3.5	12	2.8	75.5	-	7.2
D27	8	2	11	8	77	-	4.3
D28	1.1	3.5	20.5	3.6	57	33	6.3
D29	2.3	4	16	4	57.5	37	6.6
D30	1.5	2.2	17	41	78.2	-	6.4
GT-1	17	0	18	15	81	-	8.3
GT-2	0.5	0	7.5	25	65	48	6.9
GT-3	1	0	25	1.5	56	34	5.8

* Note: sign '–' indicates non-determined values.

Following the results of VES survey, the geological structures of the study area can be described. Thickness and depth of geological formations are determined by VES results considering the stratification in the boreholes. VES results provide an overview on the geological and hydraulic situation in the study area. To examine the resistivity distribution of two dimensional geological structures in the study area, four resistivity imaging (RI) profiles have been carried out (see Figure 4.1). A RI profile is located in the Xuan Hung commune (profile A), Xuan Truong district. Three profiles are located in Giao Thuy district belonging to Giao Phong (profile B), Giao Xuan (profile C) and Giao An (profile D) communes. Three RI profiles B, C and D extend from the Southwest to Northeast across the transition zone between fresh and saline water of the Pleistocene aquifer.

The RI investigation has been performed using inverse Schlumberger - Wenner configuration with three potential electrode pairs, simultaneously. The measurements were carried out with electrode spacings of 20, 40, 80, and 160 m. To reduce the noise, non-polarizable is used for potential electrode. The depth of investigation reaches down to approximately 200 m with the maximum electrode spacing of 1120 m. The RI data is inverted using the complete data set considering twelve depth levels.

The RI data were inverted by RES2DINV and DC2DSIRT programs to determine the resistivity distribution of a 2D vertical cross-section along the profiles. The RES2DINV software applies an optimization procedure with a lot of adjustable parameters. The DC2DSIRT program uses the simultaneous iterative reconstruction technique with predetermined parameters. The same data files were used as the input data for both programs to compare the resulting 2D cross-sections of resistivity distribution.

Figure 4.5 shows the resistivity distribution along profile A following the inversion by RES2DINV and DC2DSIRT programs with the same color scale. The section presented in Figure 4.5a is inverted by RES2DINV in three iterations with a resulting root mean squares (RMS) error of 7.7 %. It shows higher contrasts in the resistivity distribution compared with the section in Figure 4.5b, which is inverted by DC2DSIRT and represents a smoother image. Though the resistivity values are slightly different between two cross sections, both sections reveal a layered structure. The first layer, from the surface to the depth of 60 m, is characterized by low resistivity of around 1-5 Ωm corresponding to Holocene formations and clay sediments. The deeper layer reaches down to 150 m with resistivity in the range from 5 to 20 Ωm corresponding to Pleistocene formations. The RI result can be compared with geological units of the borehole LK16, which is located in a distance of 200 m from the profile A (at position 900 m of profile). Following the stratification of

borehole LK16, the first layer from the surface to a depth of 15 m consists of fine sand. This is the Holocene aquifer. It shows a resistivity of less than 2 Ωm in the geoelectrical section indicating that the Holocene aquifer contains saline water. The second layer is a clay layer which extends from 15 to 60 m of depth. The third layer extending from 60 m to 100 m of depth consists of sandy formations of the Pleistocene Hanoi formation ($Q_{II-III}^{1}hn$). A thin layer of clay sediments becomes evident in the borehole stratification at a depth of 80 m but it cannot be resolved by the resistivity cross section.

The 2D cross section of RI delineates the geological structure along profile A. The resistivity values are a little bit higher at the Southern part than at the Northern part of profile (Figure 4.5a). The conductivity of groundwater at the well LK16 is 198 mS/m and corresponds to a concentration of TDS=1.13 g/l. The Pleistocene aquifer contains brackish groundwater at this position. The conductivity of groundwater sample at the domestic well (position 300 m of profile) is 152 mS/m (TDS=1.02 g/l) while the conductivity of groundwater well at position 1500 m of profile is 302 mS/m (TDS=2.02 g/l). The difference of resistivity between the Southern and Northern parts of the profile is related to the changes of groundwater conductivity. A higher formation resistivity corresponds to a lower conductivity of groundwater.

Along profile A, a low resistivity anomaly can be identified at position of 450 m. The Pleistocene formation seems to be interrupted at this section. The low resistivity anomaly is related to a fracture zone where a connection between the Holocene and the Pleistocene aquifers may exist. The low resistivity anomaly may reflect a local fracture which is located between Nam Dinh and Chay river faults (see Figure 2.3 in the section 2). The width of the fracture zone is around 300 m. This fault has been mentioned in previous publication (Nguyen Trong Vu et. al., 2009).

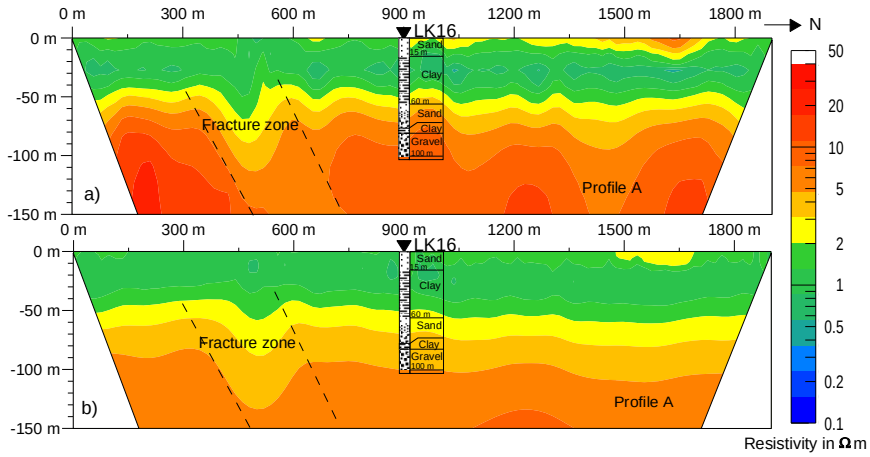

Figure 4.5. Resistivity distribution along the profile A (Xuan Hung commune):
a) Inversion by RES2DINV b) Inversion by DC2DSIRT.

The other profiles of the RI survey have been carried out along the coastline of Giao Thuy district. The RI profiles are parallel and close to the coastline. Because three RI profiles B, C, and D are located at different positions along the transition zone between fresh and saline water in the Pleistocene aquifer, the 2D cross sections of resistivity distribution are suitably displayed in one figure. It helps to compare the variation of resistivity with the changes of groundwater conductivity (Figure 4.6). The inversion process is performed by RES2DINV in three iterations with the RMS around 10 % for three profiles. The resistivity distribution of three profiles is compiled in the same horizontal and vertical scale and using a uniform colour scale of resistivity.

Figure 4.6a shows a cross section of resistivity distribution along profile B which is located in Giao Phong commune, Giao Thuy district. The RI profile B has a total length of 2350 m. It is located in the fresh groundwater area of the Pleistocene aquifer. The resistivity distribution along profile shows a layered structure. The cross section can be divided into two parts with different resistivity distribution. The Southwestern part of profile from the beginning to position of 1000 m shows a structure of three layers. A low resistivity layer is identified between two layers of high resistivity. The top layer with high resistivity is related to a sandy layer bearing fresh groundwater in the Holocene aquifer. The Pleistocene aquifer is found at approximately 90 m depth in the layer of high resistivity. The Northeastern part of profile from position of 1000 m to the end of profile reflects two layers. The top layer shows low resistivity from the surface down to a depth of 50 m. This layer is related to the Holocene formations and the clay sediments. The low resistivity of Holocene aquifer indicates that the aquifer contains saline groundwater. The layer below shows high resistivity. This layer is related to the Pleistocene aquifer.

To confirm the geological structure and the RI result along the profile B, two boreholes were drilled at the profile. The borehole GT-1 is located at position of 450 m and the borehole GT-2 is located at position of 2100 m. The stratifications of boreholes were also indicated in the resistivity image. The stratification in the two boreholes shows a good agreement with the resistivity structures. At the position of 450 m, the borehole GT-1 includes three main layers. The top layer consists of fine sand. It extends from the top down to a depth of 18 m. This layer is the Holocene aquifer corresponding to the high resistivity layer in the RI section. The clay layer is found from 18 m to 81 m of depth. The clay sediments belong to Vinh Phuc formation ($Q_{III}^{2}vp$). It is displayed as a low resistivity layer in the RI section. The Hanoi formation is found at a depth from 81 to 115 m with sand and gravel. This layer is the Pleistocene aquifer and corresponds to the deepest layer in the geoelectrical section. A high resistivity in the RI section implies that the Pleistocene aquifer contains fresh

water. The resistivity of the RI section at GT-1 position is higher than 10 Ωm for the Pleistocene aquifer. The electrical conductivity of the water at the well GT-1 shows a value of 122 mS/m (resistivity of 8.2 Ωm). It corresponds to a TDS concentration of 0.82 g/l.

Located at the position of around 2100 m of profile, the borehole GT-2 shows a slightly different structure. The fine sand layer extends from the surface down to a depth of 7.5 m. This layer corresponds to the top layer in the resistivity section with a resistivity of less than 2 Ωm. The low resistivity of the formation implies that the Holocene aquifer contains saline water or high clay content. A clay layer is identified from 7.5 to 65 m of depth. This layer belongs to Vinh Phuc formation ($Q_{III}^{2}vp$). It is an aquifuge. It plays an important role to prevent saline water intrusion into the Pleistocene aquifer. The Hanoi formation is found at a depth from 65 m to 82 m and 92 m to 113 m. It corresponds to the high resistivity layer in the RI section. The resistivity of this layer is around 20 Ωm. The water sample of the Pleistocene aquifer at depth of 110 m (well GT-2) shows an electrical conductivity of 91 mS/m (resistivity of 11 Ωm), corresponding to a TDS concentration of 0.6 g/l. A clay layer is identified at a depth from 82 to 92 m. This clay layer was not found in the borehole GT-1. It may be a local lens of clay. At a depth from 113 to 115 m, plastic clay is mixed with gravel. This sediment belongs to the Le Chi formation (Q_1lc).

A fault has been identified at the position around 1000 m. The Southwestern part of profile may be regarded as a depressed zone and the other part of profile as an up lifted zone. A fracture zone separates the two sequences of geological structures.

The profile C (Giao Xuan commune) with a total length of 1680 m is located in the brackish groundwater area of the Pleistocene aquifer. The resistivity section shows a layered structure (Figure 4.6b). The top layer has a low resistivity extending from the surface to a depth of approximately 60 m. This layer reflects the resistivity of the Holocene aquifer and a clay layer (aquiclude) with a resistivity of less than 2 Ωm. A low resistivity water bearing formation means that the Holocene aquifer contains saline water. The deepest layer presents higher resistivity, but it is less than 10 Ωm. The depth to top of the layer is slightly increased at the Southwestern part of the profile. This layer is related to Pleistocene aquifer. The resistivity gradually decreases along the profile. The resistivity at the Southwestern part of profile is higher than that at the Northeastern part. The electrical conductivity measurements confirm that the salt concentration of groundwater increases along the RI profile C. Figure 4.7 presents the results of the electrical conductivity measurements of groundwater at the depth of 110 m in wells along the RI profile C. The water wells are not exactly located on the profile, but they are close to profile with a distance of less than 100 m. The TDS

values were inferred from the electrical conductivity following equation (3.10). The TDS value of groundwater is indicated for every well. The water well at position of 350 m shows an EC of 232 mS/m (4.31 Ωm) corresponding to a TDS of 1.55 g/l. It is brackish water. At this position, the RI investigation shows a resistivity of around 10 Ωm for the Pleistocene formations. The measurement of EC at position of 1450 m presents a value of 612 mS/m (1.63 Ωm) corresponding to a TDS of 3.36 g/l. It is related to the resistivity of formation of less than 5 Ωm in the geoelectrical section. The Pleistocene aquifer at the Northeastern part of profile contains saline water with a TDS value higher than 3 g/l.

The resistivity is gradually changing from the Southwestern to the Northeastern part of the profile caused by decreasing resistivity of the Pleistocene groundwater. The resistivity at the Southwestern part of profile is higher than 5 Ωm and the Pleistocene aquifer contains brackish groundwater. The Northeastern part of profile shows a resistivity of less than 5 Ωm and the Pleistocene aquifer contains saline groundwater. This implies that the transition zone from brackish to saline groundwater of the Pleistocene aquifer is located in middle of the profile. Based on the resistivity section, the boundary between brackish and saline groundwater is identified at position around 900 m of profile. The variation of water salinity causes the changes of resistivity along the profile. Compared with the resistivity of the Pleistocene aquifer at the RI profile B, the resistivity of the Pleistocene formation at profile C is lower. It indicates that the groundwater of Pleistocene aquifer changes from fresh water at the position of profile B (Giao Phong commune) to brackish water at the position of profile C (Giao Xuan commune).

The RI profile D is located at Giao An commune, Giao Thuy district. The distance between profiles C and D is about 4 km (Figure 4.1). The profile D has a total length of 1250 m. It is located in the saline groundwater area of the Pleistocene aquifer. Figure 4.6c shows the resistivity cross section along profile D. The RI section presents a very low resistivity of formation along the whole profile. The resistivity of Holocene and Pleistocene aquifer does not exceed 5 Ωm. The resistivity section does not show any layered structure. The resistivity of all formations from the surface down to a depth of 150 m is very low. The resistivity value of sandy and clayey formations is approximately equal to each other. Therefore, the geoelectrical section shows a homogeneous distribution of resistivity from the surface down to a depth of 150 m. To reveal the geological structure along profile, the borehole GT-3 is drilled at position of 600 m. The borehole GT-3 indicates a layered structure of sediments (Figure 4.6c). The top layer from surface down to a depth of 13 m consists of fine sand. This sediment belongs to Thai Binh formation ($Q_{IV}^{3}tb_1$). The sandy formation bearing groundwater shows a very low resistivity indicating that the Holocene aquifer contains

saline groundwater. The second layer is composed of clay sediments with a thickness of 43 m (from 13 to 56 m of depth). The clays belong to Vinh Phuc formation. The Hanoi formation ($Q_{II-III}^{1}hn$) is found from 56 to 90 m of depth. The lithological components of Hanoi formation consist of coarse sand and gravel. These sediments belong to Pleistocene aquifer. A very low resistivity of sand and gravel implies that the Pleistocene formation contains saline groundwater. The water sample, which is extracted from a depth of 90 m (GT-3 well), shows a very high conductivity with 1482 mS/m (0.67 Ωm) corresponding to a TDS of 9.9 g/l. The groundwater of the Pleistocene aquifer at GT-3 well shows a very high salt concentration. The resistivity distribution along the profile is in agreement with that of a salt water bearing sandy formation. Clay mixed with gravel is found from 90 to 115 m. This sediment belongs to Le Chi formation (Q_1lc). It shows a low resistivity in the geoelectrical section. Based on the resistivity distribution along profile D, it can be concluded that both Holocene and Pleistocene aquifers contain saline water.

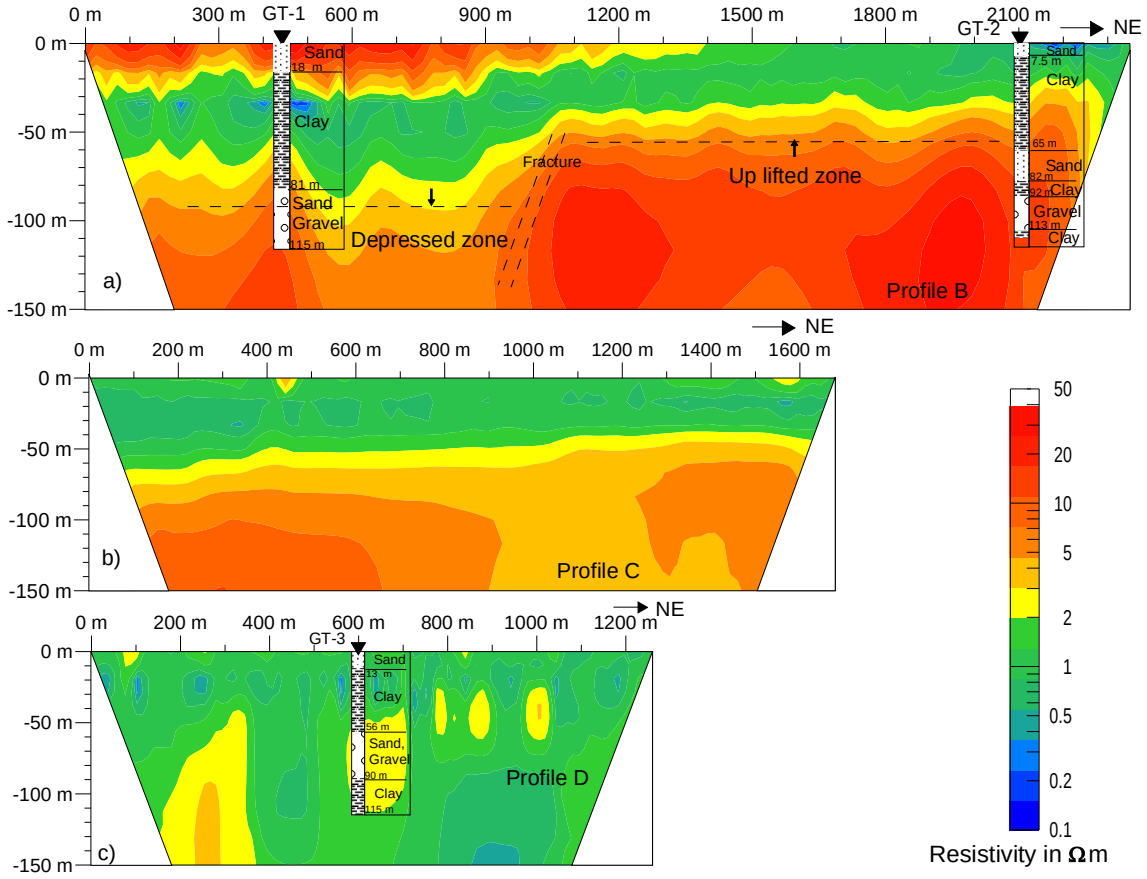

Figure 4.6. Resistivity Imaging along coastline of Giao Thuy district
a) Profile B, b) Profile C, and c) Profile D.

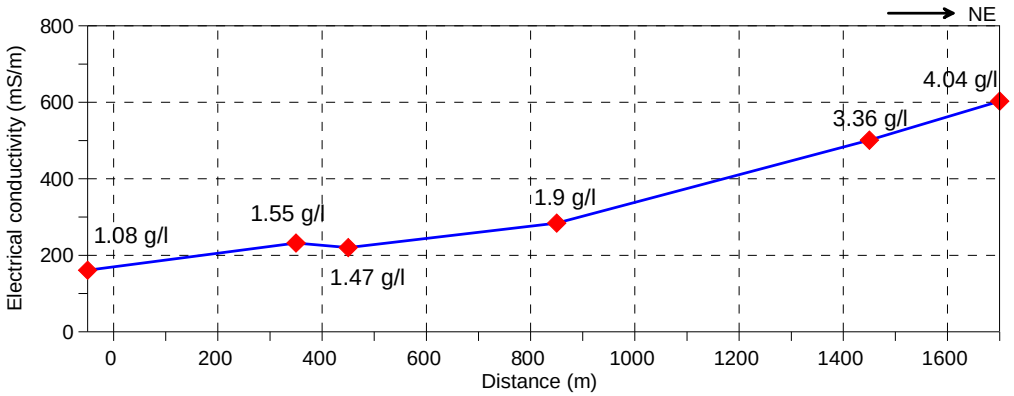

Figure 4.7. Electrical conductivity of groundwater along profile C determined at a depth of 110 m in wells.

The three profiles reveal the transition in the Pleistocene aquifer from fresh to saline water. The salt concentration of groundwater changes from freshwater in Giao Phong area (profile B) to brackish water in Giao Xuan area (profile C) and to saline water in Giao An area (profile D). The resistivity distribution along the three profiles reflects the hydrogeological situation of the local area. The Holocene aquifer contains almost only saline water except the Southwestern part of profile B. The Pleistocene aquifer contains both fresh and saline groundwater. Comparing the RI sections of the three profiles, it could be identified that the resistivity of formation in the fresh water area is higher than 10 Ωm (resistivity of Pleistocene formation along profile B). The resistivity of the formation with brackish water ranges from 5 to 10 Ωm (the Southwestern part of profile C). A resistivity below 5 Ωm indicates a saline water bearing formation (the Northeastern part of profile C and along profile D). Based on the resulting geoelectrical sections of RI, the transition zone of the Pleistocene aquifer indicates a gradual change from fresh to saline groundwater in the direction from South West to North East.

4.2.2. Transient electromagnetic method

Measurements with the transient electromagnetic method (TEM) were carried out along two RI profiles B and C. Six TEM stations are performed along profile B and twenty TEM stations are carried out along profile C. TEM measurements are carried out using the TEM FAST 48 HPC equipment. A coincided loop of transmitter and receiver antennas with a single turn is used. The square transmitter loop has a size of 100 x 100 m. The TEM soundings are analysed by TEM RESEACHER software, a component of the TEM FAST 48 HPC system. The interpretation technique is based on the fitting of theoretical and field curves. A layered model generates a theoretical

curve of TEM. An apparent resistivity $\rho_a(t)$ of a homogeneous medium is calculated by an asymptotic formula at a given moment which coincides with the time of the measured signal in the experiment. The equation (3.8) is used to calculate the theoretical curve. Resistivity and thickness of layers are adjusted to get a good fitting between modelled and measured data using the principle of equivalence. The TEM RESEACHER programme yields the values of resistivity and thickness of a horizontally layered structure. The programme enables to combine multi TEM soundings in a 2D cross section of resistivity distribution. It allows interpreting TEM data in a single curve or in a profile of multi TEM soundings.

The TEM profile B includes six soundings which are called GP1 to GP6. The position of TEM station is located close to the RI profile. The GP1 station is located in a distance of 100 m from the borehole GT-1 and the GP6 station is located in a distance of 200 m from borehole GT-2. Four TEM soundings are performed on the salt field while the TEM GP5 and GP6 stations are located on the rice field. The distance between GP5 and GP6 is approximately 1000 m because there is no available space for TEM measurement in the densely populated area. All TEM soundings are analysed according to a model with four layers. Figure 4.8 shows the field data and the layered model of TEM sounding GP2. The measured resistivity, the layered model and the theoretical curve display as a function of depth. The measurements are taken in the time range from 4.06 µs to 15304 µs after shutting off the current in the transmitter loop. The measured curve shows an increase of resistivity at later time. The TEM sounding GP2 shows a structure of four layers. The first layer shows a resistivity of 2.2 Ωm and a thickness of 18 m. This layer belongs to the Holocene aquifer. Resistivity of the Holocene aquifer is very low because the TEM is carried out on the salt field. The top layer at the salt field is infiltrated by sea water. The second layer has a low resistivity of 0.75 Ωm and a thickness 34 m. This layer consists of clay which is found in the borehole and presented by a low resistivity layer in the RI section. The third layer presents a resistivity of 16 Ωm with a thickness of 30 m. The fourth layer shows a resistivity of 2000 Ωm. This is not the true resistivity of formation. A very high resistivity of the Pleistocene formation in the TEM model implies that the electromagnetic field does not reach down to this layer. There is no measurable eddy current in the high resistivity formation. This phenomenon happens when the electromagnetic field has not enough energy to penetrate the above layers. In this case, the clay layer with high conductivity has adsorbed the energy of electromagnetic field and prevented a deeper penetration by a so-called screening effect. Thus, TEM model generates a layer with a resistivity of 2000 Ωm. Although this value of resistivity is not reliable, the resistivity of the third layer of the TEM model is assumed to be the resistivity of the Pleistocene aquifer.

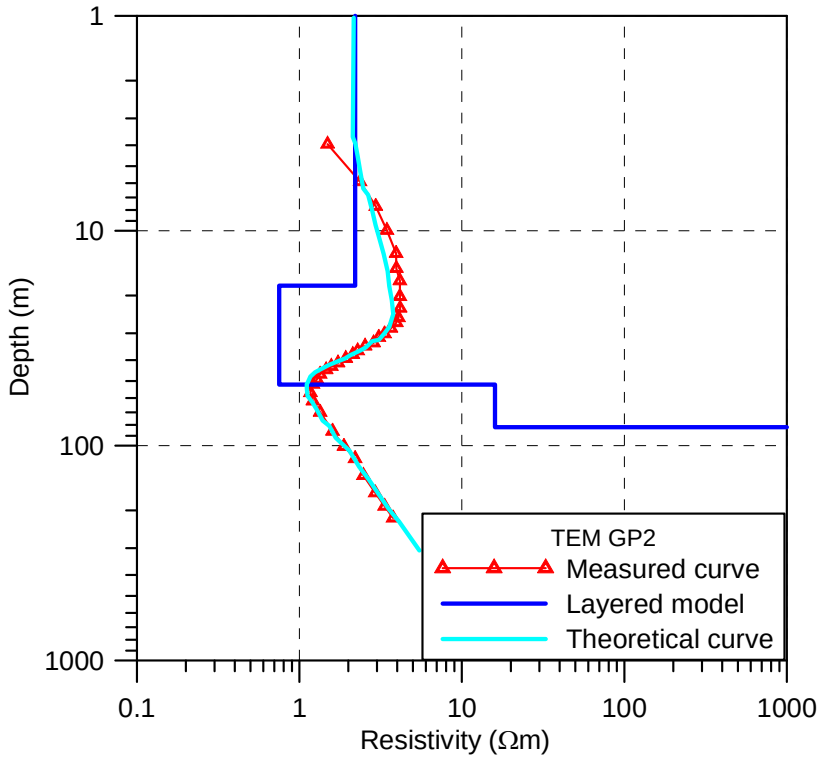

Figure 4.8. Transformed curve, layered model and theoretical curve of TEM GP2.

The modelling curve, which is generated by a model of four layers, is fitting the measured data. The TEM model seems to be appropriate to describe the local geological structure despite the deepest layer has a non-acceptable resistivity. The inversion process results in a RMS error of 2.7% for TEM GP2 sounding.

Six TEM soundings of profile B are interpreted by a four layer model. A combination of six sounding in a 2D section is performed. Figure 4.9 shows a 2D resistivity section along profile B. The resistivity distribution along profile presents four layers. The first layer has a low resistivity of around 2 Ωm and a thickness of around 18 m at the Southwestern part of the profile (from the beginning of profile to position of GP4). The resistivity value of this layer is different compared to the RI section because of sea water infiltration in the top layer on the salt fields. At the Northeastern part of the profile, the first layer has a thickness of 7.5 m (GP6 sounding). The second layer presents a very low resistivity corresponding to the clay layer with a resistivity of less than 1 Ωm. The thickness of clay layer varies from 30 to 45 m. The resistivity of the third layer is in the range from 16 to 20 Ωm. The deepest layer shows a resistivity of 2000 Ωm. This resistivity value is not acceptable.

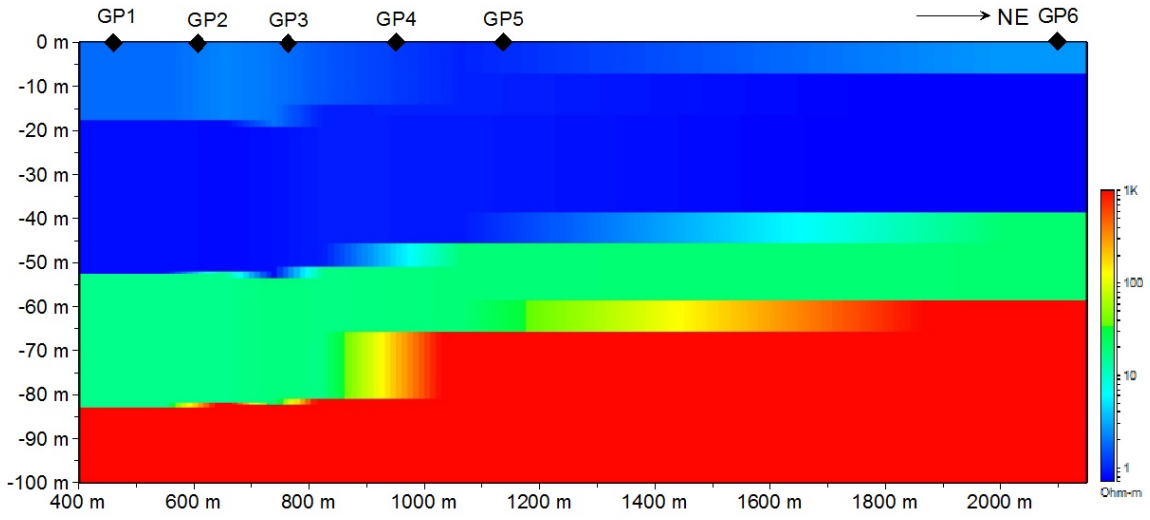

Figure 4.9. Resistivity distribution along profile B following TEM results.

Twenty TEM soundings are carried out along RI profile C using a square loop of 100 x 100 m. The loop is directly placed on the surface of rice fields. The length of TEM profile is longer than the RI profile. The RI profile C is located in the interval between T4 and T18 stations. The TEM stations are closely located to the RI profile. The TEM soundings are individually analysed using a model of four layers. The resulting models of all TEM soundings are combined in a 2D cross section of resistivity distribution along the profile. The distance between two soundings is approximately 100 m. The distance between T3 and T4 soundings is 250 m because of an electricity power line. The space between T17 and T18 is increased to 350 m in order to avoid measurements in a village. The TEM soundings are located in the transition zone from fresh to saline water in the Pleistocene aquifer. Figure 4.10 shows the structural models of two TEM soundings at the Southwestern and the Northeastern positions of the profile. The T1 station is closely located to the fresh water area of the Pleistocene aquifer (Figure 4.10a). A model of four layers generates a theoretical curve which fits well the field data of T1 sounding. The first layer has a thickness of 10 m with a resistivity of 1.8 Ωm. This layer is the Holocene aquifer bearing saline water. The second layer has a resistivity of 0.8 Ωm with a thickness of 35 m. It corresponds to the clay layer of the aquifuge. The third layer presents a resistivity of 1.8 Ωm, corresponding to the transition layer from clayey to sandy formations. This layer has a thickness of 30 m. The deepest layer shows a resistivity of 17.5 Ωm. It reflects the Pleistocene aquifer. The electrical conductivity of the Pleistocene water sample at the well, which is close to the TEM T1 sounding, shows a value of 157 mS/m corresponding to a TDS of 1.06 g/l. This is fresh water.

Figure 4.10b shows the layered model of T20 sounding. The three top layers show a similar resistivity and thickness compared to the TEM T1 sounding. The fourth layer shows a lower resistivity than that of T1 sounding. The resistivity of Pleistocene aquifer at T20 position is only 4 Ωm. This indicates that the Pleistocene aquifer contains saline water. A water sample is taken from the well which is located in a distance of 100 m from the T20 sounding. The water conductivity shows a value of 598 mS/m corresponding to a TDS of 4.01 g/l. This is saline groundwater.

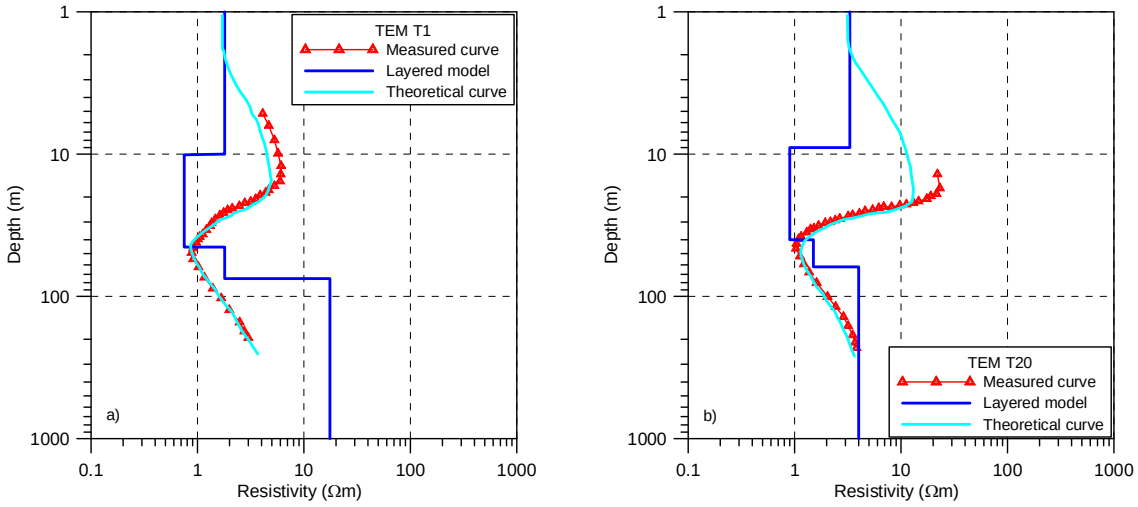

Figure 4.10. Transformed curves, layered models and theoretical curves in profile C a) TEM T1 and b) TEM T20.

All TEM soundings are individually analysed using the layered model. Along the profile C, the TEM soundings are not affected by the screening effect. The resulting TEM models are combined in a 2D cross section of resistivity distribution along profile C (Figure 4.11). The positions of TEM stations are marked in the resistivity section. Following the results of TEM interpretation, the geological structure consists of four layers with different resistivity. The top layer has a resistivity of around 2 Ωm and a thickness of 10 m. This layer is the Holocene aquifer containing saline water. Below the Holocene aquifer is a clay layer which is represented by a very low resistivity layer (around 1 Ωm). The thickness of the clay layer is around 30 m. The third layer reflects a transition from clayey to sandy formation with a resistivity of around 2 Ωm. The deepest layer is related to the Pleistocene aquifer. The resistivity of the Pleistocene formation varies in the range from 4 Ωm to 17.5 Ωm. A gradual decrease of formation resistivity from T1 to T20 reflects an increase of salinity concentration of groundwater in the Pleistocene aquifer. This implies that the conductivity of groundwater in the Pleistocene aquifer increases from Southwest to Northeast along the profile.

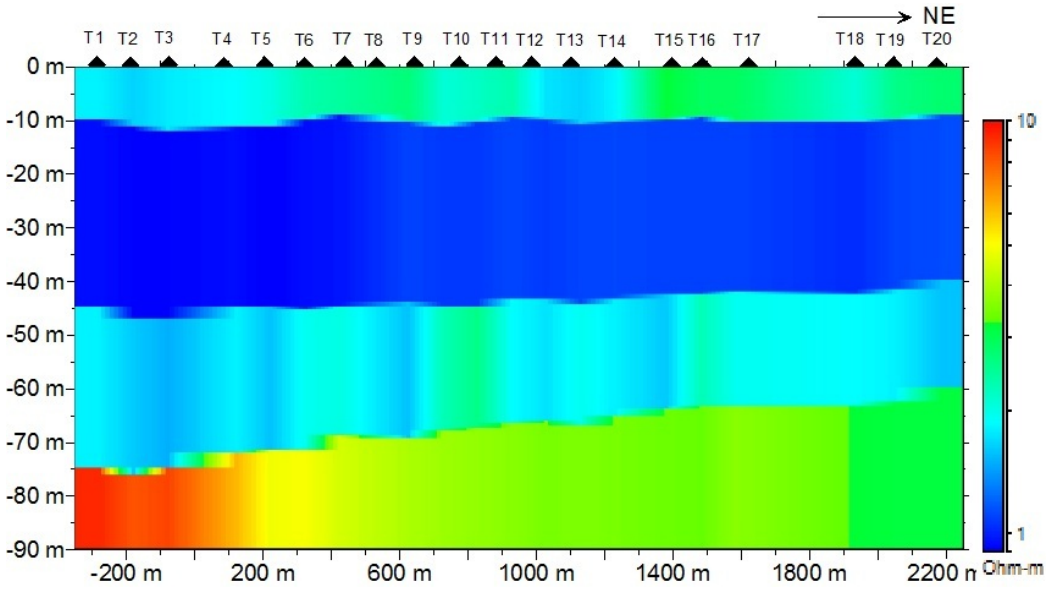

Figure 4.11. Resistivity distribution resulting from TEM along profile C.

The electrical conductivity of groundwater is measured at ten water wells at a depth of 110 – 120 m. The water wells are located in a distance up to 100 m from the TEM profile. Figure 4.12 presents the electrical conductivity of the groundwater along TEM profile C. The TDS value, which is converted from the conductivity of groundwater, is indicated at the position of water wells (Figure 4.12). Two first water wells show a TDS value of approximately 1 g/l. This implies that the Pleistocene aquifer contains fresh groundwater at this section of the profile. The T1, T2 and T3 soundings of TEM are located in the area between the first two water wells. These TEM models show a high resistivity of around 15 Ωm for the Pleistocene formation. The next three water wells show a TDS value in the range from 1 to 2 g/l. These TDS values are assumed as brackish water. The TDS value of groundwater sample is higher than 3 g/l at the five last water wells along the profile. This indicates that the Pleistocene aquifer contains saline groundwater at the Northeastern part of profile. This corresponds to the low resistivity of the Pleistocene aquifer which is presented in the resistivity cross section of TEM (Figure 4.11).

The TDS concentration of groundwater increases along the profile. It fits well with the gradual decrease of resistivity in the Pleistocene aquifer. Comparing the resistivity of water bearing formation and the electrical conductivity of groundwater along profile C, it can be inferred that the Pleistocene aquifer contains fresh, brackish, and saline water. A transition from fresh to saline water is extended from the position of TEM T4 to the position of T11 sounding. The saline water boundary is identified at the position 900 m of the profile.

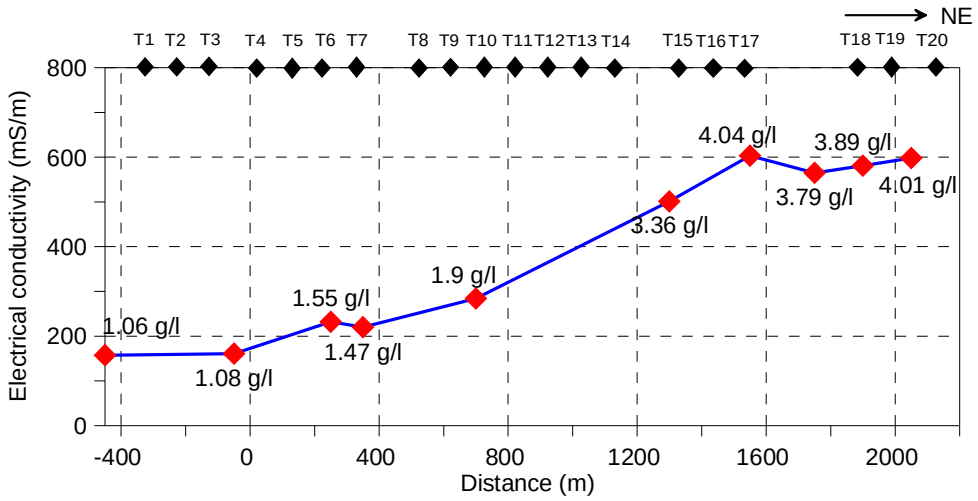

Figure 4.12. Electrical conductivity of groundwater along profile C of TEM.

4.2.3. Drilling and well logging

Drilling and well logging are carried out at three boreholes which are located on the RI profiles. The boreholes GT-1 and GT-2 are located on the profile B (Giao Phong commune) at the positions of 450 and 2100 m while the borehole GT-3 is placed at the position of 600 m of profile D (Giao An commune). The diameter of boreholes is 0.135 m. The stratification of boreholes results from observation of the drilling process and the lithological classification of soil samples of drilling cores. Forty soil samples are taken from three boreholes to be analysed in the laboratory. Well logging was performed immediately after the drilling process. Natural gamma and resistivity well logging are carried out using the GMX II well logging system. The resistivity logging includes four different spacings of the tool: 8, 16, 32, and 64 inches.

Figure 4.13 shows the detailed stratification of the borehole GT-1 and the logging curves. The stratification presents three main layers: Holocene aquifer, aquiclude and Pleistocene aquifer (Figure 4.13a). The Holocene aquifer extends from the surface to a depth of 18 m, including two subdivided layers. The first layer from the surface to a depth of 10 m is formed by fine sand, which belongs to Thai Binh formation ($Q_{IV}^{3}tb_1$). The second layer consists of clayey sand belonging to Hai Hung formation ($Q_{IV}^{3}hh$). The clay layer is represented by clayey sediments with changing viscosity from soft to plastic clay. It can be divided into four layers with different properties of samples such as viscosity, colour, and composition. The Pleistocene aquifer is identified by sandy sediments with grain sizes changing from fine to coarse particles. This sediment belongs to the Pleistocene epoch, Hanoi formation ($Q_{II-III}^{1}hn$). The Pleistocene aquifer is subdivided into three layers based on the grain size of soil samples. The sub-interfaces are estimated by the drilling process and the collected samples.

When the drilling process had been finished, well logging was carried out in the open borehole. The logging curves are presented in Figure 4.13b and 4.13c. Unfortunately, well logging has to be stopped at a depth of 80 m because the wall of the borehole had been collapsed. Well logging data is acquired from 8 to 80 m of depth. Figure 4.13b shows four curves of resistivity logs with the different spacings. The different spacings cause a varying depth of penetration. The R8 and R16 curves reflect the resistivity of the mud cake and the invaded zone. The approximately coinciding curves R32 and R64 present the resistivity of non-invaded formation. Although the resistivity curves of the four spacings are slightly different, they show common features. The resistivity values decreases from 10 Ωm to less than 1 Ωm and then increases to around 6 Ωm along the depth of the borehole. The decreasing resistivity reflects the changing sediments from sand (Holocene aquifer) to clay formation (aquiclude). Comparing to the stratification of the borehole, the interface between the two layers is located at around 18 m of depth. The increasing resistivity at the deepest section is related to the changing of lithology from clay to sand. Unfortunately, resistivity logging could not be performed in the sandy formation of the Pleistocene aquifer below 80 m of depth, but the resistivity logs show an increasing tendency with depth.

Figure 4.13c presents the gamma log of borehole GT-1. The detector of logging tool counts the number of natural gamma rays emitted by the geological formation in a time interval. The unit of natural gamma logging is counts per second (cps). A high count rate from the detector implies that the geological formation contains high clay content. The gamma logging curve of borehole GT-1 shows high values of gamma ray activity along the investigated depth interval. The minimum of count rate is 71 cps and the maximum is 131 cps. The gamma log indicates a high clay content in the Holocene aquifer. Comparing the gamma log and the stratification of borehole, it can be inferred that clay sediments show a reading of natural gamma rays higher than 100 cps.

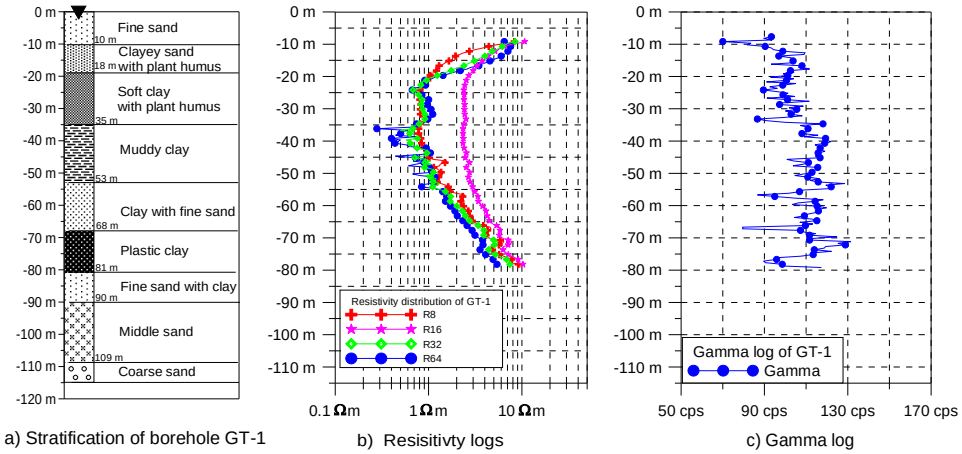

Figure 4.13. Stratification and well logging curves of borehole GT-1.

Located at position of 2100 m on profile B, the borehole GT-2 shows a slightly different geological structure. The distance between borehole GT-1 and GT-2 is 1600 m. Figure 4.14a shows the stratification of borehole GT-2. The first layer extends from the surface to a depth of 7.5 m. This layer is fine sand mixed with clay, which belongs to Thai Binh formation ($Q_{IV}^{3}tb_1$). The clayey layer is identified from 7.5 to 65 m of depth. This layer includes the Hai Hung formation ($Q_{IV}^{1-2}hh$) and Vinh Phuc formation ($Q_{III}^{2}vp$). It includes four subdivided layers which consist of clay with different compositions. The Pleistocene aquifer consists of sandy formation from coarse to fine grain size. This layer belongs to Hanoi formation ($Q_{II-III}^{1}hn$). A clay layer is found within the Pleistocene aquifer from 82 to 92 m of depth. This layer is not found in the borehole GT-1. At the bottom of the borehole, the Le Chi formation is identified from 113 to 115 m of depth. The Le Chi formation consists of clay and gravel.

The resistivity logs of borehole GT-2 are presented on Figure 4.14b. The four resistivity logs present a similar behaviour. The resistivity of the R64 log indicates a strong decrease in section from 15 to 25 m of depth with values below 0.1 Ωm. This value reflects the soft clay sediment which belongs to the Hai Hung formation. A low resistivity may be caused by a very low measured voltage because of large tool spacing and a low formation resistivity. The resistivity of all four logs increases along the depth of borehole from 25 to 65 m. The resistivity value varies from 1 to 20 Ωm within the clayey layer. The resistivity value is higher than 10 Ωm at the depth from 50 to 65 m. The increasing resistivity at this section reflects the transition from clayey to sandy sediments. The resistivity of the four logs remains stable from 65 to 82 m of depth with values of around 20 Ωm. This depth interval corresponds to the sandy formation of the Pleistocene aquifer. The high resistivity of the water bearing formation implies that the Pleistocene aquifer contains fresh water. Resistivity logs show a decreasing resistivity in the clay layer from 82 to 92 m, which was identified in the borehole GT-2. The resistivity of logs decreases from 20 Ωm to around 10 Ωm in the clay layer. At the deepest part of resistivity logs from 92 m to 106 m, the resistivity of the formation increases again to around 30 Ωm. This layer consists of sand mixed with gravel belonging to the Pleistocene formation. The fresh water, which was extracted from a depth of 110 m (GT-2 well), shows a resistivity of 11 Ωm corresponding to a TDS value of 0.6 g/l.

Figure 4.14c shows the natural gamma log of borehole GT-2. It clearly identifies the layered structure of the geological formations. A clay layer is presented from 10 to 65 m of depth by high count rates of gamma ray activity. The decreasing values of gamma log at the section from 55 to 65 m reflect the transition from clayey to a sandy formation. The clay layer, which extends from 82 to 92 m of depth in the borehole, is

identified by a high value of gamma ray activity (Figure 4.14c). The count rates of gamma ray activity in the clay layer vary from around 100 cps to 150 cps. Two layers of sandy formations are found from 65 to 82 m and from 92 to 106 m of depth with the count rates of gamma ray activity in the range from 40 to 70 cps. Both layers belong to the Pleistocene aquifer. The gamma log shows a good agreement with the resistivity logs and the stratification of borehole GT-2. The layer interfaces between the formations are clearly indicated by the gamma log. The layer interfaces are determined by the stratification of borehole and the results of well logging interpretation.

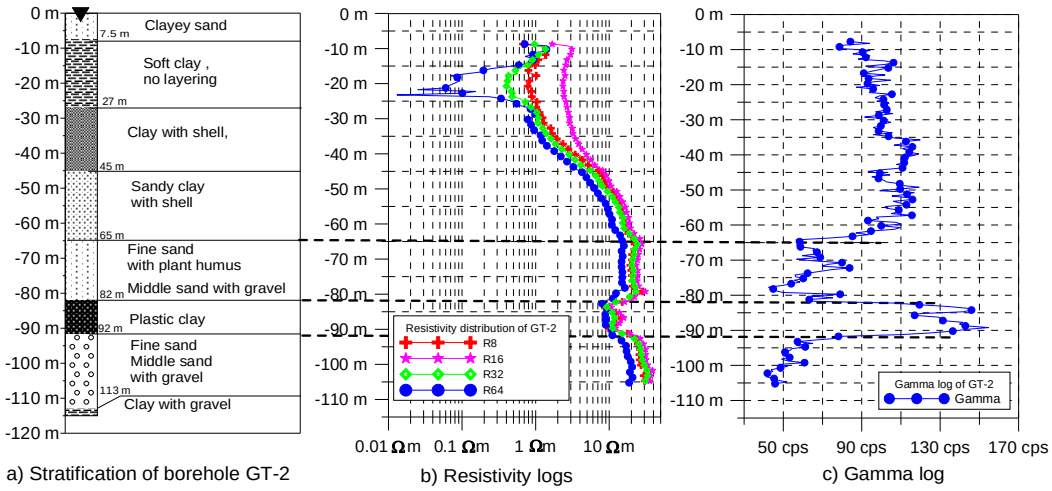

Figure 4.14. Stratification and well logging curves of borehole GT-2.

The borehole GT-3 is located in the saline water area of the Pleistocene aquifer. It is located at the position of 600 m on the profile D. The stratification of borehole GT-3 and the well logging curves are compiled in Figure 4.15. The stratification of borehole indicates four main layers. The Holocene aquifer is identified by a sandy layer, which extends from the surface to a depth of 13 m. This layer consists of sandy sediments with plant humus. The clay layer forming an aquifuge is found from 13 to 56 m of depth. The sandy formation which belongs to Pleistocene aquifer extends from 56 to 90 m of depth. The Pleistocene aquifer consists of fine to coarse grained sand mixed with gravel. It can divide into two sub layers with different grain size. The Le Chi formation (Q_1lc) is found at a depth from 90 to 115 m. The lithological components of Le Chi formation include clay with coarse sand and gravel. The detailed stratification of borehole GT-3 is presented in Figure 4.15a.

Figure 4.15b displays the resistivity logs of the borehole GT-3. The resistivity logs show a very low resistivity in the range from 1 to 3 Ωm for Holocene aquifer (from 8 to 13 m of depth). This indicates that the Holocene aquifer contains saline water. The

resistivity logs indicate a value in the range from 0.6 to 3 Ωm for the clay layer at a depth from 13 to 48 m. The resistivity slightly increases from 48 to 56 m. This reflects the transition from clayey to sandy sediments. The resistivity logs indicate slightly increased values in the range from 2 to 5 Ωm in the section from 56 to 90 m, which corresponds to the Pleistocene aquifer. The water sample, which is extracted from a depth of 90 m (well GT-3), shows a conductivity of 1482 mS/m corresponding to a TDS of 9.9 mg/l. The resistivity logs of borehole GT-3 reflect a saline water bearing sandy formation in the Pleistocene aquifer. The deepest section of resistivity logs shows a resistivity in the range from 3 to 5 Ωm. This section corresponds to a clay layer mixed with coarse sand and gravel.

Because both clayey sediments and saline water bearing sandy formations show a similar resistivity, it is not possible to distinguish the two formations based on resistivity logs. In this case, the gamma log proves to be a reliable tool to distinguish between different lithological units. Figure 4.15c presents the gamma log in the borehole GT-3. The layered structure of sediments can easily be identified. The gamma log presents a high count rate of gamma ray activity (around 100 cps) in the section down to a depth of 55 m, which corresponds to the clay layer. The count rate of gamma ray activity suddenly decreases at a depth of 56 m indicating a sharp transition from clayey to sandy sediments. The gamma log shows a value of around 50 cps in the section from 56 to 90 m, which is the sandy formation belonging to the Pleistocene aquifer. The gamma log indicates a strong increase at values of around 130 cps at a depth of 90 m reflecting the deepest clay layer. The natural gamma log of borehole GT-3 indicates three layers of geological formations.

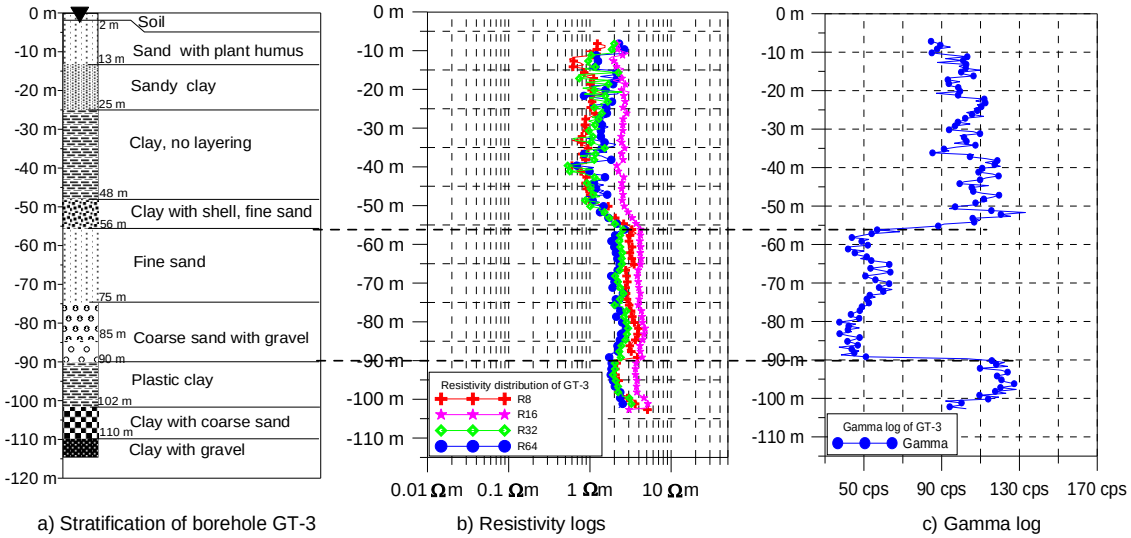

Figure 4.15. Stratification and well logging curves of borehole GT-3.

4.3. Laboratory investigations

Forty soil samples were taken from three boreholes in the study area for laboratory investigations. All soil samples are named using the letter V as the first identifier symbol (ID). The first number in the ID indicates the number of borehole. The next two numbers of the ID indicate the consecutive number of samples from the borehole. For example, the sample V316 identifies the sixteenth sample from the borehole GT-3.

4.3.1. Water content and density

The water content is determined by the evaporated amount of the water from the soil sample. The sample is dried at the room temperature and later in the vacuum oven at a temperature of 35^0 C. The gravimetric water content is determined by percentage ratio between the mass of evaporated water and mass of dry sample. The volumetric water content relates the volume of water to the total volume of the sample. In my laboratory investigations, the total volume of soil sample is given by the volume of sample holder. The volume of water is known according to the evaporated amount of water during the drying process and the density of water. The volume of solid constituents is determined by the dry weight and the grain density. The volume of air inside the original sample is inferred from equation:

$$V_{air} = V_{total} - V_{solid} - V_{water}. \tag{4.1}$$

The volumetric and gravimetric water content are determined according to equations (3.12) and (3.13). Based on the known parameters, porosity and saturation of the soil sample are calculated according to equations (3.14) and (3.15). The raw density d_n is determined by the ratio between the total weight and total volume of soil samples. Grain density of soil sample is investigated after drying process. A known mass of dried sample is placed in the ULTRAPYCNOMETER-1000 system. The ideal gas of Helium occupies the empty pore space. The solid volume of the soil sample is measured by the system using the gas expansion method. Grain density is calculated from the mass and solid volume of the dry sample.

The results of laboratory investigations of all soil samples are presented in Table 4.2. The depth and the description of soil samples are also compiled in the table. The soil samples show a value of gravimetric water content in the range from 10 to 50%. The volumetric water content of sample is in the range from 20 to 55%. The clayey sediments show a water content higher than that of sandy samples. The clayey samples show a high value of saturation factor (from 0.80 to 0.99) while the saturation of sandy samples varies in the range from 0.68 to 0.95. Porosity of sample shows a high value for clayey sediments. The value of porosity ranges from 25 to 61%. Raw density of all

samples varies in a range from 1589 to 2235 kg/m^3 while the grain density ranges from 2569 to 2670 kg/m^3.

Table 4.2. Water content and density of soil samples from the study area.

Sample ID	Depth (m)	d_n (kg/m^3)	d_k (kg/m^3)	w (%)	Θ (%)	S_w	ϕ (%)	Sample descriptions
V101	-0.5	1741.3	2684.1	27.9	37.9	0.77	49.5	Sand
V102	-4	1969.5	2655.6	17.9	29.6	0.78	37.9	Sand
V103	-13	1875.6	2629.0	32.3	45.3	0.97	46.6	Clay
V104	-29	1930.2	2649.4	28.7	42.6	0.97	44.0	Clay
V105	-35	1898.7	2606.3	31.1	44.6	0.99	45.0	Clay
V106	-39	1816.4	2687.1	33.5	45.5	0.92	49.4	Clay
V107	-54	1803.3	2671.4	40.8	51.5	0.98	52.8	Clay
V108	-56	1884.1	2621.7	30.0	43.2	0.96	45.1	Clay
V111	-77	1884.2	2673.5	31.5	44.1	0.93	47.6	Clay
V113	-81	1916.1	2682.9	27.6	41.0	0.92	44.6	Clay
V114	-85	2235.1	2684.8	11.6	23.0	0.89	25.7	Sand
V115	-90	2085.0	2641.0	16.4	28.2	0.81	34.9	Sand
V116	-101	2073.4	2652.9	16.1	27.9	0.80	34.8	Sand
V117	-115	2095.0	2592.0	16.2	28.3	0.87	32.6	Sand
V201	-0.5	1896.0	2675.1	26.9	39.9	0.89	44.7	Sand
V202	-5	1927.4	2697.2	29.6	42.9	0.93	46.3	Clay
V204	-16	1917.8	2638.7	30.5	43.7	0.96	45.6	Clay
V206	-23	1903.5	2645.2	34.5	47.6	0.99	47.8	Clay
V211	-46	1882.9	2666.2	33.2	46.6	0.98	47.4	Clay
V213	-56	1892.2	2649.9	28.5	41.5	0.92	45.0	Clay
V214	-66	2107.4	2668.0	18.0	31.4	0.91	34. 5	Sand
V215	-75	2119.4	2662.9	18.2	31.5	0.90	35.0	Sand
V216	-82	2153.5	2651.9	16.3	29.2	0.88	33.1	Sand
V217	-90	1903.3	2680.7	36.1	49.1	0.99	49.3	Clay
V218	-101	2149.1	2664.0	15.0	27.1	0.84	32.3	Sand
V219	-109	2157.3	2659.6	15.1	27.5	0.88	31.4	Sand, Gravel
V220	-115	1912.1	2699.9	30.3	43.7	0.94	46.6	Clay
V301	-3.5	1908.8	2620.5	28.8	42.0	0.95	44.3	Sand
V303	-6.5	2087.8	2688.0	16.3	28.8	0.84	34.4	Sand
V306	-11	1772.2	2676.5	27.0	37.1	0.70	48.6	Sand
V308	-24	1862.8	2671.7	31.5	44.0	0.92	47.7	Clay
V311	-37	1588.8	2603.5	53.3	54.4	0.89	60.8	Clay
V312	-48	1772.3	2613.9	35.7	46.4	0.92	50.3	Clay
V315	-61	2007.1	2655.6	20.6	34.1	0.91	37.7	Sand
V316	-75	2121.9	2656.3	14.5	25.5	0.81	31.4	Sand
V317	-85	2217.5	2656.0	9.9	17.2	0.68	25.2	Sand, Gravel
V318	-96	1878.5	2689.9	30.9	43.7	0.92	47.4	Clay
V319	-107	2014.6	2647.8	20.8	34.4	0.91	38.0	Clay
V320	-115	2248.0	2672.0	12.2	24.2	0.93	25.9	Clay, Gravel

4.3.2. Electrical resistivity

The electrical resistivity of soil sample is investigated by a SIP FUCHS system. The variation of resistivity amplitude and phase angle is recorded as a function of frequency. Figure 4.16 presents the resistivity amplitude and phase angle of sample V214, which is a sandy sample from a depth of 66 m. The resistivity of this sample varies in the range from 14.6 to 15.1 Ωm in the frequency range from 3 mHz to 750 Hz (Figure 4.16a). The resistivity amplitude slightly decreases with an increasing of frequency. This is a normal behaviour. Figure 4.16b shows the phase shift of sample V214 as a function of frequency. The phase shift angle varies in the range from 1.9 to 5.9 mrad. It increases from 3 mHz to 100 Hz and decreases at frequencies higher than 100 Hz. The errors of phase measurements are presented by vertical error bars on the phase shift data points (Figure 4.16b). The error value of phase measurements varies in the range from 0.01 to 0.8 mrad.

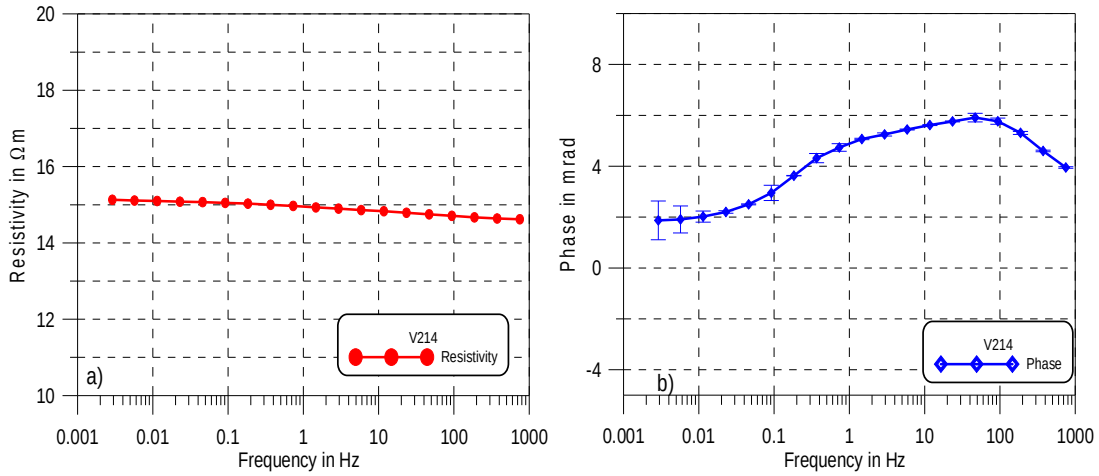

Figure 4.16. Resistivity amplitude and phase shift of the sample V214.

SIP investigation is performed for all forty samples, which were taken from three boreholes. The resulting complex resistivity spectra show negative phase behavior at low frequencies for almost all samples. The negative phase behavior may be caused by chemical reactions of organic substances with clay minerals. Due to this uncertainty in the phase measurements, only the resistivity amplitude and the positive phase angles are used for further interpretation.

Figure 4.17 shows the spectra of resistivity amplitude of soil samples from borehole GT-1. The depth and description of soil samples are indicated in the legend of the figure. The resistivity amplitude reflects the electrical properties of the lithological components and the salinity of the water in the pore space of soil samples. Clay sediments present a

resistivity of less than 5 Ωm. The increasing resistivity amplitude from 5 Ωm to 16 Ωm along with the increasing depth describes the changes of samples from clayey to sandy sediments of the Pleistocene aquifer. The soil samples from both Holocene and Pleistocene aquifers show a resistivity amplitude higher than 10 Ωm. This indicates the fresh water in the pore space of the sands.

The spectra of resistivity amplitude of soil samples from borehole GT-2 are compiled in the Figure 4.18. Generally, the resistivity amplitude does not change so much with frequencies. The sample V201 from a depth of 0.5 m is taken from the overburden layer with a resistivity of 12 Ωm. The sample V202 taken at a depth of 5 m in the Holocene aquifer shows a very low resistivity (1.5 Ωm). This value of resistivity indicates that the water of the Holocene aquifer is very conductive. The clayey samples have a resistivity in the range from 0.8 to 9 Ωm. The variation of the resistivity of the clay samples is related to the constitution of the samples. Soft clays show a resistivity of less than 2 Ωm while the clays mixed with fine sand present a resistivity in the range from 5 to 9 Ωm. The sandy formations present a resistivity higher than 10 Ωm. The resistivity of groundwater which is extracted at a depth of 110 m (well GT-2) is 11 Ωm while the sandy sample V219 taken at a depth of 109 m shows a resistivity of around 18 Ωm. This indicates that the Pleistocene aquifer at the well GT-2 contains fresh water.

The resistivity of soil samples from GT-3 varies in the range from 1 to 12 Ωm (Figure 4.19). The sandy formations from both Holocene and Pleistocene aquifers show a resistivity of less than 10 Ωm. The Holocene sample V306 taken at a depth of 11 m presents a resistivity of around 1.5 Ωm. The Pleistocene sample V316 taken at a depth of 85 m displays a resistivity of around 7 Ωm. This indicates that the groundwater containing in both Holocene and Pleistocene aquifers is very conductive. The saline groundwater from the well GT-3 (at a depth of 90 m) shows a conductivity of 1482 mS/m (0.67 Ωm) corresponding to a TDS value of 9.9 g/l. The clayey formations show a resistivity in the range from 1 to 6 Ωm.

The resistivity of samples from SIP at a fixed frequency is comparable with the resistivity of sediments, which was measured by other methods. Table 4.3 compiles the resistivity and phase shift of all soil samples according to SIP at a frequency of 1.46 Hz. The resistivity of soil sample varies in the range from 0.88 to 36.75 Ωm. The clayey formations and the saline water bearing formations show a resistivity of less than 10 Ωm. The sandy sediments which have a value of resistivity higher than 10 Ωm indicate a fresh water bearing formation. Some soil samples show a negative phase shift at a frequency of 1.46 Hz.

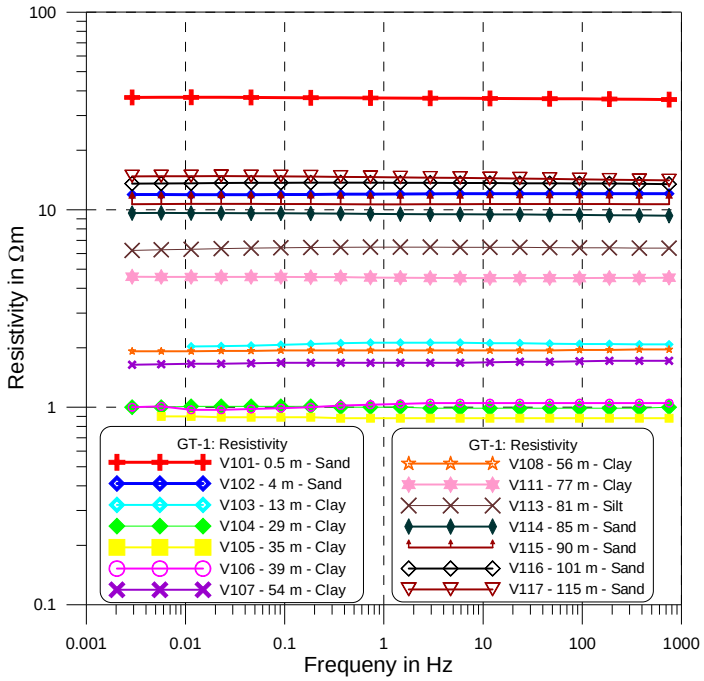

Figure 4.17. Resistivity amplitude of soil samples from borehole GT-1.

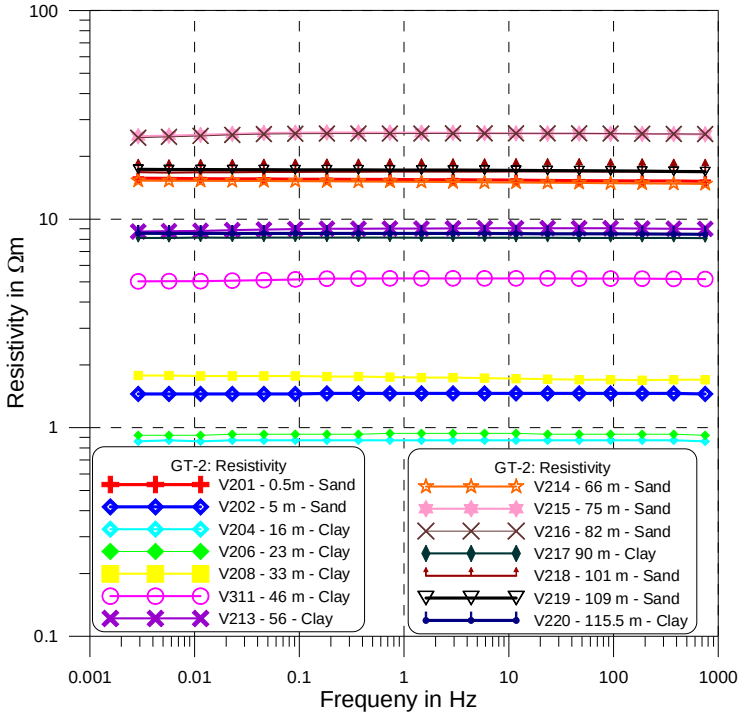

Figure 4.18. Resistivity amplitude of soil samples from borehole GT-2.

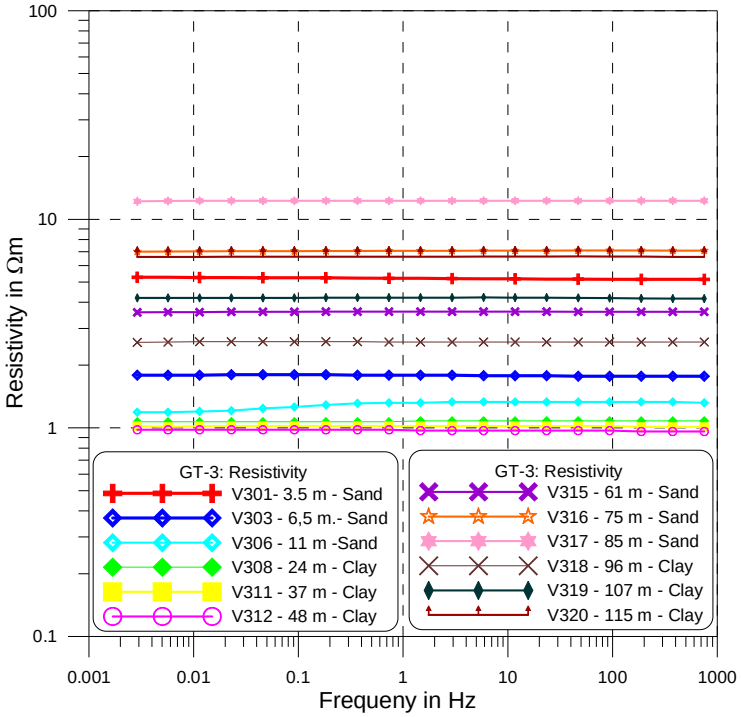

Figure 4.19. Resistivity amplitude of soil samples from borehole GT-3

Table 4.3. Resistivity amplitude and phase shift of samples at frequency of 1.46 Hz.

GT-1	ρ(Ωm)	φ (mrad)	GT-2	ρ(Ωm)	φ (mrad)	GT-3	ρ(Ωm)	φ (mrad)
V101	36.75	3.32	V201	16.42	2.34	V301	4.86	2.39
V102	11.92	-3.57	V202	1.63	-0.02	V303	1.82	4.33
V103	2.2	-2.77	V204	1.07	10.44	V306	1.38	-15.37
V104	0.96	5.56	V206	1.04	4.45	V308	1.08	-2.9
V105	0.88	3.87	V208	1.29	-1.25	V311	1.02	0.07
V106	1.04	-16.14	V211	5.2	-1.36	V312	0.97	4.1
V107	1.68	-3.27	V213	8.94	-1.45	V315	3.61	0.24
V108	1.94	0.21	V214	15.09	5.07	V316	7.06	-1.41
V111	4.53	5.28	V215	25.73	2.61	V317	12.27	0.45
V113	6.47	-1.34	V216	25.14	-1.52	V318	2.58	1.31
V114	9.51	2.01	V217	8.11	0.44	V319	4.21	-0.43
V115	10.65	-0.68	V218	16.89	-1.5	V320	6.95	6.66
V116	13.57	3.92	V219	17.89	1.99			
V117	14.62	5.23	V220	8.54	0.69			

4.3.3. Specific internal surface

The mass related specific internal surface s_m of soil samples is determined by the Nitrogen adsorption method. Figure 4.20 presents the specific internal surface values and the depth of samples respectively. The measured data is compiled in appendix A. The sandy samples, which were taken from the aquifers, are presented by a specific internal surface less than 10 m^2/g. The clayey sediments show a specific internal surface higher than that of sandy formations.

Based on the specific internal surface, it is easy to identify the sandy formation of the borehole. For example, at borehole GT-1, the three first samples, which are distributed from 0.5 to 13 m of depth, indicate a specific internal surface less than 6.52 m^2/g. These samples are sandy formations and belong to the Holocene aquifer. The Pleistocene aquifer formations are identified by the specific internal surface values in the range from 4.70 to 6.29 m^2/g. The specific internal surface of the clayey formations varies in the range from 10.89 to 38.52 m^2/g. These samples belong to the aquifuge which are distributed from 29 to 77 m of depth. The sandy and clayey samples of boreholes GT-2 and GT-3 can be distinguished by the value of specific internal surface in the same way. Sample V217 represents a clay lens within the Pleistocene aquifer at the borehole GT-2. The specific internal surface of sample V217 is 17.69 m^2/g while the sandy sample V216 shows a value of 2.42 m^2/g. The specific internal surface is strongly related to the hydraulic properties of formations. In my study, the specific internal surface of soil samples is used to calculate the hydraulic conductivity of the Pleistocene aquifer.

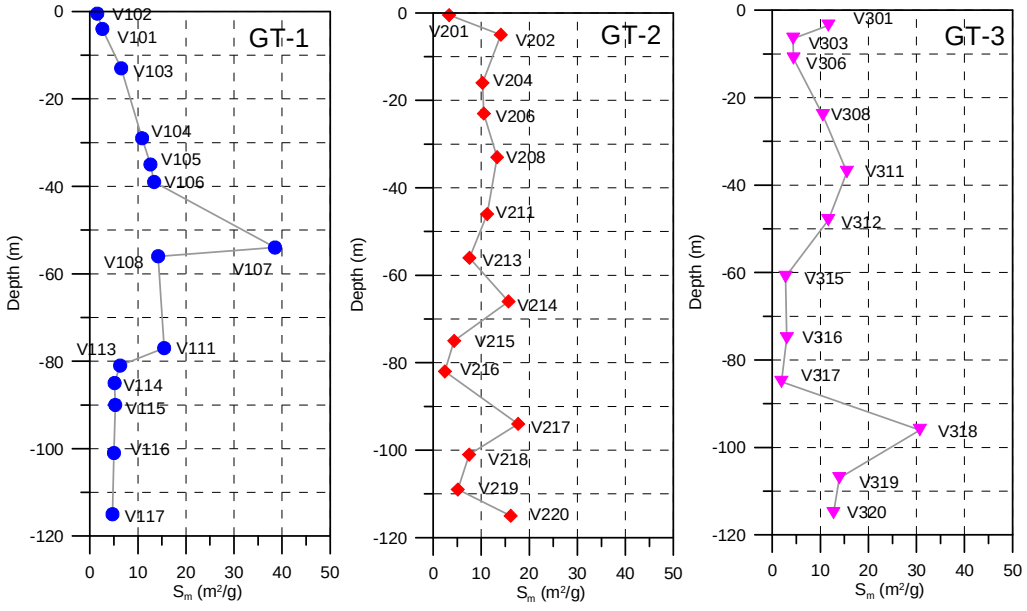

Figure 4.20. Specific internal surface of soil samples in the three boreholes.

4.3.4. Grain size distribution

The grain size of soil samples is strongly related to other petrophysical parameters such as resistivity, density, porosity, and internal surface. Sixteen samples are chosen to classify the grain size distribution using wet sieving technique. Three samples (V102, V201 and V306) come from the Holocene aquifer. Twelve samples belong to the Pleistocene aquifer. Only the sample V320 is clay sediment mixed with gravel belonging to Le Chi formation (Q_1lc). The grain size distribution of sediments is determined according to the percentage of mass of fractions from clay to gravel size particles. The grain size considers the diameter of particles in the range from 0 to larger than 400 µm. The resulting grain size fractions are compiled in Table 4.4. The sieving results indicate for all samples a clay fraction of less than 11% of mass. Most sandy samples show for the clay fraction a value of less than 5 %. Only the two samples V115 and V116 present a higher percentage of clay fractions. The silt fraction occupies a significant percentage of mass in most samples. The sandy fractions with different grain size from fine to coarse particles are dominant in the aquifer formations. A significant portion of gravel is identified in the samples at the bottom of the Pleistocene aquifer. The sample V320 shows a high percentage of gravel but also a high percentage of clay and silt fractions. Only the portion of the sandy fraction is low.

Table 4.4. Grain size distribution of soil samples from the study area.

Sample ID	Grain size distribution (%)					
	Clay < 2 µm	Silt 2 - 63 µm	Fine sand 63 - 125 µm	Middle sand 125 - 200	Coarse sand 200 - 400 µm	Gravel > 400 µm
V102	2.19	32.65	52.40	7.76	4.66	0.34
V113	1.36	28.28	31.41	32.48	5.99	0.48
V114	3.38	36.59	27.60	25.80	5.99	0.53
V115	10.85	41.54	23.12	15.03	9.19	0.26
V116	8.92	36.96	15.10	15.12	23.08	0.83
V117	2.52	30.94	20.84	11.13	12.43	22.14
V201	0.76	9.46	26.85	48.21	12.69	2.03
V214	3.44	76.65	12.03	1.24	5.80	0.83
V215	4.07	34.97	16.43	23.30	19.94	1.29
V216	2.59	21.24	6.29	6.14	58.02	5.73
V219	2.67	29.48	8.98	5.86	14.84	38.17
V306	2.71	35.29	54.50	7.50	0.00	0.00
V315	2.66	21.52	4.31	6.90	59.44	5.16
V316	2.37	32.58	9.55	15.90	33.40	6.20
V317	0.88	19.85	6.23	9.44	10.64	52.95
V320	10.47	51.64	1.85	0.81	8.97	26.25

Figure 4.21 presents the grain size distribution curves of the typical samples from the three boreholes. The graph displays the diameter of particles in mm versus the cumulative weight in percentage. The grain size distribution curves show a similar feature for the sandy samples. Only the clayey sample mixed with gravel V320 (the blue curve) shows a slightly different feature. The clay and silt fractions occupy 63% of cumulative weight. The sand fractions are not significant while the gravel fraction occupies 26% of mass. In my study, the hydraulic conductivity is calculated from the diameter of particles corresponding to the percentage of sample by weight, which has a diameter smaller grain size. The diameters d_{10}, d_{20}, d_{50}, and d_{60} are determined from the grain size distribution curves. The determined diameters are listed in appendix B. A semi-logarithm plot is used to determine the diameters of weight percent. Figure 4.22 displays the determined diameters d_{10}, d_{20}, d_{50}, and d_{60} for all samples of the Pleistocene aquifer in different symbols and colours. The depth and name of samples are indicated in the figure.

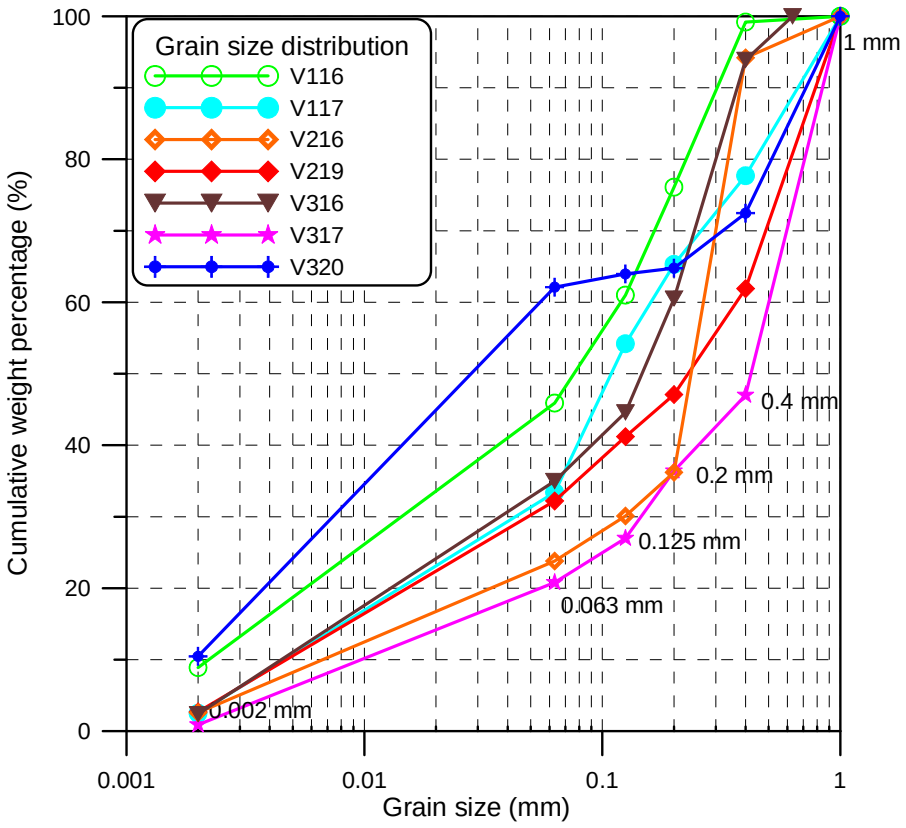

Figure 4.21. The grain size distribution curves of sandy samples from study area.

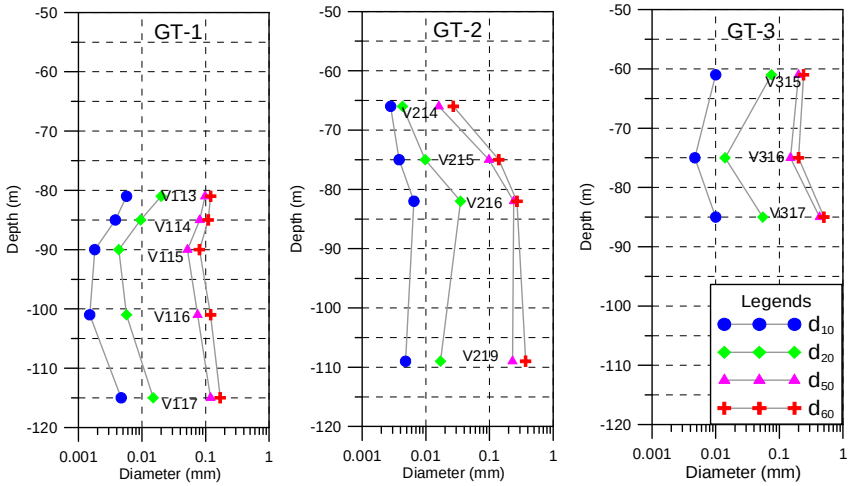

Figure 4.22. The diameters of samples determined from grain size distribution curves.

4.3.5. Magnetic susceptibility

The mass specific magnetic susceptibility of all samples is determined by a Kappabridge KLY-2 equipment. The results are displayed in Figure 2.23 following the depth of sample in the borehole. The mass specific magnetic susceptibility of soil samples varies in the range from 9.3 10^{-8} to 98.1 10^{-8} m^3/kg. The sandy samples show higher values while the clayey samples present lower values of mass specific magnetic susceptibility (see appendix C). For example, the sandy sample V116 shows a high value of 61.3 10^{-8} m^3/kg. The clayey sample V108 presents a value of 12.6 10^{-8} m^3/kg. This indicates that the sandy formation of Pleistocene aquifer contains minerals with higher magnetic susceptibility. This behavior is similar in the boreholes GT-2 and GT-3. The higher value of specific magnetic susceptibility of sandy formations may be related to an increased iron content in the aquifers (Nguyen Trong Vu et al., 2005).

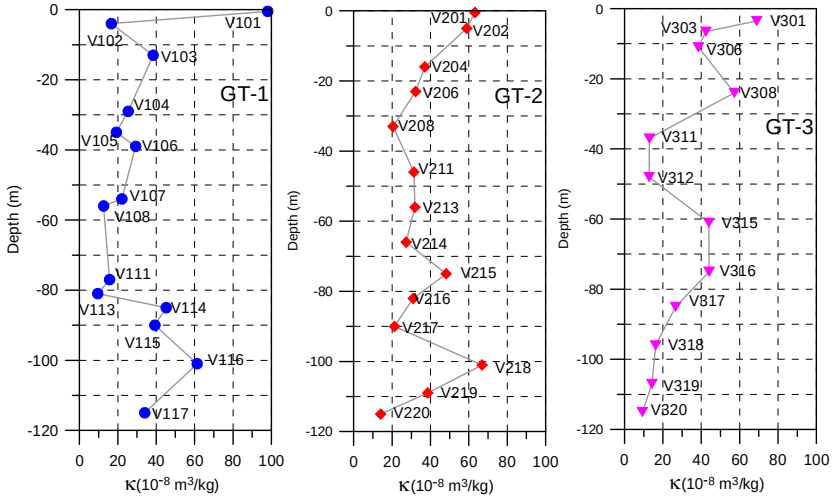

Figure 4.23. Mass specific magnetic susceptibility of soil samples.

4.3.6. Clay mineral identification

The clay fractions, which were separated from sieving process, are used for mineral identification. The sample is used for XRD measurement. Figure 4.24 presents an example of XRD investigation of sample V115. In the XRD chart, clay minerals are identified. Muscovite or illite (*M*) occupies about 40 percent of minerals. Kaolinite (*K*) and chlorite (*Chl*) occupy a total of 60 percent. K-feldspar and quartz minerals are identified at lower (non-significant) qualities.

The resulting clay mineral identification of the clay fraction is compiled in Table 4.5. The XRD investigation indicates that the clay fractions consist of muscovite (illite), kaolinite and chlorite minerals. The muscovite (illite) mineral is dominant among the clay minerals with a percentage in the range from 35 to 65 %. The percentages of kaolinite and chlorite minerals are varying in the same range from 15 to 35%.

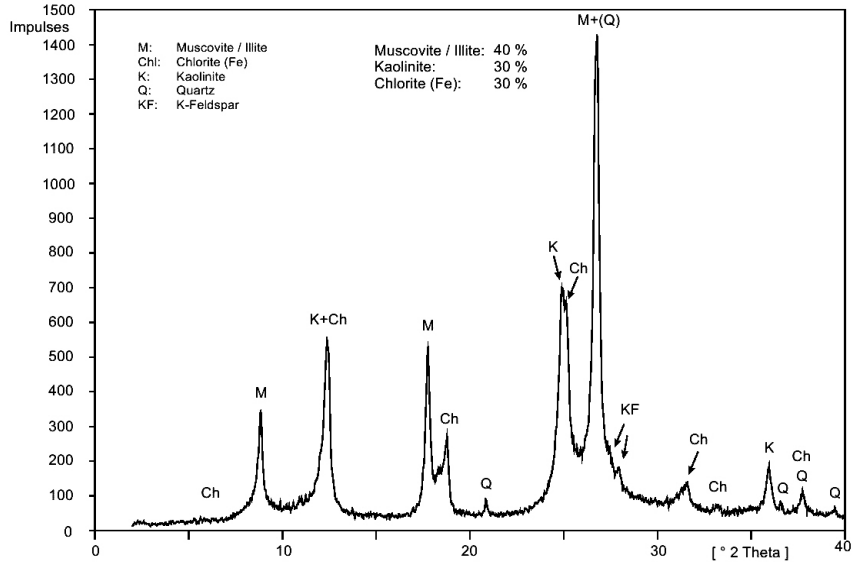

Figure 4.24. Clay mineral identification of sample V115 by XRD method.

Table 4.5. Clay mineral identification of clay fraction from boreholes.

ID	M (%)	K (%)	Chl (%)	ID	M (%)	K(%)	Chl (%)	ID	M (%)	K (%)	Chl (%)
V102	50	25	25	V201	65	15	20	V306	70	15	15
V113	50	30	20	V214	45	30	25	V315	50	25	25
V114	40	35	25	V215	45	25	30	V316	55	20	25
V115	40	30	30	V216	45	30	25	V317	50	25	25
V116	35	35	30	V219	40	35	25	V320	45	30	25
V117	40	30	30								

4.4. Hydrogeological investigations

4.4.1. Groundwater conductivity

In my study in Nam Dinh coastal area, the electrical conductivity of groundwater from the Pleistocene aquifer is investigated at 80 water wells. The groundwater is extracted from a depth of 80 to 145 m. In most wells, the groundwater is extracted from a depth of 110 m. Figure 4.25 displays the electrical conductivity distribution of groundwater for the Pleistocene aquifer. The electrical conductivity of groundwater is expressed in the unit mS/m. The position of water wells is also marked in the map. A conversion of electrical conductivity to TDS concentration is performed using equation (3.10). Fresh water is defined by a TDS value of lower than 1 g/l and saline water is determined by a TDS of higher than 3 g/l (Doan Van Canh et al., 2004). Two values of TDS concentration are indicated on the colour scale corresponding to an electrical conductivity of 150 and 450 mS/m according to equation (3.10). Following the map, the fresh groundwater of the Pleistocene aquifer is located in the Southwestern part of the study area. The saline water is distributed in the Eastern part of the study area. The boundary between fresh and saline groundwater follows the contour lines of electrical conductivity corresponding to TDS concentration. The location of contour lines is influenced by the density of the water wells in the study area. The density of water wells is larger in the fresh groundwater area while the number of wells is rare in the saline water areas. It should be noted that the distribution of wells causes distortion of the contour lines of the electrical conductivity map.

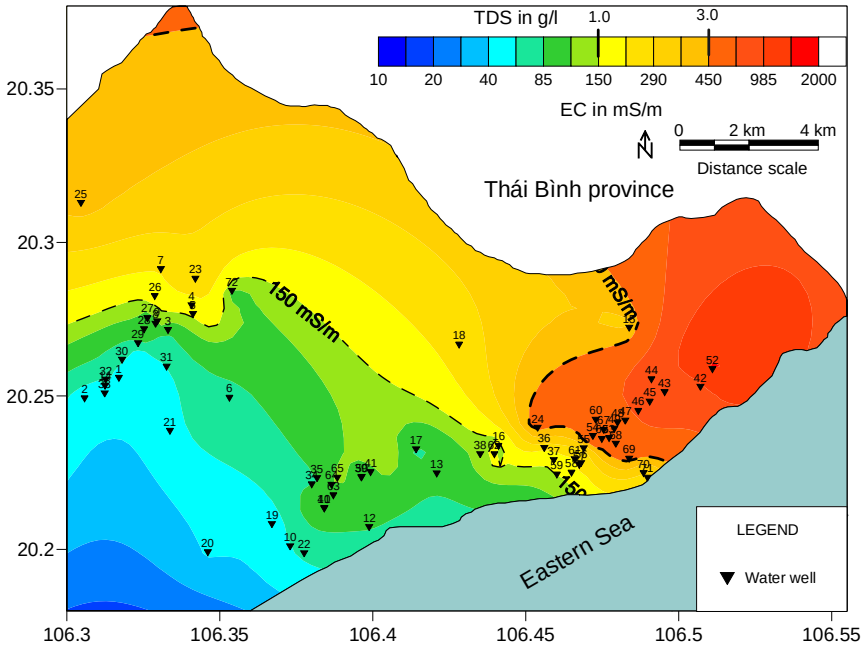

Figure 4.25. Electrical conductivity distribution in the Pleistocene aquifer.

4.4.2. Hydrological pumping test

The boreholes, which were drilled in the study area, were completed as water wells. The wells are cased by PVC pipes with a diameter of 76 mm. Pumping tests are individually performed at three wells. To calculate the hydraulic parameters of the Pleistocene aquifer, the drawdown of water table is recorded along with the pumping time. The pumping rate is constant during pumping time. The aquifer test of a well is continuously carried out for 3 hours.

The calculations of hydraulic parameters of the Pleistocene aquifer are applied according to pumping test for a single well with stable drawdown of the water table. To calculate the transmissivity parameter of the aquifer, Cooper - Jacob method is strongly suggested for aquifer test of a single well (Doan Van Canh et al., 2002). The drawdown of water table is expressed as a logarithmic function of time $S_h=f(lg(t))$, which should be presented as a straight line. The application of Cooper – Jacob method is valid for $u \leq 0.01$. The parameter u is determined by matching point using Theis curve. The transmissivity factor T_P is calculated by discharge volume of pumping test and drawdown difference Δs over a time interval of one log cycle:

$$T_P = \frac{2.3Q}{4\pi\Delta s}, \tag{4.2}$$

(Langguth, H. -R., and Voigt R., 2004). In equation (4.2), Q is in m^3/s, Δs is in m, and T_P is in m^2/s.

The hydraulic conductivity K_P of the aquifer is inferred from the transmissivity factor T_P and the thickness of aquifer h following equation:

$$K_P = \frac{T}{h}. \tag{4.3}$$

The K_P, calculated from equation (4.3), is represented for the hydraulic conductivity of the aquifer, when the well is fully screened. In my case study, only a section of 8 m at the bottom part of the aquifer is screened. Therefore, the thickness h in equation (4.3) is assigned by the length of filter screen (8 m) instead of total thickness of the Pleistocene aquifer because the ground water is extracted in the depth interval of filter screen. The K_P value is determined for the bottom part of the Pleistocene aquifer.

Figure 4.26 displays the graphs of drawdown of the water table during the pumping test at the three water wells. The drawdown of water table can be approximately described by the predicted straight line. The drawdown differences over one log cycle are indicated in the graphs. The transmissivity factor T_P and hydraulic conductivity K_P were calculated following equations (4.2) and (4.3). The resulting parameters of the pumping test and the well are compiled in the Table 4.6. The calculations of pumping tests show a slightly different value of transmissivity and hydraulic conductivity

between the boreholes. The difference of hydraulic conductivity between the water wells may be related to the grain size distribution of the Pleistocene formations. The pumping tests at the three wells result a hydraulic conductivity value of $8.5 \cdot 10^{-6}$ m/s for the bottom part of the Pleistocene aquifer.

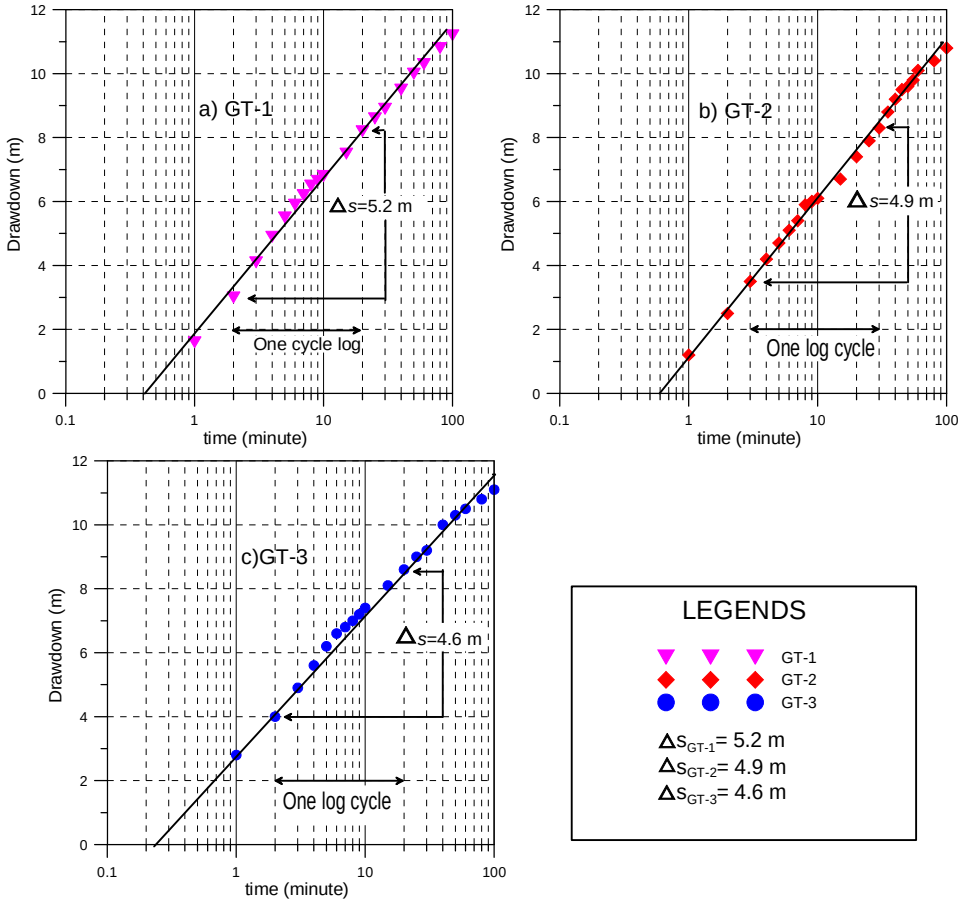

Figure 4.26. Drawdown of water table in pumping test of the three water wells.

Table 4.6. Parameters of the water wells and pumping tests.

Parameter	GT-1	GT-2	GT-3
Length of filter screen (m)	8	8	8
Bottom of screen (m)	113	110	90
Water table (m)	-3.4	-2.7	-2.3
Electrical conductivity (mS/m)	122	91	1482
TDS (g/l)	0.82	0.61	9.93
Discharge Q (m^3/s)	0.0017	0.002	0.002
Transmissivity factor T_P (m^2/s)	$5.9 \cdot 10^{-4}$	$7.5 \cdot 10^{-4}$	$7.9 \cdot 10^{-4}$
Thickness of aquifer (m)	39	38	34
Hydraulic conductivity K_P (m/s)	$7.5 \cdot 10^{-6}$	$9.3 \cdot 10^{-6}$	$9.9 \cdot 10^{-6}$

5. Data interpretation and discussion

5.1. Water content and porosity

Water content describes the volumetric fraction of water contained in the sample while the porosity regards the volumetric fraction of pore space in the sample. For a fully saturated sample, the volumetric water content is equal to the porosity in percent. The water content and porosity are related to other petrophysical parameters of the sample. The relationship between water content and porosity is related to the air volume of the sample. In my study, the water content and porosity are determined by the total volume of sample and the water quantity in the sample. Figure 5.1 shows the relationship between the porosity Φ and the volumetric water content Θ of all soil samples in the study area. The figure displays a linear relationship between porosity and water content. The fitting curve is described by a linear equation with a slope of +1:

$$\phi = \Theta + 3.9\ \% \qquad (5.1)$$

and with porosity and water content given in percent. The fitting curve results a coefficient of determination R^2=0.91. The value of 3.9 % in equation (5.1) is related to the mean volumetric air content of the samples which is generated by the evaporation of water in the sample during the transported and storage process.

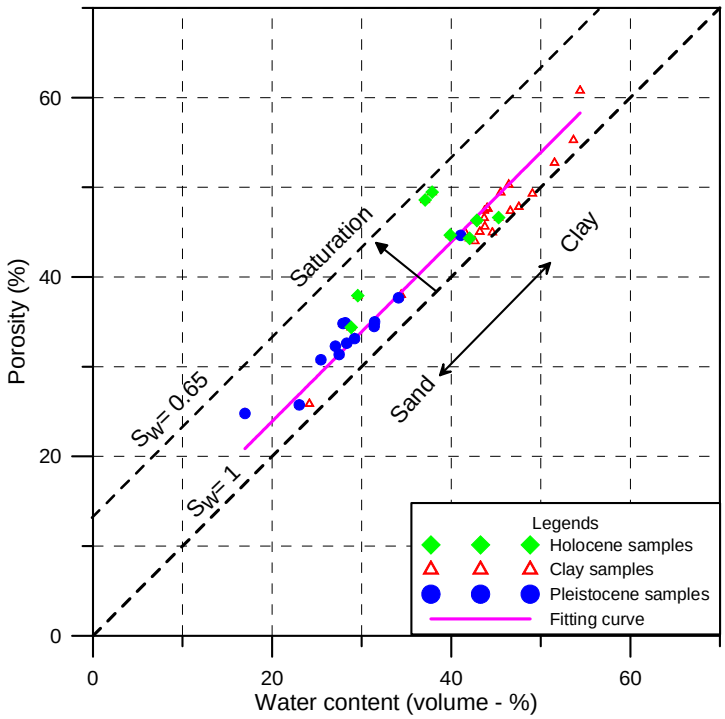

Figure 5.1. Relationship between porosity and water content of samples.

In Figure 5.1, the clayey and sandy samples are presented in different symbols and colors. The sandy samples show a lower porosity and water content while the clayey samples present higher values. The clayey samples show a value higher than 40 % for both porosity and water content. Only the samples V319 and V320 indicate a value lower than 40 % of porosity and water content because the gravel fraction is dominant in their lithological composition. A decrease in porosity and water content is related to a transition from clayey to sandy samples. The Pleistocene samples show a value of porosity and volumetric water content less than 40 %. Both porosity and volume water content of the Holocene samples is in the range from 30 to 50 %. This indicates that the clay content of the Holocene samples is higher than that of the Pleistocene samples. The saturation parameter is displayed as the lines parallel to the diagonal of figure. The fully saturated samples, S_w =1, is represented by the diagonal. All samples locate between two saturation lines of 0.68 and 1. The clayey samples distribute closely to the saturation line S_w =1. This indicates that the clayey samples are fully saturated. The sandy samples show a lower value of saturation.

5.2. Correlation of clay content and natural gamma ray activity

The natural radioactivity of formations, which is measured by gamma well logging tool, is strongly related to the clay content of sediments. To find out the correlation of the clay content and the radioactivity of geological formations, the mass related clay content (*CC*) of soil samples and the count rate of gamma rays are used. The mass related clay content of soil samples is determined from the sieving process. The count rates of gamma rays are derived from natural gamma logging. Because the gamma ray activity is recorded for every 0.05 m, a moving average of 10 reading values is applied to get the mean value of gamma log. It means that an average count rate of gamma ray activity is determined for every interval of 0.5 m in the borehole.

Figure 5.2 shows the relationship between the clay content (*CC*) of soil samples and the count rate of gamma rays (G_r), which are emitted by geological formations. Seven soil samples are taken from the Pleistocene aquifer. The count rates of gamma rays are derived at the same depth of soil samples from gamma log. The soil sample V320 belongs to Le Chi formation, which is located below the depth of 90 m at the borehole GT-3. The count rate of gamma rays corresponding to sample V320 is the average value of the Le Chi formation at the borehole GT-3. The acquired data from sieving process and gamma logging shows a good correlation. The red solid line represents the linear equation

$$G_r = 8CC + 29.7, \tag{5.2}$$

with the coefficient of determination $R^2 = 0.99$.

The equation (5.2) implies that the count rate of natural gamma rays per second reduces to 29.7 cps when the clay content of formation becomes zero. That means that the minimum value of gamma ray activity comes from other sources. This relationship indicates that the gamma ray to a large extent originates from clay minerals in the formation. Unfortunately, well logging data is not available at the depth of more than 80 m at the borehole GT-1. Therefore, the soil samples of borehole GT-1 are not used in this relationship.

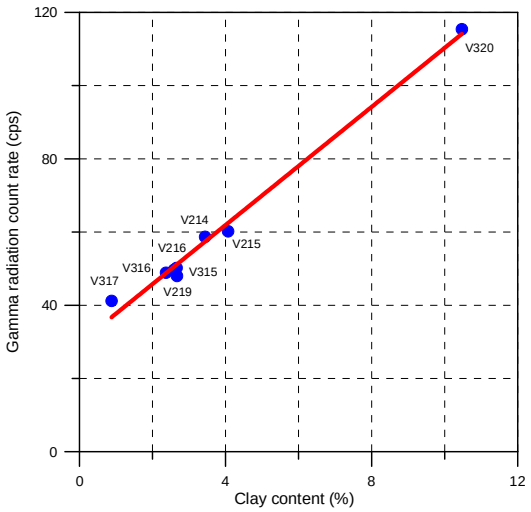

Figure 5.2. Relationship of clay content and natural gamma radioactivity.

Comparing the gamma logs of the boreholes in the study area, it is easily identified that the count rates of gamma rays becomes higher than 100 cps for the clayey sediments. The sandy formations of the Pleistocene aquifer are presented by count rate of gamma rays of around 50 cps. Based on the gamma log, the interface between sandy and clayey layers is identified. Figure 5.3 shows the gamma logs of boreholes GT-2 and GT-3. Both gamma curves indicate clearly a separation of clayey and sandy formations. At the borehole GT-2, a clay lens, which is interbedded in the Pleistocene aquifer, is identified in the depth interval from 82 to 92 m. The Pleistocene aquifer includes two phases: from 65 to 82 m and from 92 to 113 m. At the borehole GT-3, the interface between clayey and sandy formations is located at a depth of 56 m. The sediment changes from sand to clay at a depth of 90 m. In the geoelctrcial data interpretation, the equivalent problem regarding the resistivity of formations indicates that the resistivity of clay sediment is similar to the resistivity of sandy formation containing saline water. Therefore, the electrical resistivity investigations are limited to distinguish the clayey and sandy formations in the saline water area. In this case, the gamma log is useful to identify the interface between sandy and clayey layers. Sandy sediments, which have a low resistivity, are the saline water bearing formations.

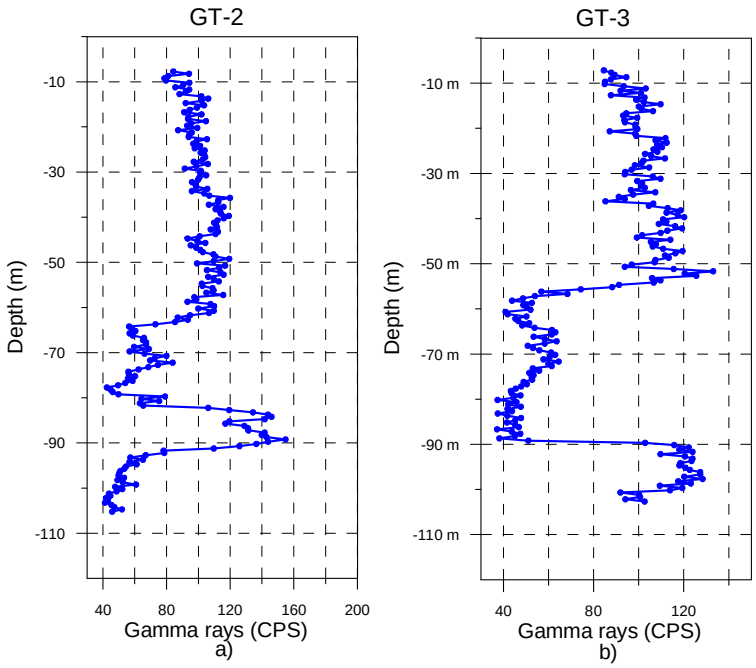

Figure 5.3. The natural gamma well logging: a) GT-2, b) GT-3.

Comparing the gamma log at boreholes GT-2 and GT-3 in the section of Pleistocene aquifer, the count rate of gamma rays of borehole GT-2 is higher than that of borehole GT-3. This implies that the clay content of the formation in the borehole GT-2 is higher than in GT-3. Based on the natural gamma logs, the clay content of formation can be estimated. Wonik (2007) used a simple way to calculate the clay volume fraction of a formation from natural gamma log based on the following equation:

$$V_{shale}(\%) = \frac{Gr - Gr_{min}}{Gr_{max} - Gr_{min}}(\%) \tag{5.3}$$

In equation (5.3), V_{shale} is the clay volume fraction (%) regarding the radioactivity of natural gamma rays. Gr is the count rate of gamma rays per second at sampling position. Gr_{min} is the count rate of gamma ray activity in a formation without any clay and Gr_{max} is the count rate of gamma ray activity in a pure clay formation. The clay volume fraction, which is estimated from the gamma log, indicates the upper limit of clay volume of the formation because the gamma ray signals may include other radioactive sources.

The clay volume fraction is estimated for the formations of the boreholes GT-2 and GT-3 at the depths of soil samples in the Pleistocene aquifer. The Gr value is directly derived from gamma logs. The G_{rmin} value is 29.7 cps, which is the minimum count rate of gamma ray activity according to the relationship in equation (5.2). For the G_{rmax}

value, a simple determination is needed. In the study area, high value of gamma ray activity is identified in the section of Le Chi formation in the borehole GT-3. The count rate of gamma ray activity is 115.4 cps for the sample V320, which shows a clay content value of 10.5 %. For the pure clay formation (100 % clay content), the count rate of gamma ray activity should be 1099 cps. Therefore, the inferred value of 1099 cps is used as the maximum count rate of gamma ray activity for whole study area.

The clay volume fractions of formations V_{shale}, which are listed in Table 5.1, are calculated according to the equation (5.3). The results show the clay volume fraction of the Pleistocene formations in the range from 0.011 to 0.029 %. For the Le Chi formation (corresponding to sample V320), the clay fraction occupies 0.8 % volume of formation. Comparing the calculated results for samples, the clay volume fraction of borehole GT-2 is higher than that of borehole GT-3. This is in agreement with mass related clay content of the Pleistocene samples, which were determined by sieving process. The average mass related clay content of samples at borehole GT-2 is 3.2 % and borehole GT-3 is 2%. The clay content of sediments is related to resistivity of formation because clay in the water acts as a conductor.

Table 5.1. Clay volume fraction calculated from gamma ray activity.

Sample ID	G_r (cps)	CC (%)	G_{rmin} (cps)	G_{rmax} (cps)	V_{shale} (%)
V214	58.7	3.4	29.7	1099	0.027
V215	60.2	4.1			0.029
V216	49.7	2.6			0.019
V219	48.2	2.7			0.017
V315	50.2	2.7			0.019
V316	48.9	2.4			0.018
V317	41.2	0.9			0.011
V320	115.4	10.5			0.080

The clay volume fractions, which are regarded to the gamma ray activity, are comparable to the mass related clay content determined by the sieving process. Figure 5.4 displays the correlation between the mass related clay content and the clay volume fraction of the Pleistocene samples. The correlation is based on the mass related clay content and the clay fraction of seven samples in the Pleistocene formation, which were listed in Table 5.1. The data base fits well to the through origin curve (the red solid line) with coefficient of determination R^2=0.99. The fitting equation has a form as

$$V_{shale}\,(\%) \sim 0.00731\ CC\,(\%), \qquad (5.4)$$

where V_{shale} is the clay volume fraction in percent, which is calculated from gamma log and *CC* is the mass related clay content determined by the sieving process. The sandy samples, which belong to the Pleistocene aquifer, show a clay fraction of less than 0.03 % of formation volume. It is corresponding with a mass related clay content of less than 4.1 %. This is a good relationship between the mass related clay content and the clay volume fraction of the samples.

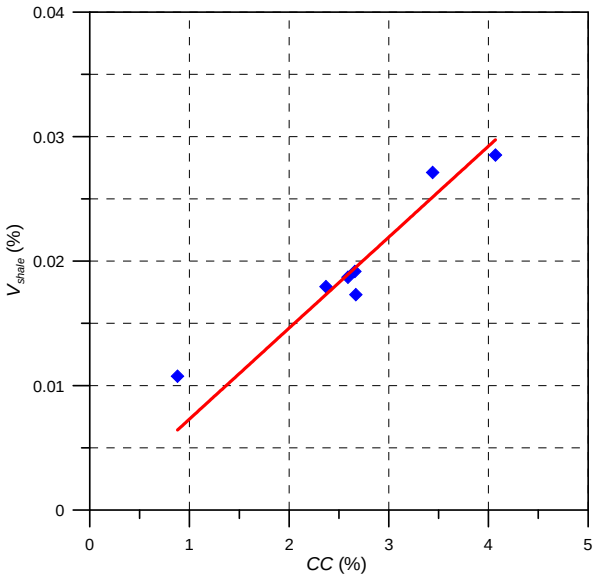

Figure 5.4. Correlation between mass related clay content and clay volume fraction.

5.3. A comparison of the electrical resistivity investigations

5.3.1 Combined inversion of VES and TEM soundings

Electrical resistivity surveys are used to evaluate the hydrogeological situation of the aquifers within the study area. The results describe the local geological structures and the electrical conductivity of the pore water in the aquifers. The resistivity of formation, which is investigated by VES, RI, TEM, resistivity logs and LAB resistivity of soil samples, can be used to estimate the hydrogeological characteristics of the aquifers. At the positions of the borehole, where the geological structure is known, a combined inversion between VES and TEM is performed to reveal the local geological structure. The results of the related inversions show the advantages of the methods for the case study in Nam Dinh coastal area. In the actual application of data interpretation, the principle of equivalence is applied to get a suitable model. The principle of equivalence indicates that the resistivity and thickness of layer cannot be determined independently (Parasnis, 1986). Regarding the so-called T-equivalence, an increasing resistivity of layer requires a decreasing thickness of layer or inversely. To

get a suitable model of local structure, several models with different resistivity and thickness of layers result from inversion of VES and TEM soundings. The RMS error after inversion and the geological information from the borehole help to decide which model is suitable to describe the local structure. In the case study in Nam Dinh coastal area, TEM soundings are performed close to the position of boreholes GT-1 and GT-2. At the position of boreholes, VES soundings are carried out by IPR-12 system with an inverse Schlumberger Wenner configuration. The IPR-12 system provides a higher power and accuracy of measurement. The VES soundings, which are carried out by IPR-12 system, are used in a combined inversion with TEM sounding at the positions of the boreholes.

Figure 5.5 shows the inversion results of the electrical resistivity investigations which are performed at the position 450 m on the RI profile B at the location of borehole GT-1. The layered model of VES D6, VES GT-1, a 2D cross section of RI, the layered model of TEM GP1, the resistivity log of R32 and the stratification of borehole GT-1 are presented in the Figure 5.5. The VES D6 is performed by the Schlumberger configuration with a distance of 50 m from the borehole GT-1. The inversion process yields a model of four layers with three main layers corresponding to the Holocene, Pleistocene aquifers and an aquitard. The first layer with a resistivity of 5 Ωm and a thickness of 1 m is the overburden layer. The model of four layers results in a RMS error of 6.5%.

VES GT-1 sounding is inverted in the same way. A model of four layers with the depth of layers regarding the stratification of borehole GT-1 generates the theoretical curve. The inversion results in a RMS of 8.3 %. This error is acceptable for 1D inversion of VES. The overburden layer is not resolved by VES GT-1 because the minimum electrode spacing is 60 m. The depth of layers is fixed regarding the interface between layers of geological structure. The inversion process yields a resistivity of 17 Ωm for the Holocene aquifer and 15 Ωm for the Pleistocene aquifer. The clay layer (aquitard) is divided into two layers. The upper clay layer corresponds to the soft and muddy clay layers in the stratification of borehole with a resistivity of 0.7 Ωm. The lower clay layer consists of clay with fine sand and plastic clay with a resistivity of 3 Ωm. This is a transition layer. Comparing the models of VES D6 and VES GT-1, the RMS error of VES GT-1 inversion is higher than that of VES D6 but the model considers the depth of layers regarding to the stratification of borehole GT-1 (Figure 5.5c). The model of VES GT-1 also reflects the variation of resistivity with depth in the resistivity log curve (Figure 5.5e).

The TEM GP1 is measured at the position of borehole GT-1 with a distance of 50 m to the borehole. Figure 5.5d depicts an inverted model of TEM GP1 sounding. The TEM model includes four layers. The depth of the layers is fixed following the stratification

of borehole GT-1. The inversion yields resistivity of each layer with a RMS error of 4.8 %. The first layer shows a resistivity of 1.8 Ωm. This resistivity value is less than the results of VES and RI because the TEM GP1 sounding is measured on the salt field, which is periodically flooded by sea water. This layer corresponds to the Holocene aquifer with a thickness of 18 m. The second layer extends from 18 to 53 m of depth with a resistivity of 0.8 Ωm. This layer corresponds to the soft clay and muddy clay layer in the bohrehole GT-1. The third layer with a thickness of 28 m and a resistivity of 16 Ωm presents the transition layer from clayey to sandy formation. The deepest layer shows a resistivity of 2000 Ωm (Figure 5.5d) and an infinite thickness. A very high resistivity of the deepest layer means that no eddy current of TEM can be solved in this layer. The above clay layer forms a screen which prevents the penetration of the electromagnetic field. This is a disadvantage of electromagnetic methods in the exploration of coastal aquifers, where a clay layer or saline water aquifer generates a screening effect on electromagnetic propagation. Due to the screening effect, the resistivity of the third layer in the TEM model is higher than the true resistivity of clay sediment. It should be noted that the resistivity of the third layer reaches the resistivity of the Pleistocene aquifer.

Figure 5.5e presents the resistivity log R32 in the borehole GT-1. Well logging data is only available in the interval of depth from 10 to 80 m. The resistivity log can be divided into three layers regarding the stratification of borehole GT-1. The first layer extends from 10 to 18 m with a resistivity in the range from 1 to 8 Ωm corresponding to the clayey sand layer. The second layer with a resistivity of less than 1 Ωm corresponds to the soft clay and muddy clay layers in the borehole. The third layer extends from 53 to 80 m of depth with a tendency of increasing resistivity, which reflects the transition from clayey to sandy formation. This layer shows a variation of resistivity from 1 to 5 Ωm. Unfortunately, the resistivity log is not available at a depth of more than 80 m. But the tendency of curve indicates an increasing resistivity with depth (Nguyen Trong Vu et. al., 2010).

Comparing the results of VES, RI, TEM, well log and stratification of the borehole GT-1 helps to determine the local geological structure and the hydrogeological situation of the aquifer. The Holocene aquifer extends from the surface to a depth of approximately 18 m. The resistivity of the Holocene formation is around 12 Ωm (resistivity of sample V102 at a depth of 4 m). VES and RI section show a resistivity of around 15 Ωm for the Holocene aquifer. These resistivity values of the layer indicate that the Holocene aquifer contains freshwater at the location of borehole GT-1. The clay layer, which extends from 18 m to 81 m of depth, approximately, is an aquitard. The electrical resistivity investigations show a resistivity from 0.4 to 5 Ωm. This layer plays an important role to separate the two aquifers but it also causes a

screening effect of the TEM investigation. The Pleistocene aquifer lies below a depth of 81 m. The electrical resistivity results show a resistivity of around 15 Ωm for the Pleistocene aquifer. The resistivity of groundwater at the well GT-1 is 8.2 Ωm corresponding to a TDS of 0.82 g/l. The electrical resistivity investigations indicate that the Pleistocene aquifer contains fresh water.

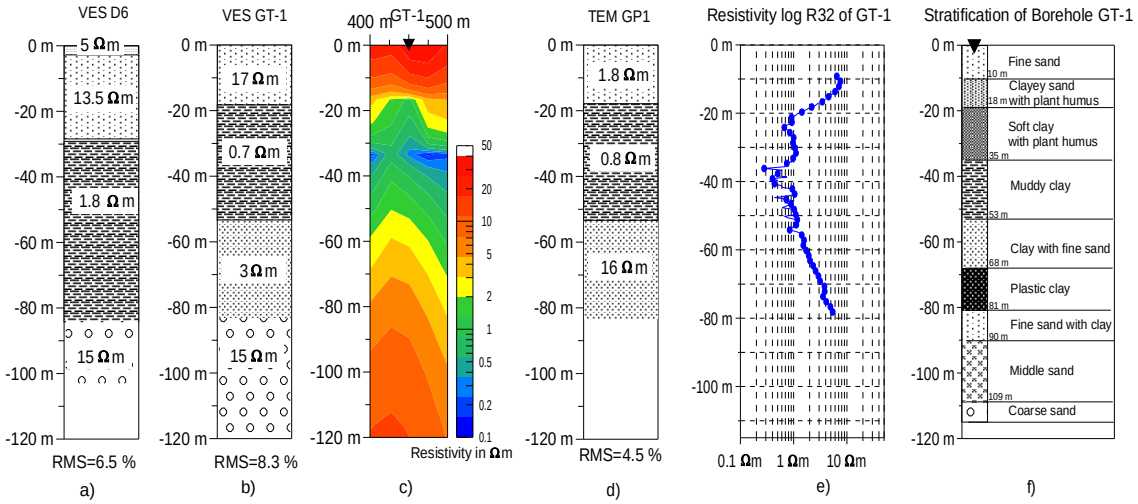

Figure 5.5. Comparison of the electrical resistivity investigations at position 450 m at profile B: a) model of VES D6, b) model of VES GT-1, c) RI section d) TEM GP1, e) R32 log, f) Stratification of borehole GT-1.

Borehole GT-2 is located at the position 2100 m at the RI profile B. VES GT-2 is performed at position of borehole while TEM GP6 is carried out in a distance of 200 m from the borehole. Figure 5.6 shows two models of VES GT-2, a 2D section of RI, the model of TEM, the log R32 curve and the stratification of borehole GT-2. The inversion of VES GT-2 yields two models with different numbers of layers. The first model presents eight layers and the depth of layers is fixed according to the stratification of borehole GT-2. The inversion results in a RMS error of 5.8 % but the structure seems to be more complex than the second model in which the intermediate layers are hidden. The second model shows a simple structure of geological formation including five layers. The Holocene aquifer extends from the surface down to a depth of 7.5 m with a resistivity of 0.5 Ωm. This indicates the saline water containing Holocene aquifer. The clay layer shows a resistivity of 1.4 Ωm. A transition layer with resistivity of 8 Ωm extends from 45 to 65 m of depth. The Pleistocene aquifer locates from 65 to 113 m of depth with a resistivity of 25 Ωm. This resistivity value is in agreement with RI and resistivity log investigations. The deepest layer with a resistivity of 4.8 Ωm is clay layer, which belongs to Le Chi formation. The second

model results in a RMS error of 6.9 %. Although, the RMS error is higher than in the first model, the second model is more reliable than the first model. The clay layer, which is embedded in the Pleistocene aquifer, is not resolved by RI (Figure 5.6c) and VES.

Figure 5.6d sketches a model of four layers for TEM GP6 sounding. The first layer is the Holocene aquifer with a resistivity of 2.6 Ωm and a thickness of 7.5 m. The clay layer presents a resistivity of 0.65 Ωm. This layer is an aquitard including soft clay and clay with shells. The third layer indicates a transition layer with a thickness of 20 m and a resistivity of 19 Ωm. The resistivity of the third layer reaches to the resistivity of the Pleistocene aquifer indicated by VES, RI, and log R32 investigations. The deepest layer (Figure 5.6d) results in a resistivity of 2000 Ωm because of screening effect. The inversion of TEM GP6 results in a RMS error of 6.1 %.

The resistivity log R32 curve is available in the interval of depth from 8 to 106 m (Figure 5.6e). In the interval from 8 to 45 m of depth, the log R32 shows a resistivity of less than 2 Ωm. This section corresponds to the clay layer of VES, TEM model and the stratification of borehole GT-2. The resistivity of the transition layer varies in the range from 2 to 20 Ωm in the interval of depth from 45 to 65 m. The Pleistocene aquifer is presented by a resistivity of around 30 Ωm in the log R32. A clay layer with a resistivity of around 10 Ωm is determined in the interval of depth from 82 to 92 m. This layer is also identified by the stratification of borehole GT-2. The resistivity of the Pleistocene aquifer indicates a fresh water bearing formation. The resistivity of groundwater at the well GT-2 is 11 Ωm, corresponding to a TDS of 0.66 g/l.

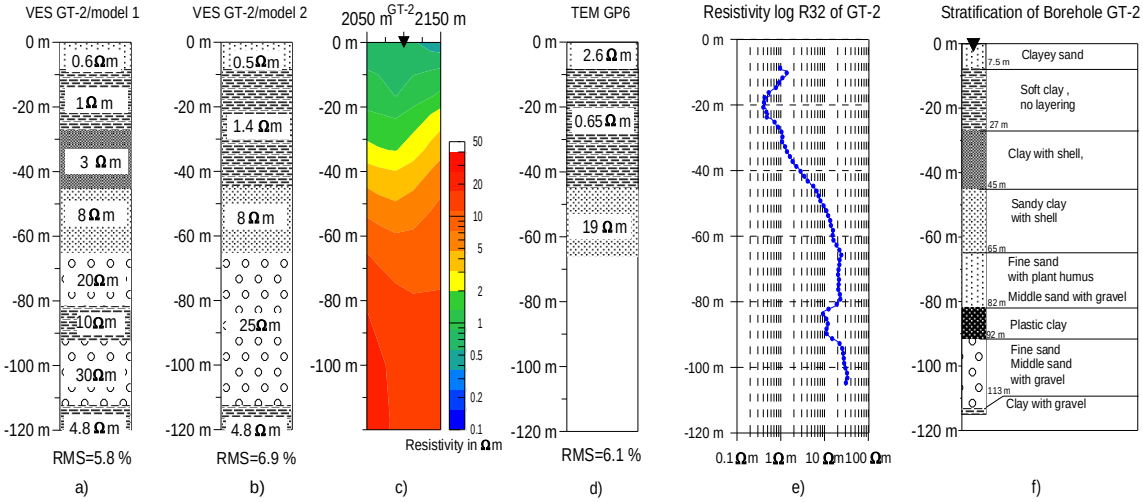

Figure 5.6. Comparison of the electrical resistivity investigations at position 2100 m at RI profile B: a) VES GT-2/model 1, b) VES GT-2/model 2, c) RI section, d) TEM GP6, e) R32 log, f) Stratification of borehole GT-2.

5.3.2. A comparison of RI and TEM results

RI and TEM investigations are carried out along the profile C (Giao Xuan commune). To evaluate the hydrogeological situation of the Pleistocene aquifer along profile C, the results of RI and TEM investigation are compared. Figure 5.7 shows the resistivity of the Pleistocene formation, which results from RI and TEM investigation along profile C. The resistivity of the water, which is extracted from the Pleistocene aquifer, is also presented in Figure 5.7. The TDS value is indicated for every well. The TEM soundings along profile C are inverted by a model of four layers. The resistivity of the deepest layer in the TEM models is comparable with formation resistivity from RI investigation at the same position. The resistivity of RI is derived at a depth of around 100 m. The positions of TEM soundings are also indicated in the graph. Generally, both RI and TEM show a tendency of decreasing resistivity from the Southwestern part to the Northeastern part of the profile. The same tendency is indicated by the resistivity values of water in the Pleistocene aquifer. The resistivity value of TEM inversion is slightly lower than that of RI. The result of RI and TEM inversion show a resistivity in the range from 4 to 8 Ωm along profile. The resistivity of the Pleistocene aquifer is higher than 5 Ωm from Southwestern beginning of the profile to the position of 900 m and less than 5 Ωm in the remaining part of profile. This corresponds to the resistivity of ground water in the Pleistocene aquifer. The TDS values of ground water are less than 3 g/l in the Southwestern part and higher than 3 g/l in the Northeastern part of the profile. Considering the resistivity of RI, TEM and Pleistocene water, the saline water boundary can be determined at the position of around 900 m of the profile.

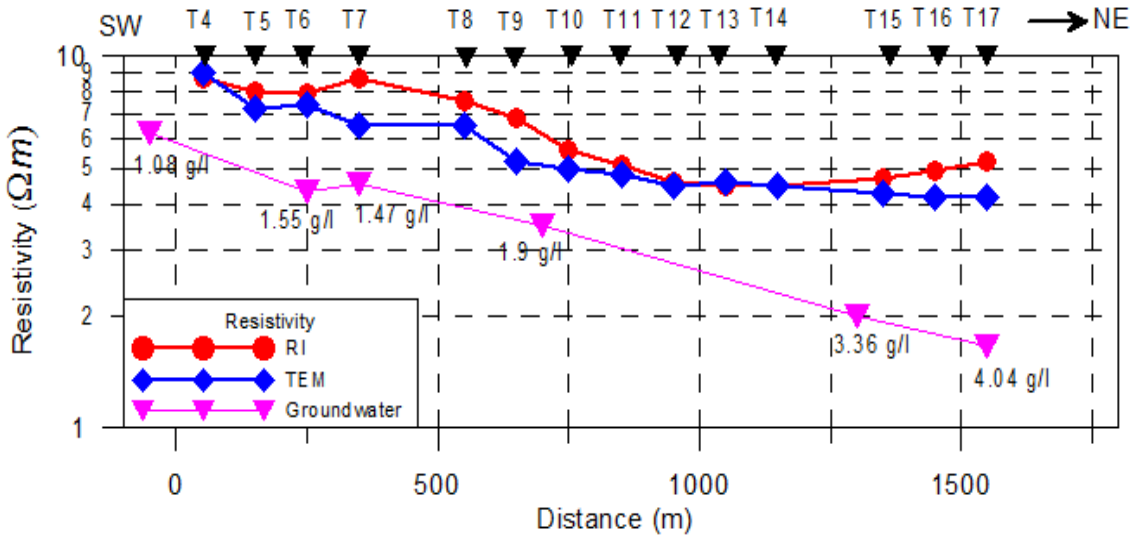

Figure 5.7. Resistivity of the Pleistocene aquifer derives from RI, TEM and resistivity of the Pleistocene water along profile C.

5.3.3. A comparison of field and laboratory resistivities

The formation resistivity depends to a large extent upon the conductivity of pore water. Assuming a nearly identical lithologic formation, the formation resistivity can be used to classify fresh and saline water bearing formations. In my study, the electrical resistivity investigations, which are carried out both in the field and laboratory, show a wide range of formation resistivity. Although, the measurements in field and laboratory have different resolution, the results of electrical resistivity investigations at the same location should be comparable.

The results of the electrical resistivity investigations, which are performed at the location of three boreholes, are used to compare the formation resistivity. The electrical resistivity investigations are individually performed at different time. First, RI was performed. Well logging is carried out after the drilling process. The laboratory resistivity is measured on the drilling cores of the boreholes. Figure 5.8 shows the results of the electrical resistivity investigations at the locations of three boreholes varying with the depth. The laboratory (LAB) investigation yields the resistivity of soil samples. Another resistivity is derived from RI investigation at different depths. A moving average of log R32 resistivity is applied to determine a characteristic resistivity of the formation. The log R32 resistivity reflects the true resistivity of formation. To compare the results of electrical resistivity investigation, the relative error between LAB, RI and log measurements is calculated. The relative error e_r between two measurements is calculated by

$$e_r(\%) = \frac{|\rho_m - \rho_{Log}|}{\rho_{Log}} = \frac{\Delta\rho}{\rho_{Log}}\,(\%), \tag{5.5}$$

where ρ_m is the measured formation resistivity (LAB or RI resistivity), ρ_{Log} is resistivity of formation derived from log R32.

For a certain borehole, the Root Mean Square (RMS) deviation is calculated for all measured data. The RMS deviation between two investigations is determined by

$$RMS(\%) = \sqrt{\frac{1}{N}\sum_{i=1}^{n}\left(\frac{\rho_{mi} - \rho_{Logi}}{\rho_{Logi}}\right)^2}\,(\%), \tag{5.6}$$

where N is the number of measurements. The RMS deviation measures the accuracy between two investigations. A small relative error or RMS deviation reflects a good measure of agreement between two investigations. In my case study, the log resistivity is derived from log R32 at the sample depth of LAB and RI resistivity. The relative error is calculated following equation (5.5). The LAB, RI, log R32 resistivity and the calculated relative error are listed in Table 5.2.

Figure 5.8a shows the resistivity distribution of RI, Log R32 and LAB versus depth at the location of borehole GT-1. Generally, the electrical resistivity investigations present a similar value of resistivity at the same depth. For the Holocene aquifer, the investigations show a resistivity higher than 10 Ωm. The clay layer shows a resistivity of less than 2 Ωm. An increasing of resistivity from 2 to 10 Ωm in the section from 60 to 80 m of depth reflects the changing of sediments from clayey to sandy formations. The resistivity of LAB investigations is higher than 10 Ωm for the Pleistocene samples (from 90 to 115 m of depth). The RI resistivity presents an increase from 8 to 11.6 Ωm in the section from 96 to 115 m. The resistivity log is not available in the Pleistocene aquifer but tendency of increasing resistivity with depth is assumed. This is in agreement with the RI and LAB resistivity results. The relative error between the LAB and log R32 measurements varies in the range from 15.3 to 53 %. The RMS deviation between LAB and log R32 measurements is 35 %. The relative error between RI and log R32 investigations is in the range from 9 to 78.1 % and RMS shows a value of 45 %.

Figure 5.8b displays the results of resistivity investigations at the location of borehole GT-2. The resistivity distribution varying with the depth shows a similar shape for all three curves. The Holocene formation, which extends from surface to a depth of around 10 m, shows a resistivity of less than 2 Ωm. This value indicates the Holocene aquifer containing saline water. The minimum resistivity of the clay layer is 0.4 Ωm (resistivity log R32) at the depth of around 20 m. This value is smaller than the resistivity of the clay layer in the borehole GT-1 because saline water may exist in the clay layer at the location of borehole GT-2. The resistivity increases with the depth and indicates a change in the lithological components of the sediments. The Pleistocene formation extends from 65 to 113 m of depth. A clay layer is identified within the Pleistocene aquifer by the LAB and resistivity log R32. Although RI does not resolve the clay layer, the RI resistivity approaches the true resistivity of formation. The statistics of data show a relative error in the range from 13 to 70.3 % for LAB and log resistivity measurements. The RMS calculation between LAB and log R32 resistivities of borehole GT-2 is 43.9 %. The relative error between RI and log R32 resistivity measurements varies in the range from 20.9 to 60.2%. The RMS deviation between RI and log R32 resistivity investigations is 43.1%.

The results of the electric resistivity investigations are slightly different at the location of borehole GT-3 (Figure 5.8c). The Holocene formation and clay layer show a resistivity of less than 2 Ωm in the section from surface down to a depth of 50 m. This confirms that the Holocene aquifer contains saline water. In the section from 56 to 115 m of depth, RI and log R32 investigations show a value of less than 3 Ωm while the LAB resistivity results in a resistivity in the range from 3 to 12.3 Ωm. The LAB

resistivity is much higher than RI and log resistivities at a similar depth. The difference between LAB resistivity and log or RI resistivities is caused by saturation factor. The log and RI resistivity are assumed fully saturated formation resistivity. The soil samples were taken in Vietnam and transported to Germany in a long time. The evaporation of water during the transport of samples reduces the saturation and increases the resistivity of samples. Amount of evaporated water is not significant for clayey samples because the clay mineral confines the water. For sandy samples, the evaporation process is stronger and quicker. Therefore, the strong deviation happens for sandy samples. In this case, to get the saturated resistivity of soil samples, a correction is needed. Using the second Archie's equation, the fully saturated resistivity of soil sample can be determined:

$$\rho_0 = \rho_t S_w^n, \tag{5.7}$$

where ρ_t is LAB determined resistivity and S_w is saturation factor, which are determined by the LAB investigation, and n is saturation exponent. For most rocks, the saturation exponent n is about 2 (Schön, 1996). The saturated resistivity of samples, which is calculated by equation (5.7) with $n=2$, is used instead of LAB resistivity for all Pleistocene samples. The two corrected resistivity values of samples V316 and V317 are presented by the triangle symbols with black color in Figure 5.8c.

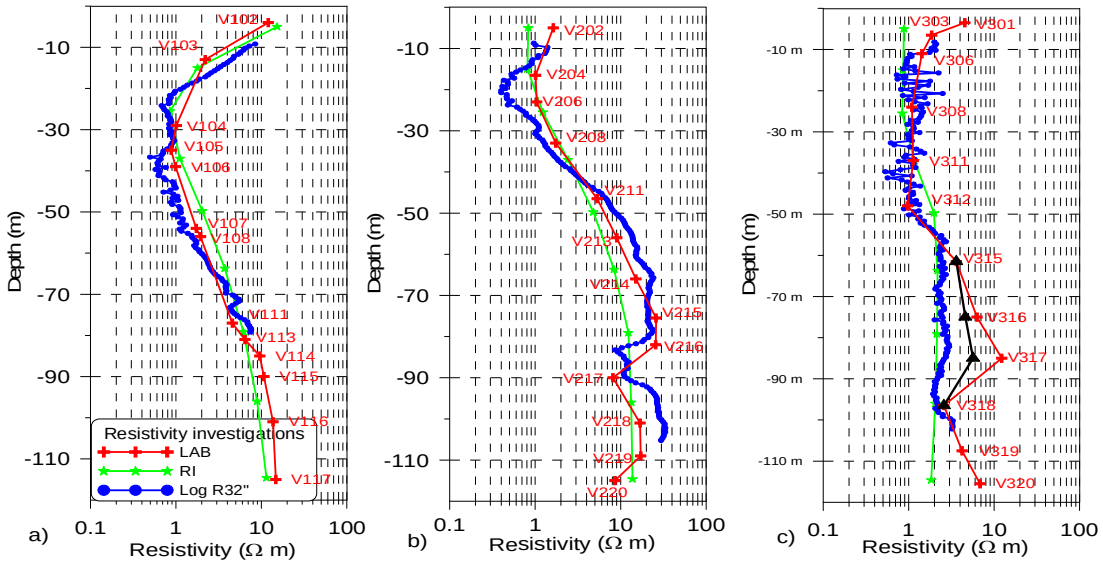

Figure 5.8. Comparison of LAB, RI and Log resistivity investigations at the locations of the three boreholes: a) borehole GT-1, b) borehole GT-2, c) borehole GT-3.

A strong deviation between LAB and log R32 resistivity measurements for the Pleistocene formations leads to a high value of relative error between LAB and log R32 resistivity measurements. Most measurements show a relative error value of less

than 41%. Two samples V316 and V317 present the relative error value of 84.0 and 108.4 %. Although these values are higher than the other one, they are acceptable. The RMS deviation between LAB and log R32 resistivity measurements is 53.4 %. For RI and log R32 resistivity measurements, the relative error varies in the range from 2.6 to 46.7 % and the RMS deviation results in a value of 21.9 %.

Table 5.2. Resistivity of formation at certain depths derived from electrical resistivity investigations and relative errors.

	Depth (m)	ρ_{LAB} (Ωm)	ρ_{Log} (Ωm)	e_r *(%)*		*Depth (m)*	ρ_{RI} (Ωm)	ρ_{Log} (Ωm)	e_r *(%)*
GT-1	-13	2.15	4.32	50.2		-15	1.79	3.1	42.3
	-29	0.99	0.86	15.3		-25	0.85	0.78	9.0
	-35	0.87	0.71	21.9		-37	1.11	0.66	68.2
	-39	0.97	0.76	28.0		50	2.03	1.14	78.1
	-54	1.70	1.11	53.0		-64	3.73	2.62	42.4
	-56	1.90	1.55	22.5		-79	6.15	7.43	17.2
	-77	4.46	6.91	35.5					
GT-2	-16	1.01	0.6	68.3		-15	0.81	0.67	20.9
	-23	1.04	0.66	57.6		-25	1.23	0.78	57.7
	-33	1.74	1.32	31.8		-37	2.42	1.86	30.1
	-46	5.31	6.1	13.0		-50	4.8	8.48	43.4
	-56	9.02	13.4	32.7		-64	8.38	21.07	60.2
	-66	15.09	22.5	32.9		-79	12.3	22.88	46.2
	-75	25.94	21.2	22.4		-96	15.16	26.67	43.2
	-82	25.72	15.1	70.3					
	-90	8.15	10.8	24.5					
	-101	16.89	29.9	43.5					
GT-3	-11	1.43	1.04	37.5		-15	0.86	1.20	28.3
	-24	1.09	1.42	23.2		-25	0.84	1.47	42.9
	-37	1.13	1.14	0.9		-37	1.17	1.14	2.6
	-48	0.97	0.92	5.4		-49	1.98	1.35	46.7
	-61	3.61	2.56	41.0		-64	2.17	2.47	12.1
	-75	4.63*	2.50	84.0		-79	2.14	2.50	14.4
	-85	5.71*	2.74	108.4		-96	2.05	2.18	6.0
	-96	2.58	2.18	18.3					

- Note: sign ‘‘*’’ - corrected resistivity value regarding the saturation of sample.

The resistivity values of formations at the same depth are comparable. Comparing the results of the electrical resistivity investigations at the locations of three boreholes, it can be inferred that the resistivity of the clay layer is less than 2 Ωm. The sandy

formations, including the Holocene and Pleistocene formations, show a variation range of resistivity from 0.4 to 26 Ωm. The resistivity of the sandy formation depends greatly upon the conductivity of pore water. The sandy formations, which have resistivity of less than 5 Ωm, are related to saline water bearing formations (the Pleistocene aquifer at borehole GT-3 and the Holocene aquifer at borehole GT-2 and GT-3). The fresh water bearing formations show a resistivity higher than 10 Ωm (the Pleistocene aquifer at the boreholes GT-1, GT-2 and the Holocene aquifer at the borehole GT-1). The water bearing formations, which have a resistivity in the range from 5 to 10 Ωm, are assumed to be filled by brackish groundwater. These limits of classification between saline and fresh ground water should be adjustable for different formations because the resistivity of formations not only depends on the conductivity of pore water but also on grain size fraction of formations. For example, the sandy formation of the Pleistocene aquifer at the locations of boreholes GT-1 and GT-2 shows different resistivity values although the two wells are located in the fresh ground water area. The differences of the Pleistocene formation resistivity may be related to the grain size fraction of the formation at the two boreholes. The clay and silt fraction dominate in the soil samples of borehole GT-1 while the sandy fractions are significant in the soil samples of borehole GT-2 (see Table 4.4).

5.4. Estimation of groundwater conductivity from electrical resistivity investigations for the Pleistocene aquifer

The Pleistocene aquifer is the main water bearing formation in the study area. The geophysical investigations try to evaluate the hydraulic condition of the aquifer. For an aquifer, the resistivity of the fully saturated formation is proportional to the resistivity of the water. As the result of this proportionality, the formation factor F is characterized by the first Archie equation:

$$\rho_0 = F\rho_w, \tag{5.8}$$

(Schön, 1996). In the equation (5.8), ρ_0 is the resistivity of saturated formation, ρ_w is the resistivity of pore water and F is the resistivity formation factor of the aquifer.

In the area of my study, the Pleistocene aquifer consists of unconsolidated sediment, composed of sand and gravel mixed with clay and silt. The geophysical investigations yield the resistivity of formations following individual investigations. Resistivities of formations, which are determined by VES, RI, TEM and well logging, can be assumed as the saturated resistivity. Resistivity of soil samples, which is determined by LAB investigation, does not represent the saturated resistivity because the saturation factor is less than 1. The saturation factor changes due to the evaporation of water in the samples. The decrease of the saturation factor leads to an increase in resistivity.

Therefore, in this correlation, the saturated resistivity of the Pleistocene samples, which is calculated by equation (5.7) with saturation exponent $n=2$, is used for all Pleistocene samples.

Based on the resistivity of groundwater at 36 domestic wells and 52 resistivity values of the Pleistocene formations according to the electrical resistivity investigations, the formation factor of the Pleistocene aquifer is determined. Position of the wells is close to the location of the electrical resistivity investigations with a distance of less than 100 m. The groundwater is extracted from a depth of around 110 m. The resistivity of the Pleistocene formation is derived from VES, RI, TEM, log R32 and LAB investigations. Figure 5.9 shows a relationship between resistivity of formation and the resistivity of groundwater in the Pleistocene aquifer. The solid line presents the fit through origin of the data base. It has a form

$$\rho_0 = 1.97\rho_w, \tag{5.9}$$

with a coefficient of determination $R^2=0.98$. The slope of fitting line is 1.97. This value is the apparent resistivity formation factor of the Pleistocene aquifer relating the resistivity of both the formation and pore water.

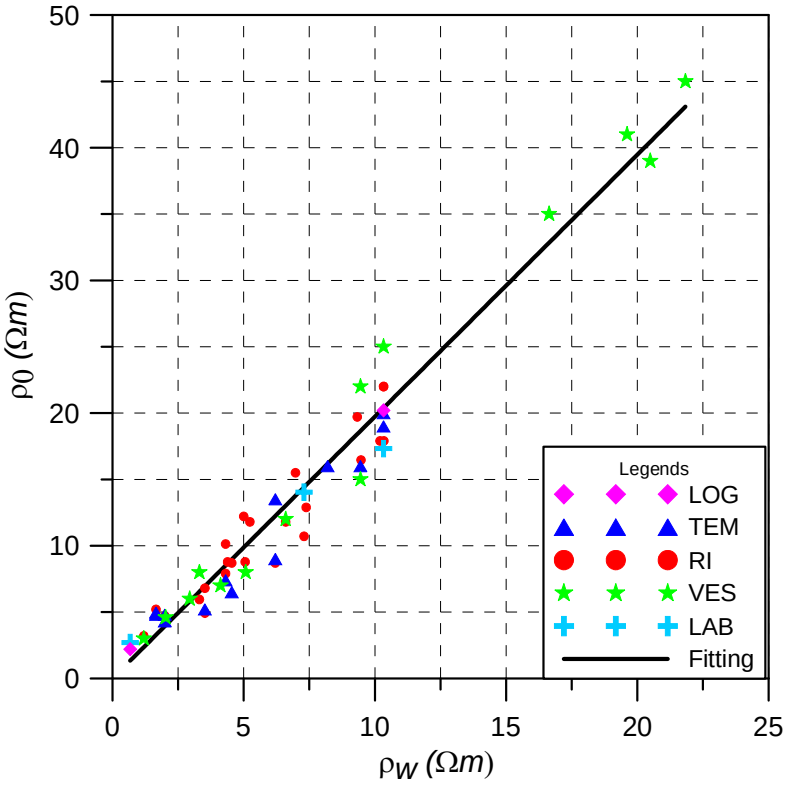

Figure 5.9. The relationship between resistivity of formation and pore water in the Pleistocene aquifer.

All soil samples in a borehole were investigated by SIP using a water conductivity that is close to the water conductivity measured in the borehole. The apparent formation factor related to the resistivity of the samples varies in the range from 1.01 to 10.23. The value of formation factor varies in a large range because of the existence of clay in the sample. Clay in wet samples acts as a conductor, therefore resistivity of sample decreases with increasing clay content. Tiab and Donaldson (2004) showed that for a clayey sand aquifer, the formation factor decreases as brine resistivity, ρ_w, increases. However, the resistivity of the formation and the apparent formation factor are not proportionally increased. The difference in formation factor between soil samples indicates the existence of clay in the water bearing formations of the Pleistocene aquifer. The presence of clay in the soil sample leads to a decrease of resistivity due to the increasing interface conductivity. To get a reliable value of formation factor, Börner et al. (1996) used a correction for the fully saturated conductivity by subtraction the interface conductivity component of conductivity. When the water conductivity σ_w is known, the formation factor F can be obtained from

$$F = \frac{\sigma_w}{\sigma_0 - \sigma''/l}\ , \tag{5.10}$$

(Börner et al., 1996). In equation (5.10), σ_0 is the conductivity of the fully saturated sample, σ'' is the imaginary component of complex conductivity, and l is the ratio between the interface conductivity and the imaginary component. Generally, l varies from 0.01 to 0.15. In my case study of the unconsolidated sediments, l was chosen to be 0.04, an average value of the range. The imaginary component is derived from phase angle φ of SIP measurements following equation:

$$\sigma'' = \sigma_0 \sin(\varphi). \tag{5.11}$$

The true formation factor of the Pleistocene samples can also be calculated from the porosity of formations according to the first Archie's equation:

$$F = \frac{1}{\phi^m}\ , \tag{5.12}$$

where m is the so-called cementation factor. For unconsolidated sands, m is assumed to be 1.3 (Schön, 1996). Table 5.3 presents the values of the formation factors which are calculated from resistivity of the samples following equation (5.10) and from porosity of the samples according to equation (5.12). The true formation factor regarding the porosity of sample varies in the range from 3.9 to 6.1. These values are higher than most values of the formation factor that were determined by equation (5.10). The deviation of formation factor values between two calculations indicates the existence of clay in the samples.

Table 5.3. Formation factor of sandy samples of the Pleistocene aquifer.

ID	ρ_t (Ωm)	S_w	ρ_0 (Ωm)	ρ_w	σ'' (S/m)	F (σ'')	ID	Φ	$F = \Phi^{-1.3}$
V114	9.5	0.89	7.62	6.90	$2.2 \cdot 10^{-4}$	1.51	V114	0.26	5.8
V115	10.7	0.81	6.95	6.90	-	1.01	V115	0.35	3.9
V116	13.6	0.80	8.73	6.90	$4.5 \cdot 10^{-4}$	1.30	V116	0.35	3.9
V117	14.6	0.87	11.03	6.90	$4.7 \cdot 10^{-4}$	1.85	V117	0.33	4.3
V214	15.1	0.91	12.51	8.33	$3.6 \cdot 10^{-4}$	1.95	V214	0.34	4.0
V215	25.7	0.90	20.78	8.33	$1.0 \cdot 10^{-4}$	3.22	V215	0.35	3.9
V216	25.1	0.88	19.54	8.33	-	2.35	V216	0.33	4.2
V218	18.9	0.84	13.28	8.33	-	1.59	V218	0.32	4.3
V219	17.9	0.88	13.74	8.33	$1.2 \cdot 10^{-4}$	2.14	V219	0.31	4.5
V315	3.6	0.91	2.96	0.77	$8.1 \cdot 10^{-5}$	3.86	V315	0.38	3.6
V316	7.1	0.81	4.63	0.77	-	6.02	V316	0.31	4.6
V317	12.3	0.68	5.67	0.77	$5.7 \cdot 10^{-5}$	7.38	V317	0.25	6.1

- Note: sign '-' is non-determined because of negative phase shift.

In the process of evaluation of the hydrogeological situation of the Pleistocene aquifer in the study area, the resistivity of water is derived from the resistivity of the formations according to the electrical resistivity investigations in the study area. A formation factor of 2.0 is used to derive the resistivity of the water. The conductivity of the water is the inverse value of water resistivity.

Figure 5.10 shows the distribution of water conductivity, which is derived from the resistivity of formation according to the electrical resistivity investigations for the Pleistocene aquifer. 117 values of formation resistivity, which were derived from VES, RI, TEM, and laboratory investigations, are used to calculate the water conductivity of the Pleistocene aquifer. The squared black dots, which are indicated in Figure 5.10, are the locations of the electrical resistivity investigations in the study area. Following the conductivity distribution of water, the Pleistocene aquifer contains fresh water at the Southwestern part and saline water at the Northeastern part of the study area. Two dashed contour lines of 150 and 450 mS/m, corresponding to TDS of 1 and 3 g/l, are presented in the map to separate between fresh and saline groundwater. The area, which is confined between these contour lines, is assumed to be the brackish water area. The transition zone runs parallel to the Red River and perpendicular to the coastline. Compared to the map of water conductivity derived from the domestic wells (Figure 4.25), the saline water boundary is well resolved at the Northern part, where the domestic wells are sparse.

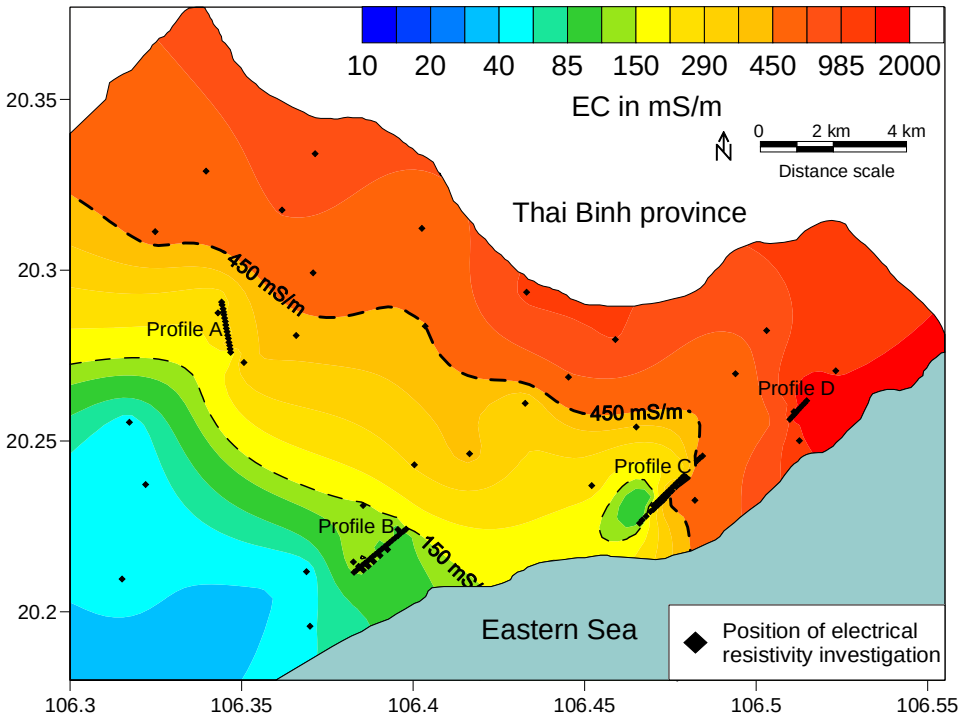

Figure 5.10. Water conductivity distribution of the Pleistocene aquifer derived from the electrical resistivity investigations.

The water conductivity distribution in Figure 5.10 shows an anomaly of conductivity distribution in the Southwestern part of profile C. This anomaly does not reflect the hydrogeological situation of the area because there is no resistivity investigation in space between profiles B and C. The anomaly indicates the fresh water bearing formation at the Southwestern part of profile C. The water conductivity of water samples from domestic wells indicated that the Pleistocene aquifer contains fresh water in the space between two profiles (Figure 4.25). That means that the fresh water extends from the profile B area to the profile C area. This is not resolved by the water conductivity distribution related to resistivity investigations. To get a reliable groundwater conductivity distribution in the study area, the locations of the electrical resistivity investigations can be assumed to be water wells and the electrical conductivity values, which are derived from electrical resistivity investigations, are assigned for groundwater at the same position. A combination of the water conductivity related to resistivity investigations and the water conductivity from the domestic wells helps to increase the number of water wells in the study area. By the way, the sparseness of water wells in the saline water area can be solved while the characteristic distribution of the groundwater in the fresh water area can be maintained. This combination provides a better image of groundwater conductivity distribution.

Figure 5.11 shows the electrical conductivity distribution of groundwater for the Pleistocene aquifer according to the water wells and the derived resistivity investigations. The locations of the water wells and resistivity investigations are indicated by different symbols. The combined map of the electrical conductivity shows a better hydrogeological situation of the Pleistocene aquifer in the study area. Two contour lines 150 and 450 mS/m of electrical conductivity corresponding to TDS values 1 and 3 g/l are used to separate the fresh and saline water area in the Pleistocene aquifer. The TDS values are indicated on the color scale. The boundary between fresh and saline water is clearly determined. The anomaly at Southwestern part of profile Giao Xuan in Figure 5.10 is instead of gradual changing in electrical conductivity distribution. The hydraulic situation in the space between two profiles is determined. However, some local anomalies of electrical conductivity are identified in Figure 5.11. These anomalies are presented by electrical conductivity value of a single well. The area with an electrical conductivity of lower than 150 mS/m (a TDS value of less than 1 g/l) contains fresh water while the area with an electrical conductivity of higher than 450 mS/m (a TDS value of higher than 3 g/l) is bearing saline water. The area, which is confined between the two contour lines, is assumed to be the transition zone, which contains brackish water. The saline water originates from the fault system, which runs along Red river, and extends to Southwest direction.

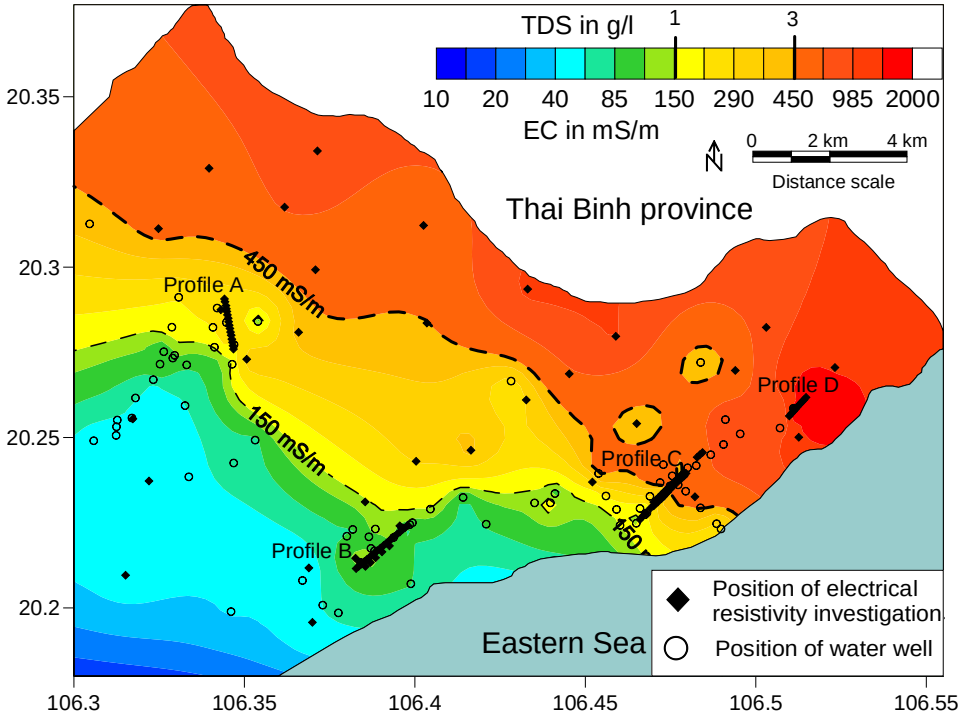

Figure 5.11. Distribution of electrical water conductivity in the Pleistocene aquifer.

5.5. Hydraulic conductivity of the Pleistocene aquifer

Hydraulic conductivity (K) is one of the most important parameters of an aquifer. Its amplitude varies in a large range because it significantly depends on characteristic parameters of aquifer such as grain size distribution, sorting of particles, porosity, and clay content. Accurate estimation of hydraulic conductivity helps to evaluate the properties of the aquifer. Hydraulic conductivity can be determined by several methods such as pumping tests at the well sites, grain size distribution analysis, permeability tests in laboratory, and related geophysical investigations. In my case study in Nam Dinh province, the hydraulic conductivity of the Pleistocene aquifer is estimated by pumping tests at the well sites (field scale), grain size distribution analysis and related geophysical investigations (laboratory scale). The pumping tests of the Pleistocene aquifer were performed at the positions of three boreholes GT-1, GT-2, and GT-3. The hydraulic conductivity value K_p of the three boreholes is approximately $8.5 \cdot 10^{-6}$ m/s (Table 4.6). This value can be assumed to be the hydraulic conductivity value of the Pleistocene aquifer in the study area. The laboratory investigations including grain size distribution analysis, mass related internal surface and complex resistivity measurements provide another estimation of hydraulic conductivity of the Pleistocene formations. These methods provide an indirect estimation of hydraulic conductivity of the aquifer.

Statistical grain size analysis is a standard method for estimation of hydraulic conductivity of an aquifer. Compared to aquifer tests, this method is less dependent on the geometry and hydraulic boundaries of the aquifer but reflects the transmitting properties of the aquifer. There are a lot of publications on hydraulic conductivity estimation of an aquifer based on grain size distribution analysis (Hazen, 1911; Beyer, 1964; Uma, 1989; Arya et. al., 1999; Carrier, 2003). For unconsolidated sediments, the fine particles play a more important role with respect to hydraulic conductivity. Therefore, it is plausible to select a central tendency value biased toward fine grain size diameter. Therefore, d_{10} has been named as the effective diameter in hydraulic conductivity estimation. It corresponds to the diameter of the fraction with 10% of sample by weight, which has a smaller grain size. A well known equation, which was given by Hazen (1911, after Hördt et al., 2009), is based on an effective diameter d_{10} and includes a temperature dependence:

$$K_H = 0.0116 d_{10}^2 (0.7 + 0.03T) \tag{5.13}$$

where K_H is in m/s, d_{10} is in mm and T is in degree Celsius. Hazen's equation is only valid for small uniformity coefficients $U < 5$ with $U = d_{60}/d_{10}$. This is a restriction because most unconsolidated sediments have a higher uniformity coefficient. To solve this restriction, Beyer (1964) suggested using the equation:

$$K_B = C(U)d_{10}^2, \quad (5.14)$$

where *C(U)* is a tabulated function, ranging from 0.011 to 0.006. Beyer's equation includes the uniformity coefficient by a uniformity-dependent factor *C(U)* (Kirsh and Yaramanci, 2006). This equation is based on a single effective diameter and does not require a small uniformity coefficient.

Alyamani and Sen (1993) have shown that the hydraulic conductivity is related to the effective diameter d_{10}, average diameter d_{50}, and their combinations. Hence, instead of an effective diameter, they used an effective range of grain size diameters in hydraulic conductivity calculation. The grain size distribution curve is commonly a straight line at fine particle size. Based on the slope and intercept of grain size distribution curve, Alyamani and Sen (1993) proposed an empirical equation to estimate the hydraulic conductivity of unconsolidated sediments using the effective diameter d_{10} and the average diameter d_{50}:

$$K_A = 1300[I_0 + 0.025(d_{50} - d_{10})]^2, \quad (5.15)$$

where I_0 is the intercept point of the straight line with the horizontal axis. In the equation (5.15), K_A is in m/day; d_{10}, d_{50}, and I_0 are in mm. The intercept value is expected to be very close to zero.

In the case of study in Nam Dinh coastal area, the Pleistocene aquifer consists of unconsolidated sediments with a significant fraction of fine particles. Hydraulic conductivity of the Pleistocene samples is calculated according to equations (5.14) and (5.15). The effective diameter d_{10}, and the average diameter d_{50} are determined from grain size distribution curves. For Beyer's formula, the uniformity-dependent factor *C(U)* is chosen to be equal to 0.09, regarding the particle size of sediments. For the equation (5.15), the intercept point I_0 is very close to zero, therefore this value is fixed equal to 0.001 mm for all of samples. Twelve samples, which belong to the Pleistocene aquifer, are used for the hydraulic conductivity estimation from grain size distribution analysis. Figure 5.12 displays three typical grain size distribution curves of the three samples in the three boreholes. All grain size distribution curves are characterized by a straight line at the fine particle size domain. Using the logarithm scale for the grain size axis, the effective diameter d_{10} and the average diameter d_{50} are easily determined. The values of determined diameter are presented in Table 5.4.

The results of hydraulic conductivity calculation are listed in Table 5.4. The hydraulic conductivity value of soil samples, which are calculated according to Beyer (K_B) and Alyamani (K_A) equations, varies in the range from 10^{-8} to 10^{-6} m/s. For a certain sample, K_A and K_B provide an approximate value of hydraulic conductivity. The hydraulic conductivity values according to two empirical equations (Beyer and Alyamani) are comparable.

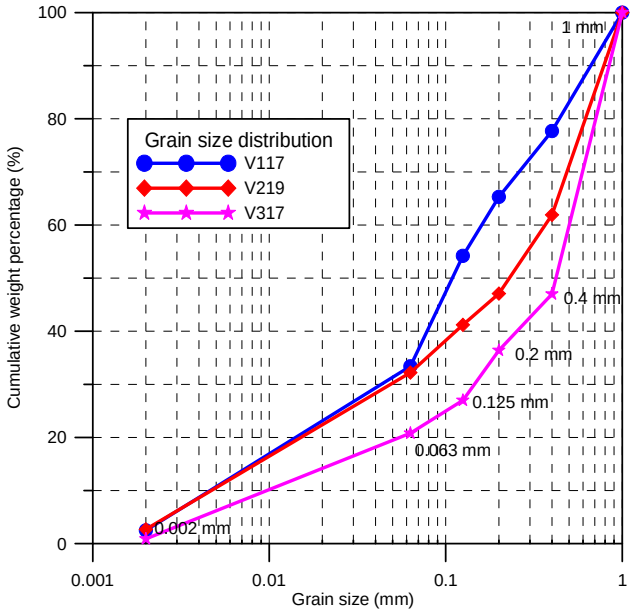

Figure 5.12. Grain size distribution curves of the Pleistocene samples.

Figure 5.13 shows a comparison of hydraulic conductivity values according to Beyer equation K_B and Alyamani equation K_A. The hydraulic conductivity values vary within one order of magnitude. The distance to diagonal line presents the error between two values K_A and K_B. The hydraulic conductivity values K_p of the Pleistocene aquifer, which are obtained from pumping tests, are also indicated in Figure 5.13. These values are located on the diagonal of the figure because the graph uses the same value for both axes. Compared to the pumping test, the hydraulic conductivity values from grain size distribution are smaller. This difference is related to the scale of investigations. The hydraulic conductivity of samples represents a thin layer where it is taken. To retrieve the hydraulic conductivity of the whole Pleistocene aquifer, a model of numerous layers is constructed with the representation of every sample for each layer. The thickness of layers is estimated from the depth interval between samples. The tranmissivity parameter T of the Pleistocene aquifer is calculated for every borehole according to equation:

$$T = \sum_{i=1}^{n} K_i h_i \quad , \tag{5.16}$$

where h_i is thickness of the i^{th} layer, and K_i is hydraulic conductivity of the i^{th} sample. The thickness h_i and the transmissivity T of every borehole are listed in Table 5.4. Two values of transmissivity correspond to two values of hydraulic conductivity from grain size distribution. An average of two transmissivity values for the whole aquifer is around $2.5 \cdot 10^{-5}$ m^2/s. This value is approximate value of transmissivity, which was obtained from pumping tests at the well sites (see Table 4.6).

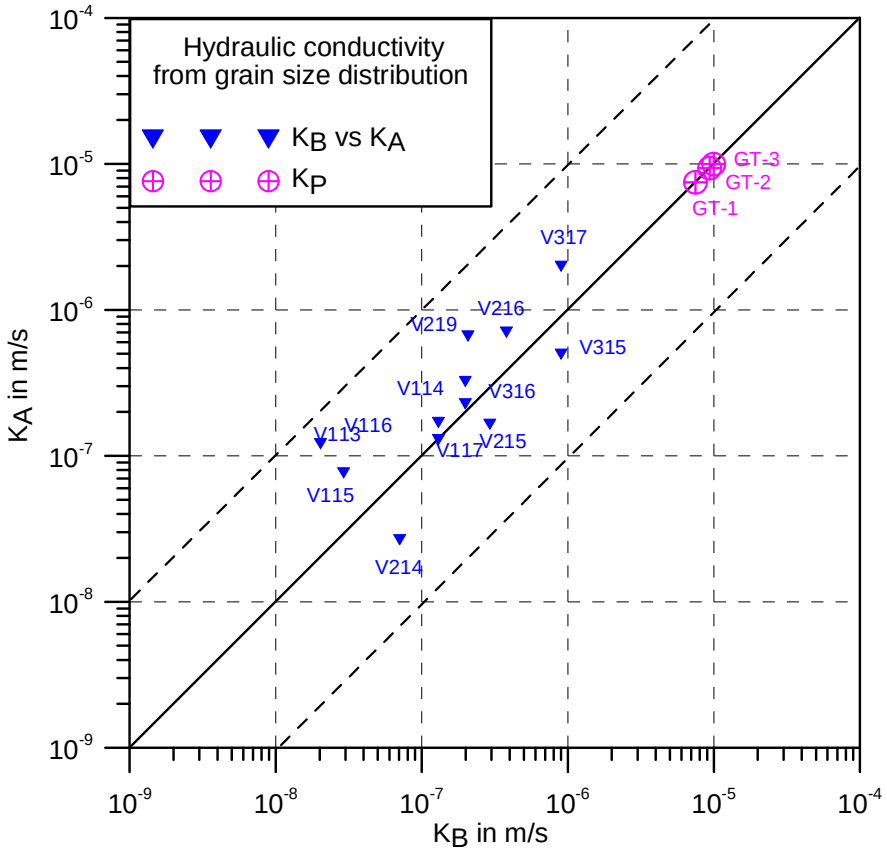

Figure 5.13. Hydraulic conductivity calculated from grain size distribution.

Table 5.4. Hydraulic conductivity and transmissivity calculated from grain size.

Layer i	*ID*	*d10 (mm)*	*d50 (mm)*	K_A *(m/s)*	K_B *(m/s)*	h_i *(m)*	T_{KA} *(m^2/s)*	T_{KB} *(m^2/s)*
1	V113	0.0057	0.098	$1.6\cdot10^{-7}$	$2.9\cdot10^{-7}$	3	$6.1\cdot10^{-6}$	$4.8\cdot10^{-6}$
2	V114	0.0038	0.081	$1.3\cdot10^{-7}$	$1.3\cdot10^{-7}$	4		
3	V115	0.0018	0.052	$7.7\cdot10^{-8}$	$2.9\cdot10^{-8}$	6		
4	V116	0.0015	0.075	$1.2\cdot10^{-7}$	$2.0\cdot10^{-8}$	11		
5	V117	0.0047	0.12	$2.3\cdot10^{-7}$	$2.0\cdot10^{-7}$	15		
1	V214	0.0028	0.016	$2.7\cdot10^{-7}$	$7.1\cdot10^{-8}$	3	$2.1\cdot10^{-5}$	$9.5\cdot10^{-6}$
2	V215	0.0038	0.098	$1.7\cdot10^{-7}$	$1.3\cdot10^{-7}$	5		
3	V216	0.0065	0.240	$6.6\cdot10^{-7}$	$3.8\cdot10^{-7}$	14		
4	V219	0.0048	0.230	$5.0\cdot10^{-7}$	$2.1\cdot10^{-7}$	16		
1	V315	0.01	0.200	$3.2\cdot10^{-7}$	$9.0\cdot10^{-7}$	6	$4.2\cdot10^{-5}$	$2.4\cdot10^{-5}$
2	V316	0.0045	0.150	$2.0\cdot10^{-6}$	$2.0\cdot10^{-7}$	10		
3	V317	0.01	0.430	$6.6\cdot10^{-7}$	$9.0\cdot10^{-6}$	18		

Hydraulic conductivity calculation of soil samples can not only be derived from grain size but also from related geophysical data. The fine particles have a strong effect on some petrophysical parameters. Relationships between hydraulic properties of unconsolidated sediments and specific internal surface area S_{por} or complex interface conductivity σ'' have been found in both laboratory and field measurements (Börner et al., 1996; Weller and Börner, 1996). To estimate the transport and storage properties from complex electrical investigation, Börner et al. (1996) performed numerous spectral induced polarization (SIP) measurements on unconsolidated sediments in both laboratory and field scale. Their results have shown that the phase shift for most of the samples was constant over a broad frequency range of up to 10 kHz. Based on the constant phase angle model, they suggested a set of empirical equation to estimate the hydraulic conductivity from SIP data at one frequency of around 1 Hz. This method is based on the PaRiS equation, which was derived by Pape et al. (1987, after Böner et al., 1996) from a fractal pore space model to estimate the hydraulic conductivity from formation factor and specific internal surface area S_{por} (related to the inverse hydraulic radius of porous media). The PaRiS equation has a form as:

$$K = \frac{a}{F(S_{por})^c}, \tag{5.17}$$

where K is in m/s and S_{por} is in μm^{-1}.

Equation (5.17) can also be used to calculate the hydraulic conductivity of formation based on the mass related internal surface S_m, which is determined by nitrogen adsorption method. The relation between S_{por} and S_m is given by Riepe et al. (1979, after Börner et al., 1996) with

$$S_{por} = \frac{d_k S_m (1 - \emptyset)}{\emptyset}, \tag{5.18}$$

where d_k is matrix density in kg/m^3 and S_m is the mass related specific internal surface area in m^2/kg, and Φ is porosity of sample. The required parameters in equation (5.18) are available based on the results of laboratory investigations. Using S_{por} from equation (5.18) in equation (5.17), the hydraulic conductivity can be estimated.

In the equation (5.17), a is an empirical constant. Weller and Börner (1996) recommended to use $a=0.00475$ for unconsolidated sediments. This value of a was successfully applied by Hördt et al., (2009) for SIP data at field scale investigations. The exponent c is another adjustable parameter. The exponent c is found to be in the range between $2.8 < c < 4.6$ (Börner et al., 1996; Lesmes and Friedman, 2005). The variation of exponent c strongly influences the result. Weller and Börner (1996) suggested to use exponent $c=3.1$. This value is derived by Pape et al. (1987) from their model based on a fractal description of the pore space. An adjustment of exponent c

requires a change of constant *a*. In my study, the equation (5.17) is applied with $a=0.00475$ and $c=3.1$ for unconsolidated samples from the Pleistocene aquifer.

A relationship between complex interface conductivity and specific internal surface area has been identified. Börner et al. (1996) suggested a procedure to derive the S_{por} directly from imaginary component of conductivity:

$$S_{por} = b\sigma'' \tag{5.19}$$

with a factor b=86000. The specific internal surface from equation (5.19) is inserted into equation (5.17) to estimate hydraulic conductivity of the formation from the complex interface conductivity and the formation factor

$$K = \frac{a}{F(b\sigma'')^c}\,. \tag{5.20}$$

In my study, the hydraulic conductivity of the Pleistocene samples is calculated by equation (5.20) according to SIP data. The imaginary component of conductivity is obtained from the phase angle using equation (5.11). Börner et al. (1996) formulated the empirical equation (5.20) with a requirement of constant phase angle over a broad frequency range. They recommended using one frequency of around 1 Hz. In the case study of Nam Dinh coastal samples, the phase behavior of complex conductivity measurements is not really constant over the frequency range because of negative phase angle at low frequencies. Almost all soil samples show a positive phase angle at the frequency of 1.46 Hz. According to the observation of phase behavior over the frequency range, the positive phase values vary in one order of amplitude. This is only a weak variation of phase values observed in the frequency range of around 1.46 Hz.

Figure 5.14 shows the phase angles of three silty sand samples in the frequency range from 10^{-2} to 10^{2} Hz. The error of measurement is indicated as vertical error bar if it is larger than the symbol. Although the phase angle behavior is not really constant over the frequency range, it seems to be stable at the frequency range from 10 mHz to 10 Hz. Thus, the application of the empirical equation (5.20) for the frequency of 1.46 Hz is possible.

Hydraulic conductivity of the Pleistocene samples is estimated by both equations (5.17) and (5.20), regarding the surface-area-to-porosity ratio S_{por} and the complex interface conductivity σ'', respectively. The formation factor was calculated by equation (5.10). Using the results of laboratory investigations, two values of hydraulic conductivity K_{Spor} and $K_{\sigma''}$ are estimated.

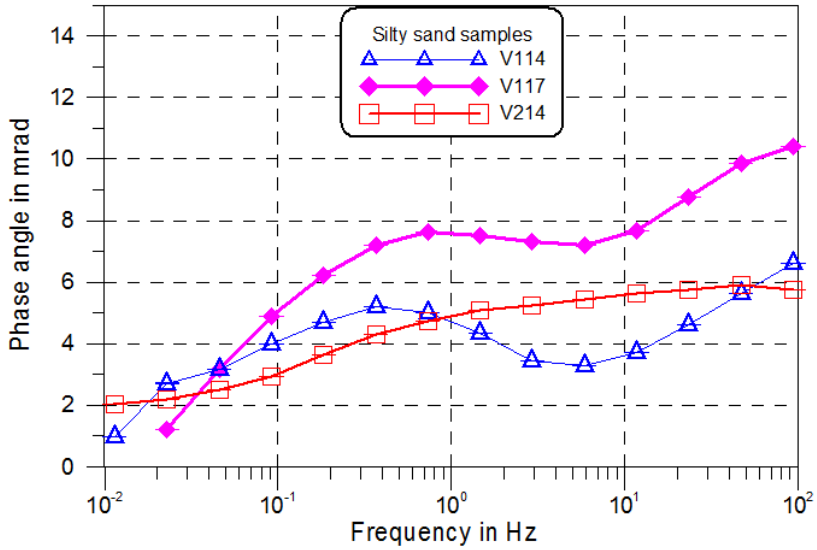

Figure 5.14. The phase shift behavior of the Pleistocene samples.

Table 5.5 lists the hydraulic conductivity of the Pleistocene samples and related parameters. K_{Spor} and $K_{\sigma''}$ are the hydraulic conductivity, which were calculated from specific internal surface area and complex interface conductivity, respectively. The variation of K_{Spor} value is in the range from $3.7 \cdot 10^{-9}$ to $5.2 \cdot 10^{-7}$ m/s while $K_{\sigma''}$ value varies from $5.9 \cdot 10^{-8}$ to $3.3 \cdot 10^{-6}$ m/s. These values are smaller than the hydraulic conductivity K_P of the Pleistocene aquifer which is obtained from pumping tests. The deviation of hydraulic conductivity K_{Spor} and $K_{\sigma''}$ is within two orders of magnitude. Strong variation is observed on samples with a high gravel fraction (V219, V315 and V317).

Table 5.5. Hydraulic conductivity calculated from *Spor* and σ''.

Sample ID	F	S_{por} (μm^{-1})	K_{Spor} (m/s)	φ (rad)	σ'' (S/m)	$K_{\sigma''}$(m/s)
V114	1.51	37.0	$3.4 \cdot 10^{-8}$	$2.0 \cdot 10^{-3}$	$2.2 \cdot 10^{-4}$	$3.6 \cdot 10^{-7}$
V115	1.01	26.0	$1.9 \cdot 10^{-7}$	-	-	-
V116	1.30	24.9	$1.6 \cdot 10^{-7}$	$3.9 \cdot 10^{-3}$	$4.5 \cdot 10^{-4}$	$4.4 \cdot 10^{-8}$
V117	1.85	25.2	$1.2 \cdot 10^{-7}$	$5.2 \cdot 10^{-3}$	$4.7 \cdot 10^{-4}$	$2.6 \cdot 10^{-8}$
V214	1.95	75.5	$3.1 \cdot 10^{-9}$	$5.1 \cdot 10^{-3}$	$3.6 \cdot 10^{-4}$	$5.9 \cdot 10^{-8}$
V215	3.22	19.9	$1.4 \cdot 10^{-7}$	$2.6 \cdot 10^{-3}$	$1.0 \cdot 10^{-4}$	$1.7 \cdot 10^{-6}$
V216	2.33	13.0	$7.2 \cdot 10^{-7}$	-	-	-
V218	1.43	41.8	$3.1 \cdot 10^{-8}$	-	-	-
V219	2.14	27.4	$5.9 \cdot 10^{-8}$	$2.0 \cdot 10^{-3}$	$1.2 \cdot 10^{-4}$	$1.8 \cdot 10^{-6}$
V315	3.86	12.2	$4.9 \cdot 10^{-7}$	$2.4 \cdot 10^{-4}$	$8.1 \cdot 10^{-5}$	$3.0 \cdot 10^{-6}$
V316	7.43	18.0	$9.5 \cdot 10^{-8}$	-	-	-
V317	7.42	15.4	$1.3 \cdot 10^{-7}$	$4.5 \cdot 10^{-4}$	$5.7 \cdot 10^{-5}$	$1.7 \cdot 10^{-6}$

Note: sign '-' = values are not determined because of negative phase angle.

The hydraulic conductivity of the Pleistocene samples was individually estimated by grain size distribution analysis, specific internal surface area and complex interface conductivity. Finally, the results should be compared. The hydraulic conductivity determined from grain size distribution varies in the range from $7 \cdot 10^{-8}$ to $6 \cdot 10^{-6}$ m/s, while the hydraulic conductivity values determined from specific interface surface area and the complex internal conductivity are in the range from $3 \cdot 10^{-9}$ to $3 \cdot 10^{-6}$ m/s. The grain size analysis yields two approximate values of hydraulic conductivity, K_A and K_B, for a certain sample. Therefore, one of them, K_A or K_B, can be used to compare with the hydraulic conductivity values K_{Spor} and $K_{\sigma''}$. Here, I propose to use the value K_A for this comparison.

Figure 5.15 plots the values of hydraulic conductivity related to grain size distribution versus the hydraulic conductivity related to complex interface conductivity $K_{\sigma''}$ and specific internal surface area K_{Spor}. The horizontal axis presents the values of hydraulic conductivity values of K_A, which were estimated by the effective diameter d_{10} and average diameter d_{50} (equation 5.15). The vertical axis shows the values of hydraulic conductivity $K_{\sigma''}$ and K_{Spor} by different symbols and colors. The blue dots display the hydraulic conductivity of grain size versus the hydraulic conductivity derived from complex interface conductivity $K_{\sigma''}$. The hydraulic conductivity values of all samples vary in the range of one order of magnitude. The distance to diagonal line reflects the difference between two values of hydraulic conductivity K_A and $K_{\sigma''}$.

The red squared symbols display the hydraulic conductivity derived from grain size K_A versus the hydraulic conductivity derived from internal surface-to-porosity ratio K_{Spor}. Most samples present a difference within one order of magnitude. Only sample V317 show a slightly higher deviation. For the sample V317, a high fraction of gravel leads to a higher value of the formation factor. A higher formation factor results in a lower hydraulic conductivity.

A comparison of hydraulic conductivity values of all samples regarding to grain size distribution, complex interface conductivity and specific internal surface area, shows that the deviation between hydraulic conductivity values are within one and half order of magnitude with the exception of the sample V214. For the sample V214, the grain size classification results in a 80 % of clay and silt fractions (Table 4.4). A domination of fine particles causes a higher value of specific internal surface and a lower value of hydraulic conductivity. The green circle, which has a radius of one and a half order of magnitude, is displayed in the Figure 5.15 to indicate the variation of hydraulic conductivity of the samples in the Pleistocene aquifer. Almost all samples are confined by the green circle. The deviation of hydraulic conductivity regarding the different methods is within one order of magnitude. This is acceptable because of the

uncertainty of the measured parameters. Hördt et al. (2009) concluded that one order of magnitude is the typical uncertainty arising from inversion ambiguity in their estimation of hydraulic conductivity regarding the grain size distribution and SIP data at field scale.

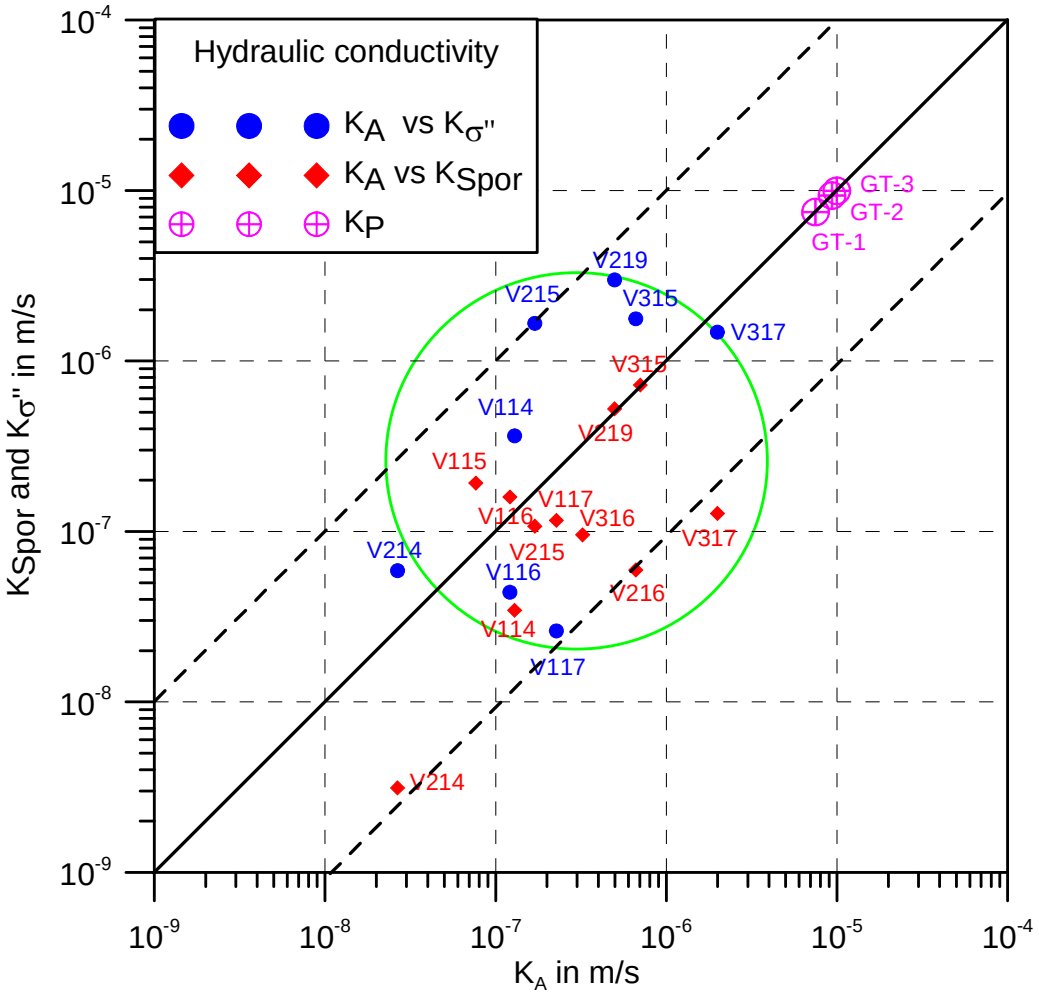

Figure 5.15. Comparison of hydraulic conductivity of the Pleistocene samples.

The hydraulic conductivity values K_P of the Pleistocene aquifer, which are obtained from pumping tests in the three boreholes, are also indicated in the Figure 5.14. These values are located on the diagonal line of the graph. Compared to the laboratory results, the hydraulic conductivity values from pumping tests (field scale) are generally higher within two orders of magnitude. The strong deviation may be caused by the different scales of the investigations. A dominance of more permeable layer is only detectable at larger scale of investigation. For the coarse grained samples, (V215; V219; V315; and V317), the hydraulic conductivity values determined by complex

interface conductivity indicate a weaker deviation from the pumping tests within one order of magnitude. These samples are located at the depths where the groundwater is extracted. The pumping tests provide information only in the vicinity of the borehole where the screen filter placed. The hydraulic conductivity also depends on the geometry and homogeneity of the aquifer. The pumping test more or less reflects the horizontal flow of groundwater at macroscopic scale. A comparison of the hydraulic conductivity values K_B with the hydraulic conductivity values $K_{\sigma''}$ and K_{Spor} shows a similar behavior as the aforementioned discussion.

For the laboratory investigation, the soil samples are representative only for a small section around the sampling position. No undistorted samples were investigated. The grain size distribution does not consider the original degree of compaction of the material. Considering the same grain size distribution, but different compaction or porosity, a wide variation in hydraulic conductivity can be caused. A variation in porosity may also result in varying values of S_{por} (see equation 5.18). A slightly change in S_{por} causes a stronger variation in K because of the large exponent $c=3.1$ in equation (5.17). The relation between S_{por} and σ'', which is described by the linear equation (5.19), could be confirmed by further investigations on an extended data base integrating sandstone samples and unconsolidated material (Weller et al., 2010a). A slightly variation of factor b in equation (5.19) indicates the uncertainty of this relation. It should be noted that the factor b also depends on the salinity of the pore water (Weller and Slater, 2012). A slightly variation in b causes also a considerable variation in K. A variation of hydraulic conductivity values determined by different empirical methods within one order of magnitude should be accepted as a good result. The larger hydraulic conductivity, which results from the pumping test, may be caused by preferential horizontal flow paths in coarse grained material. This effect cannot be recognized by the determination of the laboratory methods on disturbed samples. An upscaling of the laboratory values to the field scale generally results in a higher hydraulic conductivity. The shift of one and a half order seems to be reasonable.

5.6. Hydrogeological situation along coastline

The geological and hydrogeological situations of the aquifers in the study area have been determined. An estimation of hydraulic properties of the aquifers has performed. To evaluate the aquifers in the coastal area, a cross section reflecting the geological and hydrogeological situation along the coastline was constructed. All information, which was collected during geophysical and hydrogeological investigations, is integrated to sketch the hydrogeological conceptual model along the coastline of the study area (Figure 5.16). The profile extends from the Southwest to the Northeast,

from profile B (Giao Phong area) to profile D (Giao An area). The positions of geophysical investigations are not exactly located on the profile but they are close to the profile. Based on the results of the geophysical investigations, the geological structure is constructed along the profile. The fault, which is determined by RI results, is also sketched in the figure. The hydraulic conductivity of the soil samples, which are calculated from the grain size distribution analyses, is indicated in the model. The red text numbers indicate the TDS values of the groundwater from the Pleistocene aquifer at three new boreholes.

The conceptual model reflects the hydrogeological situation along the coastline of the study area. The Holocene aquifer contains fresh water at the Southwestern part of profile. The saline water may be infiltrated into the Holocene aquifer by the local canals which are normally connected to sea water. For the Pleistocene aquifer, the transition zone separates the water bearing formation into two parts: fresh and saline water area. The width of the transition zone is around 1 km. It is located in the middle of profile C (Giao Xuan commune). Saline water, which originates from the fault system, intrudes into the Pleistocene aquifer towards the Southwest. The transition zone moves in Southwestern direction.

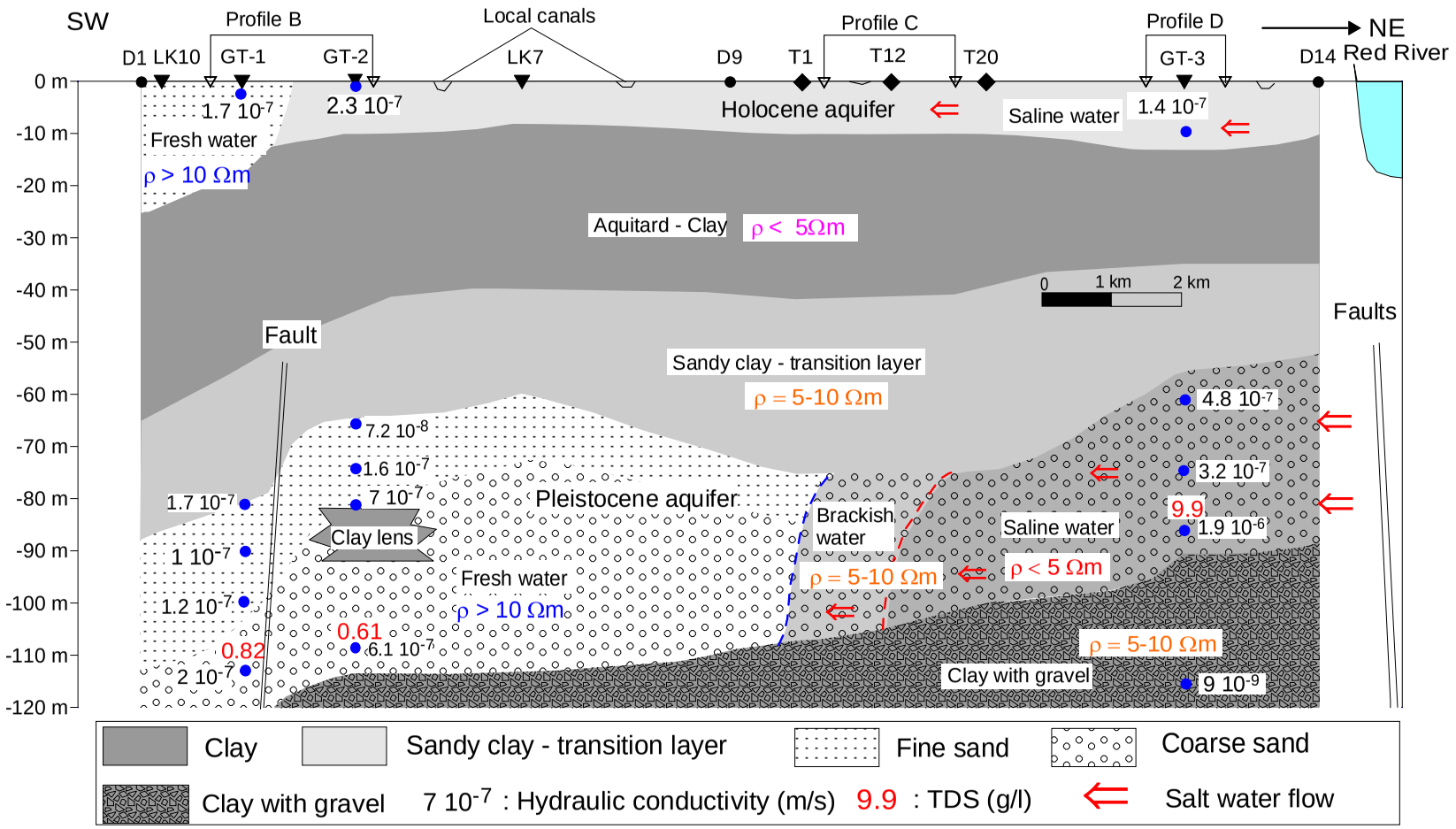

Figure 5.16. Sketch of hydrogeological conceptual model of the study area by the integration of the whole information collected during the geophysical and hydrogeological investigations.

6. Conclusions and recommendations

Salt water intrusion into aquifers is an important process in coastal areas and therefore it is the subject of scientific researches. Geophysical and hydrogeological techniques have proven to be valuable tools for evaluating the hydraulic situation of the coastal aquifers and for identifying the extension of salt water intrusion. In my study, geophysical and hydrogeological investigations have been focused on the Pleistocene aquifer, a deep water bearing formation, in which the boundary between fresh and saline water extends perpendicular to the coastline. The geological structures and the hydrogeological situation of the aquifers have been determined by geophysical and hydrogeological investigations. The hydraulic and storage properties of the Pleistocene aquifer have been determined on the basis of petrophysical parameters.

Based on geophysical, hydrogeological, and petrophysical investigations in the field and in laboratory, the following results regarding the aquifers and saline water intrusion can be summarised.

In the study area, the resistivity surveys provided valuable information on the geological structures and resistivity distribution of the aquifers. 33 VES stations provide an overview on the geological structure of the study area in the deltaic region of Red river. The geological structures are characterized by more or less horizontally layered sedimentary sequences. The thicknesses and resistivities of the layers are determined by VES. Comparing to the stratification of boreholes, the VES models include three main layers. The first layer, which belongs to the Holocene formation, extends from surface to a depth of around 30 m with a resistivity in the range from 0.7 to 15 Ωm. Most VES models show a resistivity of less than 5 Ωm for the Holocene formations. A low resistivity of the formation indicates that the Holocene aquifer contains saline water. The second layer has an average thickness of 40 m and a resistivity of less than 5 Ωm. It is a clay layer, an aquitard belonging to Vinh Phuc formation. The third and deepest layer corresponds to the Pleistocene formation with a resistivity in the range from 1 to 45 Ωm. A higher formation resistivity is reflected by the fresh water area of the Pleistocene aquifer while a lower formation resistivity is indicated by the saline water. The VES survey provides valuable information on the geological structure and hydraulic properties of the aquifers and aquicludes. However, VES data interpretation presents an ambiguous result. A low data density of VES in the study area affects the resolution of the maps of resistivity distribution due to the interpolation process. To investigate the Pleistocene aquifer at a depth of 100 m, a distance of 1000 m between two VES stations is recommended.

Resistivity imaging provides a confirmation of VES investigation and a detailed 2D resistivity section. RI data is simultaneously interpreted by RES2DINV and DC2DSIRT programs. The RES2DINV enables the locations of small anomalies, while the DC2DSIRT better reflects gradual changes in resistivity. The RES2DINV software yields higher contrast in resistivity section, while the DC2DSIRT results in smoother images. The non-commercial DC2DSIRT software uses predetermined parameters for inversion process. A lot of parameters are adjustable in RES2DINV. The inversion process is faster with RES2DINV program. The resulting vertical sections of RI present layered structures corresponding to the Holocene formation, the aquitard, and the Pleistocene aquifer. For the Holocene sediments, only the Southwestern part of profile B (Giao Phong commune) shows a high resistivity corresponding to fresh water area. The other parts of RI profiles present a low resistivity corresponding to the saline water bearing formations. The clay layer is presented by a low resistivity. The Pleistocene aquifer is characterized by a large variation of formation resistivity reflecting the transition from fresh water to saline water. Along RI profiles from Southwest to Northeast, the formation resistivity gradually decreases. The saline water boundary is located in the middle of profile C (Giao Xuan commune). RI is not able to distinguish between saline water bearing formations and the clay sediments. Therefore, in the saline water area of profile D (Giao An commune), the RI section shows a homogeneous resistivity distribution. In this case, the stratification of the borehole and the gamma logging curves are used to distinguish between the lithologic units. The resulting vertical sections clearly indicate the locations of two geological fault zones in the study area.

A TEM sounding provides a layered model. The combination of several TEM soundings along a profile can be compiled as a vertical 2D section. In the study area, most TEM soundings result in a model of four layers including the Holocene aquifer, an aquitard layer, a transition layer, and the Pleistocene aquifer. The Holocene formations show a very low resistivity. The Pleistocene formation indicates a decrease in resistivity from the Southwest to Northeast. The TEM models yield a resistivity of around 20 Ωm for the fresh water bearing formations and a resistivity of less than 10 Ωm for the saline water bearing formations.

The comparison of TEM models from stations along profile B with the corresponding models derived by VES indicates severe differences for deeper layers. The VES models are in good agreement with the stratification of the boreholes. But the TEM models indicate an unreasonably high resistivity of the deepest layer. It is supposed that a highly conductive overburden layer caused by salt production areas, the saline Holocene aquifer and a thick clay layer reduce the depth of penetration of the transmitted electromagnetic field. The conductive top layers form a kind of screening

that prevents receiving electromagnetic signals from greater depth. As a consequence, non-reliable resistivity values are attributed to the deepest layer in the resulting models. A resistivity value of 2000 Ωm, which is determined for the depth of the Pleistocene aquifer, cannot be accepted considering a resistivity of 20 Ωm determined by well logging as the true value. The reduced depth of penetration in the case of conductive overburden layers demonstrates a considerable disadvantage of electromagnetic methods in the exploration of deep aquifers.

The stratification of three new boreholes reveals the geological structures and the constituents of sediments. Thai Binh and Hai Hung sediments (Q_{IV}^{3}*tb* and Q_{IV}^{1-2}*hh*) found from the surface to the depth of 28 m correspond to the Holocene aquifer. The clay sediment (Vinh Phuc formation - Q_{III}^{2}*vp*) forms the aquitard, which extends from 28 to 81 m of depth. The geophysical results are in agreement with the stratification of boreholes. Hanoi formation (Q_{II-III}^{1}*hn)*, which consists of sand and gravel and is found from 56 to 115 m, corresponds to the Pleistocene aquifer. Le Chi sediment (Q_{1}*lc*) is found in the borehole GT-2 at a depth of 113 m and in the borehole GT-3 at a depth of 90 m. The stratification of the boreholes GT-1 and GT-2 confirms the depressed and uplifted zones, which correspond to two sides of a fault zone at position of 1000 m in profile B. A 10 m clay layer, which is embedded within the Pleistocene aquifer, is identified in the borehole GT-2. This layer is not resolved by VES, TEM and RI investigations. The stratification of borehole GT-3 shows a layered structure, which cannot be resolved by resistivity measurements because of the missing contrast in resistivity between salt water bearing sandy formation and clay layers.

Well logging results reflect the local structure of geological formations. Resistivity logs indicate a variation of the lithological components. The clay sediments show a low resistivity of less than 10 Ωm. The resistivity value of clay formations depends on the kind and condition of clay. The sandy formations of the Pleistocene aquifer present a large variation of resistivity between the boreholes. A high resistivity of the Pleistocene formation is measured at borehole GT-2 (30 Ωm), corresponding to a fresh water bearing formation. The resistivity logs display the clay layer within the Pleistocene aquifer at the borehole GT-2. The sandy formation containing saline groundwater shows a resistivity of around 3 Ωm (borehole GT-3). The clay sediments and saline water bearing formations are presented by similar resistivity. It is not possible to distinguish them by resistivity logs. In this case, the gamma ray activity log proves to be useful. The decrease of natural gamma ray activity reflects a transition from clayey to sandy formations. Clayey sediments are characterized by a gamma ray activity $\geq$ 100 cps while sandy formations show a value of around 40 cps. The gamma curves reflect the layered structure. Clayey and sandy formations can be well

distinguished by natural gamma log. However, well logging requires a borehole and the logs provide information only on the vicinity of the borehole.

Forty soil samples were investigated in a petrophysical laboratory. The results can be well compared with those of the geophysical investigation in field. The electrical resistivity was determined by an equipment that measures complex resistivity spectra in a wide frequency range. The amplitude of complex resistivity shows a slight decrease with increasing frequency. The resistivity of samples at a frequency of 1.46 Hz is chosen for further data interpretation. Clayey samples show a resistivity of less than 10 Ωm. Sandy samples at the boreholes GT-1 and GT-2 present a higher resistivity corresponding to a fresh water bearing formation. Sandy samples of borehole GT-3 show a resistivity of less than 5 Ωm. This indicates that the sandy formation contains saline water. The formation resistivity of sandy samples changes with a variation of grain size fractions. A high clay content of sediment leads to a decrease of formation resistivity because clay minerals in wet samples act as conductors. A sample with high clay content corresponds to a high value of specific internal surface area. The sandy sample with a high value of magnetic susceptibility is related to a higher iron content in the aquifer. The complex resistivity spectra indicate negative phase shifts between current and voltage signals for a variety of samples at low frequencies. The negative behavior of phase angle may be caused by ongoing chemical reactions between clay minerals and organic substances. This phenomenon should be further investigated.

Electrical conductivity of water samples from the Pleistocene aquifer, together with geophysical investigations, has confirmed the hydrogeological situation of the Pleistocene aquifer. Electrical conductivity of water samples, as well as TDS converted value, indicates the transition from fresh to saline water in the Pleistocene aquifer. The electrical conductivity map shows the distribution of areas of fresh and saline water. The fresh water area exists at the Southwestern part and the presence of saline water dominates the Northeastern part of study area. Because most of the water wells are located in the fresh water area, the water conductivity distribution of the Pleistocene aquifer is not so densely documented in the saline water area. The three new boreholes, which were drilled for this study, are completed as water wells. A pumping test has been performed in each well. The hydraulic conductivity of the Pleistocene aquifer is estimated from single well monitoring. The experiments result in a hydraulic conductivity of around $8.5 \cdot 10^{-6}$ m/s for all three water wells. Considering this value extrapolating to the thickness of the aquifer, a transmissivity value of the Pleistocene aquifer was determined.

The new geophysical investigations confirm existing models of geological structure in the study area. An aquitard lies between the Holocene and the Pleistocene aquifers. The clay layer is present in the whole study area. The average thickness of the clay layer is around 40 m. This layer plays an important role to prevent the migration of saline water between the Holocene and the Pleistocene aquifers in vertical direction. Geophysical results confirm the previous findings that the Holocene aquifer contains almost saline water. The Pleistocene aquifer is located at a depth of more than 56 m. A transition from fresh to saline water is observed in Northeastern direction. According to geophysical results the boundary between fresh and saline can be determined with an accuracy of around 100 m in the study area. The electrical conductivity distribution map of the Pleistocene aquifer shows a large transition zone from fresh to saline water area. The saline water boundary extends in perpendicular direction to the coastline and parallel to the Red river (and the fault system running along Red river). Considering the stratification of the boreholes and the results of geophysical investigations in both field and laboratory, it can be concluded that all investigations have contributed to get detailed information to improve the resolution of the geological and hydraulic models of the study area.

Based on the geophysical and the hydrogeological data in the study area, fundamental relationships between petrophysical and geophysical parameters are verified. These relationships can be used to improve the knowledge on the properties of the Pleistocene aquifer. In the laboratory investigations, the relationship between volumetric water content and porosity of soil samples has yielded an average air content of the samples. The air content is related to the evaporation of water in the sample during transported and storage process. The actual air or water content should be known to correct the electrical resistivity to full water saturation. The correlation between clay content of soil samples and gamma ray count rate of well logging indicates that the gamma ray activity of soil samples is in the range from 30 to 1100 cps, corresponding to a variation in clay content from non-clay formation to pure clay sediment. The clay volume fraction has been calculated using the count rate of gamma ray measurements. A higher clay content in the sample is related to a lower resistivity.

The principle of equivalence has been applied for a combined inversion of VES and TEM data regarding the stratification in the boreholes. Related inversion between VES and TEM soundings provides a reliable model, which is in accordance with the local geological structure. The related models consider the layer boundaries identified in the boreholes. The resulting formation resistivity of the individual layers is in good agreement with the results of RI and laboratory investigations. The boundary between

brackish and saline groundwater in the Pleistocene formation could be fixed using the resistivity derived from RI and TEM inversions along profile C (Giao Xuan area).

A comparison of RI, log and laboratory resistivities has shown a good agreement of different investigations at the position of the boreholes. For a certain depth, the RI and log investigation present a similar resistivity. Formation resistivity derived from RI and well logging corresponds to the resistivity of the fully saturated formation. Only for the sandy samples, the resistivity, which is determined in laboratory, shows a strong deviation in comparison with the log resistivity. The loss of water in the sample during transport and storage causes a decrease of saturation and an increase of sample resistivity.

Based on the resistivity of groundwater samples from the Pleistocene aquifer and the resistivity of formation at a close position, the apparent resistivity formation factor was determined. A mean value of 1.97 is inferred for all the available positions. A calculation of the apparent formation factor for soil samples indicates that most samples show a value of around 2. The presence of clay in the sample causes a decrease in resistivity and apparent formation factor. A value of 2 is assigned for the apparent resistivity formation factor of the Pleistocene aquifer. Following the formation resistivity and the apparent formation factor of the Pleistocene aquifer, the conductivity of water at the position of resistivity investigation can be derived.

The pumping test at well sites provides a hydraulic conductivity K_P value of $8.5 \cdot 10^{-6}$ m/s while the hydraulic conductivity estimations from the laboratory investigation predict lower values with a moderate variation. Based on characteristic value of grain size distribution, the hydraulic conductivity is calculated by two empirical equations (Beyer equation and Alyamani equation). The calculation presents an approximate value for a certain sample. The deviation between two values is within one order of magnitude. Using PaRiS equation, the hydraulic conductivity is calculated from the specific internal surface area and the complex interface conductivity. The values K_{Spor} and $K_{\sigma''}$ vary within one order of magnitude compared to the hydraulic conductivity derived from grain size distribution. The variation of hydraulic conductivity values of all samples is within one and a half order of magnitude. This variation reflects the variability of samples in grain size distribution (e.g. clay content) and compaction (e.g. porosity). The hydraulic conductivity $K_{\sigma''}$ of sandy samples in the depth interval of filter casing is about one order of magnitude lower compared to the pumping test results K_P. All hydraulic conductivity values derived from laboratory data are lower than the hydraulic conductivity obtained from pumping tests. The deviation between field and laboratory hydraulic conductivity reaches one and a half order of magnitude. This difference might be caused by the scale of investigation. The pumping test

reflects the horizontal water flow within the depth interval of filter casing. Preferential flow paths and an increased hydraulic conductivity in horizontal direction may result in higher values. The laboratory calculations are based on grain size, specific internal surface or imaginary part of conductivity considering the intrinsic properties of isotropic samples. It is justified to assume a higher hydraulic conductivity at a larger scale. The uncertainty of the degree of upscaling is a limitation of the methods to estimate the hydraulic conductivity from petrophysical parameters.

The whole information, which is collected during geophysical and hydrogeological investigation, has been integrated in a cross section of a hydrogeological conceptual model. The hydrogeological situation along the coastline of the study area is clearly indicated in the model. The saline water may be infiltrated into the Holocene aquifer via the local canals. For the Pleistocene aquifer, the saline water originates from the fault systems. The width of transition zone is about 1 km. An extension of the transition zone in Southwest direction will be expected when the ground water extraction increases in the freshwater area.

The methodological approach used in my study has shown that a combination of geophysical methods at field scale (VES, RI, TEM), in boreholes (resistivity, gamma log), and in laboratory (resistivity, specific internal surface, grain size distribution) provide sufficient data at different scale that can be integrated in a reliable hydrogeological model. Geoelectrical methods are generally recommended for hydrogeological investigations related to varying water salinity. The combination of sounding and mapping tools provides valuable structural information. The limitations caused by the principle of equivalence can be reduced if boreholes are available to calibrate the geoelectrical models with known depth data. Electrical investigations on samples provide insight into petrophysical relations that are helpful to estimate water conductivity or hydraulic conductivity of the investigation formations.

Proposals for the further research

Although the hydrogeological situation of the aquifers in the study area has been determined, the following further activities are recommended.

To study the extension of saltwater intrusion in a new area, VES should be carried out to identify the layering of geological structures and the electrical properties of formations. The distance of VES stations should consider the depth of investigation. For the Pleistocene aquifer at a depth of 100 m, the spacing between VES stations should be about 1 km. RI and TEM measurements are performed to present the geological structure in 2D sections. RI and TEM profiles should be extended across the transition zone of the saline water in the aquifer. Drilling and well logging should

be performed to confirm the geological structure and the physical properties of formations. Laboratory investigations of soil samples provide the petrophysical properties of the formations. The physical parameters, which are derived from well logging and laboratory investigations, should be used to verify the resistivity model in the data interpretation of VES, TEM and RI. The conductivity and chemical composition of groundwater samples at the position of geophysical investigations should be determined.

A comparison of laboratory and field results helps to determine the intrinsic properties of formations. SIP measurements at the borehole sites is recommended to calculate the hydraulic conductivity of the aquifers at the field scale and to compare it with the hydraulic conductivity estimated from laboratory investigations. Pumping tests at more water wells should be carried out to maps the distribution of hydraulic conductivity and transmissivity in the aquifer. The water wells should be equipped with a filter casing for all thickness of the aquifer.

The present boundary between fresh and saline water and the transition zone in the Pleistocene aquifer has been determined with high accuracy. It seems to be more important but also more difficult to observe the temporal shift of this boundary. A monitoring concept should be developed to get reliable information on the changes of water salinity in the aquifer. Regular water probing in the existing wells close to the present boundary would provide useful local data. A repetition of VES at the same positions would provide information on changes of formation resistivity. The changing formation resistivity with time indicates a variation of groundwater salinity. In a similar way, RI can be repeated along the same profile to maps the changes in a 2D section. VES and RI proved to be useful for long term observation. The installation of fixed electrode arrays in borehole or along surface with permanent registration can be recommended if faster changes are expected. These systems can also be applied to monitor seasonal and short term changes of water salinity in the Holocene aquifer.

Appendices

Appendix A. Specific internal surface of soil samples.

GT-1	S_m (m^2/g)		GT-2	S_m (m^2/g)		GT-3	S_m (m^2/g)
V101	1.53		V201	3.30		V301	11.68
V102	2.60		V202	14.08		V303	4.36
V103	6.52		V204	10.28		V306	4.41
V104	10.89		V206	10.53		V308	10.52
V105	12.60		V208	13.30		V311	15.52
V106	13.37		V211	11.24		V312	11.63
V107	38.52		V213	7.54		V315	2.78
V108	14.20		V214	15.69		V316	3.01
V111	15.46		V215	4.37		V317	1.90
V113	6.29		V216	2.42		V318	30.71
V114	5.14		V217	17.69		V319	13.96
V115	5.28		V218	7.48		V320	12.74
V116	5.01		V219	5.13			
V117	4.70		V220	16.131			

Appendix B. The diameter of samples determined from grain size distribution curves.

ID	d_{10} *(mm)*	d_{20} *(mm)*	d_{50} *(mm)*	d_{60} *(mm)*
V113	0.0057	0.02	0.098	0.12
V114	0.0038	0.0095	0.081	0.11
V115	0.0018	0.0043	0.052	0.08
V116	0.0015	0.0057	0.075	0.12
V117	0.0047	0.015	0.12	0.17
V214	0.0028	0.0043	0.016	0.027
V215	0.0038	0.0098	0.098	0.14
V216	0.0065	0.035	0.240	0.27
V219	0.0048	0.017	0.230	0.37
V315	0.01	0.075	0.200	0.24
V316	0.0047	0.014	0.150	0.20
V317	0.01	0.055	0.430	0.5

Appendix C. Mass specific magnetic susceptibility of soil samples.

Sample ID	κ (10^{-8} m^3/kg)	Sample ID	κ (10^{-8} m^3/kg)	Sample ID	κ (10^{-8} m^3/kg)
V101	98.1	V201	63.2	V301	68.9
V102	16.6	V202	58.9	V303	42.4
V103	38.4	V204	37.1	V306	38.5
V104	25.4	V206	32.3	V308	57.3
V105	19.2	V208	20.5	V311	13.0
V106	29.3	V211	31.4	V312	12.8
V107	22.1	V213	31.9	V315	44.0
V108	12.6	V214	27.3	V316	44.1
V111	15.7	V215	48.2	V317	26.6
V113	9.5	V216	31.0	V318	16.2
V114	45.2	v217	21.3	V319	14.3
V115	39.3	V218	66.9	V320	9.3
V116	61.3	V219	38.6		
V117	34.0	V220	14.1		

References

Alyamani, M. S., and Sen, Z., (1993). Determination of hydraulic conductivity from complete grain size distribution curves. *Ground Water*, 31, 551-555.

Arya, L. M., Leji, F. J., Shouse, P. J., and Genuchten, M., T., (1999). Relationship between the hydraulic conductivity function and the particle size distribution. *Soil Science Society of America Journal,* 63, 1063-1070.

Bear, J., Cheng, A. H.-D, Sorex, S., Ouazar, D. and Herrera I., (1999). Theory and application transport in porous media: Seawater intrusion in coastal aquifers – Concepts, Methods and Practices. *Kluwer Academic Publisher, Netherlands.*

Beck, A. E., (1981). Physical principles of exploration methods – An introduction text for geology and geophysics students. *The Macmillan Press.*

Beyer, W., (1964). Bestimmung der Wasserdurchlässigkeit von Kiesen und Sanden aus der Kornverteilung. *Wasserwirtschaft – Wassertechnik*, 14, 165-168.

Börner, F. D., Schopper, J. R., and Weller, A., (1996). Evaluation of transport and storage properties in the soil and groundwater zone from induced polarization measurements. *Geophysical prospecting*, 44, 583 – 601.

Carrier III, W. D., (2003). Technical notes: Goodbye, Hazen; Hello, Kozeny-Carman. *Journal of Geotechnical and Geoenvironmental Engineering,* 129, 1054-1056.

Choudhury, K., Saha, D. K., and Chakraborty, P., (2001). Geophysical study for saline water intrusion in coastal alluvial terrain. *Journal of Applied Geophysics,* 46, 189-200.

Christiansen, A. V., Auken, E., and Sorensen, K., (2006). Chapter 6: The transient electromagnetic method. In: Kirsch R. (ed.): Groundwater geophysics – A tool for Hydrogeology. *Springer*.

Dakhnov, V. N. and Keller, G. V., (1962). Geophysical well logging. Quarterly of the Colorado school of mines. Volume 52, number 2, *Golden Colorado Press.*

Dang Dinh Phuc, (2000). Prediction of salt water intrusion in the coastal aquifers of Hai Hau and Giao Thuy dictricts, Nam Dinh province. Water managements and irrigations department, Ministry of Agriculture and Rural Development (in Vietnamese).

Dang Thanh Hai, Nguyen Ba Duan, Nguyen Duy Tieu, Nguyen Trong Vu, and Lai Cao Khiem, (2009). Exploration of deep groundwater aquifers in a predominantly saline water region. Intitute of Geophysics, Hanoi (in Vietnamese).

Doan Van Canh, Bui Hoc, Hoang Kim Hung, and Nguyen Kim Ngoc, (2002). Methodologies of hydrogeological investigation. *Trafic and Transport Press.* Hanoi, 241 pages (in Vietnamese).

Doan Van Canh, Le Thi Lai, Nguyen Duc Roi, Pham Thai Nam, Pham Quy Nhan, Nguyen Duc Binh, and Nguyen Van Nghia, (2004). *Report of project*: 'Estimating the groundwater potentials and proposal for safe exploitation methods for Nam Dinh province'. Institute of Geology. Hanoi, 100 pages (in Vietnamese).

Doan Van Canh, Le Thi Lai, Hoang Van Hung, Nguyen Duc Roi, and Nguyen Van Nghia, (2005). Groundwater potential of Nam Dinh province. *Journal of Geology*, Series B, 25, 31-42.

Ellis, D. V. and Singer, J. M. (2007). Well logging for Earth Scientists. *Springer*.

Ernstson, K. and Kirsch, R. (2006). Chapter 3: Geoelectrical methods. In: Kirsch, R. (ed.): Groundwater geophysics – A tool for Hydrogeology. *Springer*.

Falgas, E., Ledo, J., Marcuello, A., and Queralt, P., (2009). Monitoring freshwater-seawater interface dynamics with audiomagnetotelluric data. *Near Surface Geophysics*, 7, 391-399.

Franco, R., Biella, G., Tosi, L., Lozej, A., Chiozzotto, B., Giada, M., Rizzetto, F., Claude, C., Mayer, A., Bassan, V., and Gasparetto-Stori, G., (2009). Monitoring the saltwater intrusion by time lapse electrical resistivity tomography: The Chioggia test site (Venice Lagoon, Italy). *Journal of Applied Geophysics*, 69, 117-130.

Goes, B. J. M., Oude Essink, G. H. P., Vernes, R. W., and Sergi, F., (2009). Estimating the depth of fresh and brackish groundwater in a predominantly saline region using geophysical and hydrological methods, Zeeland, the Netherland. *Near Surface Geophysics*, 7, 401-412.

Hamzah, U. Samudin, A. R., and Malim E. P., (2007). Groundwater investigation in Kuala Selangor using vertical electric sounding (VES) surveys. *Environment Geology*, 51, 1349-1359.

Hazen, A., (1911). Discussion: Dam on sand foundation. *Transaction of the American Society of Civil Engineer,* 73, 199-203.

Hodlur, G. K., Dhakate, R., and Andrade, R., (2006). Correlation of vertical electric souding and borehole-log data for delineation of saltwater and freshwater aquifers. *Geophysics*, 71, G11-G20.

Hördt, A., Druiventak, A., Blaschek, R., Binot, F., Kemna, A., Kreye, P., and Zisser, N., (2009). Case histories of hydraulic conductivity estimation with induced polarization at the field scale. *Near Surface Geophysics*, 7, 529 – 545.

Hydrogeological Federation of North Vietnam (2006). Yearly report on situation of ground water at national monitoring water wells 2005. *Journal of Geology,* Series A, 292, 59-65 (in Vietnamese).

Hwang, S., Shin, J., Park, I., and Lee, S., (2004). Assessement of seawater intrusion using geophysical well logging and electrical soundings in a coastal aquifer, Youngkwang-gun, Korea. *Exploration Geophysics*, 35, 99-104.

Kearey, P., and Brooks, M., (1984). An introduction to geophysical exploration. *Blackwell Scientific Publications.*

Keller, G. V. and Frischknecht, F. C., (1970). Electrical methods in geophysical prospecting. *Pergamon Press, Oxford, NewYork.*

Kafri, U. and Goldman, M., (2005). The use of the time domain electromagnetic method to delineate saline groundwater in granular and carbonate aquifers and to evaluate their porosity. *Journal of Applied Geophysics*, 57, 167 – 178.

Khalil, M. A., Ramalho, E. C., and Santos, F. A. M., (2011). Using resistivity logs to estimate hydraulic conductivity of a Nubian sandstone aquifer in southern Egypt. *Near Surface Geophysics,* 9, 349-355.

Kirsch, R. (2006). Chapter 14: Groundwater quality – saltwater intrusions. In: Kirsch, R. (ed.) Groundwater geophysics – A tool for Hydrogeology. *Springer*.

Kirsch, R. and Yaramaci U. (2006). Chapter 15: Geophysical characterization of aquifers. In: Kirsch, R. (ed.) Groundwater geophysics – A tool for Hydrogeology. *Springer.*

Land, L. A., Lautier, J. C., Wilson, N. C., Chianese, G., and Webb, S., (2004). Geophysical monitoring and evaluation of coastal plain aquifers. *Ground Water,* 42, 59-67.

Langguth, H.-R. and Voigt, R., (2004). Section 4: Pumpversuche - Hydrogeologische Methoden. *Springer.*

Lesmes, D. P., and Friedman, S. P., (2005). Relationship between the electrical and hydrogeological properties of rocks and soils. In: Rubin, Y. and Hubbard, S. S. (eds.): Hydrogeophysics. *Spinger.*

Loke, M.H., (1999). Electrical imaging surveys for environmental and engineering studies – A practical guide to 2D and 3D surveys. *http://www.georentals.co.uk*.

Loke M.H., (2001). Tutorial: 2-D and 3-D electrical imaging surveys. 128 pages. *http://www.cas.umt.edu/geosciences//faculty/.../Loke_elect_tutorial.pdf*.

Manual of software RES2DINV, (2004). Geotomo software company, Malaysia. www.geoelectrical.com.

Manual of TEM FAST 48 instrument, (2006). Applied Electromagnetic Research (AEMR), the Netherlands. www.aemr.net.

Maurer, H., Friedel, S., and Jaeggi, D., (2009). Characterization of a coastal aquifer using seismic and geolectric borehole methods. *Near Surface Geophysics,* 7, 353-366.

Meju, M. A., Fenning, P. J., and Hawkins, T. R. W., (2000). Evaluation of small-loop transient electromagnetic sounding to locate the Sherwood Sandtone aquifer and confining formations at well sites in the Vale of York, England. *Journal of Applied Geophysics*, 44, 217-236.

Nam Dinh Statistic Office, (2009). Nam Dinh statistical yearbook 2008. *Statistical press.*

Nguyen, F., Kemna, A., Antonsson, A., Engesgaard, P., Kuras O., Ogilvy, R., Gisbert, J., Jorreto, S., and Pulido, B. A., (2009). Characterization of seawater intrusion using 2D electrical imaging. *Near surface Geophysics*. 7, 377-390.

Nguyen Nhu Trung, (2005). Application of geolectrical methods for groundwater investigation and salt water intrusion in coastal zone of Hai Phong province and Cat Ba island. Institute of Marine Geology and Geophysics, Hanoi (in Vietnamese).

Nguyen Nhu Trung, Trinh Hoai Thu, and Nguyen Van Nghia, (2008). Application of electrical resistivity and hydrogeology modelling methods to map and forecast the salt water intrusion in Thai Binh province. *Journal of Geology*, Series B, 31-32, 241-248.

Nguyen Thi Kim Thoa, Pham Van Ngoc, and NguyenVan Giang, (1995). Groundwater exploration in Mekong Delta by geophysical methods. Institute of Geophysics, Hanoi (in Vietnamese).

Nguyen Trong Vu, Weller A., and Tran Canh, (2005). Petrophysical investigation of material from Vietnamese river dikes. *Journal of Geology*, Series B, 23, 99-105.

Nguyen Trong Vu, Tang Dinh Nam, and Weller, A., (2007). Delineating the boundary between fresh and brackish groundwater by geophysical methods in Nam Dinh coastal area. *Journal of Geology*, series B, 29, 51 - 58.

Nguyen Trong Vu, Tang Dinh Nam, and Weller, A., (2009). Resistivity imaging measurements in Nam Dinh coastal area for delineation of aquifer. *Journal of Geology*, series B, 33, 29 - 35.

Nguyen Trong Vu, Tang Dinh Nam, and Weller, A., (2010). Geohysical measurements in coastal area of Nam Dinh province (Vietnam) for delineation of aquifers. *Near surface Geophysics Meeting*, P21, Zurich, Switzerland.

Nguyen Van Do, Ta Duc Bon, Do Van Quoc, and Bui Minh Duc, (1996). Hydrogeological map of Nam Dinh province and adjacent areas in scale 1:50.000. University of Mining and Geology, Hanoi (in Vietnamese).

Nguyen Van Giang, Dang Thanh Hai, and Nguyen Trong Vu, (1998). Groundwater investigation by geophysical methods in Ninh Binh province. Institute of Geophysics, Hanoi (in Vietnamese).

Pape, H., Riepe, L., and Schopper, J. R., (1987). Theory of self-similar network structures in sedimentary and igneous rocks and their investigation with microscopical and physical methods. *Journal of Micoscopy*,148, 121-147.

Parasnis, D. S. (1986). Principles of Applied Geophysics. *Chapman and Hall, USA.*

Payne, J. D., Kress, W. H., Shah, S. D., Stefanov, J. E., Smith, B. A., and Hunt, B. B., (2007). Geophysical delineation of the freshwater / saline water transition zone in the Barton Springs segment of the Edwards aquifer, Travis and Hays Counties, Texas, 5244. *US Geological Survey, Reston, Virginia*.

Rabinovich, M. B., (1995). Errors of 1D interpretation of 3D TDEM data in the application of mapping saltwater / freshwater contact. *Journal of Applied Geophysics*, 34, 23-34.

Reynolds, J. M., (2005). An introduction to applied and environmental geophysics. *John Wiley and Sons.*

Roy, A. and Apparao, A., (1971). Depth of investigation in direct current methods. *Geophysics*, 36, 943-959.

Riepe, L., Rink, M., and Schopper, J. R., (1979). Relation between specific surface dependent rock properties. *Transactions of the 8th European Logging Symposium, London, Paper D.*

Schön, J. H., (1996). Physical Properties of Rocks: Fundamentals and Principles of Petrophysics. Volume *18. Pergamon Press.*

Sharma, V. P., (1997). Environmental and engineering geophysics. *Cambridge University Press.*

Sheriff, E. R., (1989). Geophysical methods. *Prentice Hall, University of Houston.*

Seidel K. and Lange G., (2007). Section 4.3: Direct current resistivity methods. In: Knödel, K., Lange, G., and Voigt, H. -J., (eds.): Environmental geology – Hanbook of field methods and case studies. *Springer*, 205-238.

Spichak, V. V., (2007). Electromagnetic sounding of the earth's interior - Methods in Geochemistry and Geophysics. Volume 40. *Elsevier*.

Steward, M., (1999). Chapter 2: Geophysical investigations. In: Bear, J., Cheng, A. H.-D, Sorex, S., Ouazar, D., and Herrera I., (eds.): Theory and application transport in porous media: Seawater intrusion in coastal aquifers – Concepts, Methods and Practices. *Kluwer Academic Publisher, Netherlands.*

Tang Dinh Nam, Nguyen Tien Phong, Phung Van Huy, and Luong Thu Trang, (2004). Estimating the salt water intrusion and groundwater contamination in middle coastal zone of Vietnam from Quang Binh province to Quang Ngai province. Institute of Geosciences and Mineral Resources, Hanoi (in Vietnamese).

Telford, W. M. , Geldart, L. P., Sheriff, E. R., and Keys A. A., (1976). Applied Geophysics. *Cambridge University Press*.

Tiab, D., and Donaldson, E. C., (2004). Petrophysics: Theory and practice of measuring reservoir rock and fluid transport properties. *Elsevier Publisher*.

Tran Van Thang, (2009). *Report of project:* 'Characteristics of dynamic tectonics and geoenvironment hazards in the Red River delta and estimation of their effects to infrastructures'. Vietnamese Tectonics Association, Hanoi (in Vietnamese).

Tucker, M., (1988). Techniques in sedimentology. *Blackwell Scientific Publication*.

Uma, K. O., Egboka, B. C. E., and Onuha, K. M., (1989). New statical grain size method for evaluating the hydraulic conductivity of sand aquifers. *Journal of Hydrogeology,* 108, 343-366.

Weller, A., and Börner, F. D., (1996). Measurement of spectral induced polarization for environmental purposes. *Environmental Geology*, 27, 329-334.

Weller, A., Gruhne, A., Seichter, A., and Börner, F. D., (1996). Monitoring hydraulic experiments by complex conductivity tomography. *European Journal of Enviromental and Engineering Geophysics*, 1, 209 – 228.

Weller, A., Slater, L., Nordsiek, S., and Ntarlagiannis, D., (2010a) On the estimation of specific surface per unit pore volume from induced polarization: A robust empirical relation fits multiple datasets. *Geophysics* 75, No. 4, WA105-WA112.

Weller, A., Nordsiek, S., and Debschütz, W., (2010b). Estimating permeability of sandstone samples by nuclear magnetic resonance and spectral-induced polarization. *Geophysics*, 75, E215-E226.

Weller, A., and Slater, L., (2012). Salinity dependence of complex conductivity of unconsolidated and consolidated materials: Comparisons with electrical double layer models. *Geophysics*, 77, D182-D189.

Wiederhold, H., Simon, B., Steuer, A., Schaumann, G., Meyer, U., Binot, F., and Kühne, K., (2010). Coastal aquifers and saltwater intrusion in focus of airborne electromagnetic surveys in northern Germany. 21st *Salt Water Intrusion Meeting, Azores Portugal*.

Wonik, T., (2007). Section 4.8: Borehole logging. In: Knödel, K., Lange, G., Voigt, H. -J., (eds.): Environmental geology – Hanbook of field methods and case studies. *Springer*, 431-470.

Yang, C. -H., Tong, L. –T., and Huang, C. F., (1999). Combined application of dc and TEM to sea-water intrusion mapping. *Geophysics*, 64, 417-425.